

Alma Mater Studiorum – Università di Bologna

DOTTORATO DI RICERCA

Scienze Chimiche

Ciclo XXI

CHIM/03

Biomimetic Materials for Biomedical Applications

Presentata da: Dott.ssa Chiara Capuccini

Coordinatore Dottorato

Chiar.mo Prof. G. Longoni

Relatore

Chiar.ma Prof. A. Bigi

Esame finale anno 2009

Contents

Contents	2
Summary	4
1. Introduction	7
Biomimetic Materials	7
Biomaterials for Hard Tissue Repair	9
1.1 Bone Tissue.....	10
1.2 CaPs of Biological Interest	16
1.2.1 Hydroxyapatite.....	17
1.2.2 OctaCalcium Phosphate.....	21
1.2.3 α -TriCalcium Phosphate	23
1.2.4 DiCalcium Phosphate Dihydrate	25
1.3 CaPs for Hard Tissue Repair	26
1.3.1 Modified CaPs	28
1.3.1.1 Strontium	29
1.3.1.2 Magnesium.....	30
1.3.1.3 Manganese	31
1.3.1.4 Bisphosphonates	32
1.3.2 Coatings	33
1.3.2.1 Pulsed Laser Deposition	34
1.3.2.2 Matrix Assisted Pulsed Laser Evaporation.....	38
1.3.3 Bone Cements	43
1.3.4 Scaffolds	44
1.3.4.1 Drug Delivery	46
2. Aim of the Research	49
3. Materials	52
3.1 Syntheses	52
3.1.1 Sr-substituted Hydroxyapatite	52
3.1.2 Alendronate-Hydroxyapatite Nanocrystals.....	52
3.1.3 Substituted OctaCalcium Phosphate.....	53
3.1.4 α -TriCalcium Phosphate.....	53
3.2 Thin films deposition	53
3.2.1 Pulsed Laser Deposition	53
3.2.2 Matrix Assisted Pulsed Laser Evaporation.....	54

3.3 Hydrolysis	54
3.4 Microspheres	54
3.4.1 Alginate dialdehyde	54
3.4.2 Gelatin microspheres cross-linked with Alginate Dialdehyde and Calcium ..	55
3.4.3 Synthesis of the inorganic shell	55
3.4.4 Aspirin-loaded microspheres	56
4. Methods.....	57
4.1 X-Ray Diffraction	57
4.1.1 Scherrer analysis	57
4.1.2 Rietveld refinement analysis.....	58
4.2 Fourier Transform Infra-Red Spectroscopy	58
4.3 Atomic Absorption Spectroscopy	59
4.4 Scanning Electron Microscopy	59
4.5 Transmission Electron Microscopy	59
4.6 Surface Area Analysis by Gas Adsorption (BET)	59
4.7 Pulsed Laser Deposition	60
4.8 Matrix Assisted Pulsed Laser Evaporation.....	60
4.9 UV – Phosphorous, Gelatin and Drug Release Determination.....	60
4.10 Cell Culture	61
4.10.1 Osteoblast culture	61
4.10.2 Isolation of mononuclear cells for osteoclast culture	62
5. Results and Discussion.....	64
5.1 Strontium-Substituted Hydroxyapatite	64
5.2 Pulsed Laser Deposited Sr-Hydroxyapatite	77
5.3 Alendronate-Hydroxyapatite Nanocrystals.....	84
5.4 Bivalent Ions Modified OCP	89
5.4.1 Strontium Substitution	91
5.4.2 Magnesium Substitution	94
5.4.3 Manganese Substitution.....	97
5.5.1 Hydrolysis in Gelatin Solutions	107
5.6 Microspheres.....	111
6. Conclusions.....	118
7. References.....	121

Summary

Objects with complex shape and functions have always attracted attention and interest. The morphological diversity and complexity of naturally occurring forms and patterns have been a motivation for humans to copy and adopt ideas from Nature to achieve functional, aesthetic and social value.

Biomimetics is addressed to the design and development of new synthetic materials using strategies adopted by living organisms to produce biological materials. In particular, biomineralized tissues are often sophisticated composite materials, in which the components and the interfaces between them have been defined and optimized, and that present unusual and optimal chemical-physical, morphological and mechanical properties. Moreover, biominerals are generally produced by easily traceable raw materials, in aqueous media and at room pressure and temperature, that is through cheap process and materials. Thus, it is not surprising that the idea to mimic those strategies proper of Nature has been employed in several areas of applied sciences, such as for the preparation of liquid crystals, ceramic thin films computer switches and many other advanced materials.

On this basis, this PhD thesis is focused on the investigation of the interaction of biologically active ions and molecules with calcium phosphates with the aim to develop new materials for the substitution and repair of skeletal tissue, according to the following lines:

I. Modified calcium phosphates.

A relevant part of this PhD thesis has been addressed to study the interaction of Strontium with calcium phosphates. It was demonstrated that strontium ion can substitute for calcium into hydroxyapatite, causing appreciable structural and morphological modifications. The detailed structural analysis carried out on the nanocrystals at different strontium content provided new insight into its interaction with the structure of hydroxyapatite.

At variance with the behaviour of Sr towards HA, it was found that this ion inhibits the synthesis of octacalcium phosphate. However, it can substitute for calcium in this

structure up to 15 atom %, in agreement with the increase of the cell parameters observed on increasing ion concentration. A similar behaviour was found for Magnesium ion, whereas Manganese inhibits the synthesis of octacalcium phosphate and it promotes the precipitation of dicalcium phosphate dehydrate.

It was also found that Strontium affects the kinetics of the reaction of hydrolysis of α -TCP. It inhibits the conversion from α -TCP to hydroxyapatite. However, the resulting apatitic phase contains significant amounts of Sr^{2+} suggesting that the addition of Sr^{2+} to the composition of α -TCP bone cements could be successfully exploited for its local delivery in bone defects.

The hydrolysis of α -TCP has been investigated also in the presence of increasing amounts of gelatin: the results indicated that this biopolymer accelerates the hydrolysis reaction and promotes the conversion of α -TCP into OCP, suggesting that its addition in the composition of calcium phosphate cements can be employed to modulate the OCP/HA ratio, and as a consequence the solubility, of the set cement.

II. Deposition of modified calcium phosphates on metallic substrates.

Coating with a thin film of calcium phosphates is frequently applied on the surface of metallic implants in order to combine the high mechanical strength of the metal with the excellent bioactivity of the calcium phosphates surface layers. During this PhD thesis, thank to the collaboration with prof. I.N. Mihailescu, head of the Laser-Surface-Plasma Interactions Laboratory (National Institute for Lasers, Plasma and Radiation Physics – Laser Department, Bucharest) Pulsed Laser Deposition has been successfully applied to deposit thin films of Sr substituted HA on Titanium substrates. The synthesized coatings displayed a uniform Sr distribution, a granular surface and a good degree of crystallinity which slightly decreased on increasing Sr content. The results of *in vitro* tests carried out on osteoblast-like and osteoclast cells suggested that the presence of Sr in HA thin films can enhance the positive effect of HA coatings on osteointegration and bone regeneration, and prevent undesirable bone resorption.

The possibility to introduce an active molecule in the implant site was explored using Matrix Assisted Pulsed Laser Evaporation to deposit hydroxyapatite nanocrystals at different content of alendronate, a bisphosphonate widely employed in the treatments of pathological diseases associated to bone loss. The coatings displayed a good degree of crystallinity, and the results of *in vitro* tests indicated that alendronate promotes

proliferation and differentiation of osteoblasts even when incorporated into hydroxyapatite.

III. Synthesis of drug carriers with a delayed release modulated by a calcium phosphate coating.

A core-shell system for modulated drug delivery and release has been developed through optimization of the experimental conditions to cover gelatin microspheres with a uniform layer of calcium phosphate. The kinetics of the release from uncoated and coated microspheres was investigated using aspirin as a model drug. It was shown that the presence of the calcium phosphate shell delays the release of aspirin and allows to modulate its action.

As result of the research, the papers produced are reported below:

- A. Bigi, E. Boanini, C. Capuccini, M. Gazzano, *Strontium-substituted hydroxyapatite nanocrystals*. DOI:10.1016/j.ica.2006.07.074.
- A. Bigi, C. Capuccini, P. Torricelli, F. Sima, E. Boanini, C. Ristoscu, B. Bracci, G. Socol, M. Fini, I. Mihailescu. *Strontium-substituted hydroxyapatite coatings synthesized by pulsed laser deposition: in-vitro osteoblast and osteoclast response*. DOI:10.1016/j.actbio.2008.05.005.
- C. Capuccini, P. Torricelli, E. Boanini, M. Gazzano, R. Giardino, A. Bigi, *Interaction of Sr-doped hydroxyapatite nanocrystals with osteoclast and osteoblast-like cells*. DOI: 10.1002/jbm.a.31975.

1. Introduction

Biomimetic Materials

Objects with complex shapes and functions have always attracted attention and fascination. The morphological diversity and complexity of naturally occurring forms and patterns have been a motivation for humans to copy Nature and to adapt ideas from Nature to achieve functional, aesthetic, and societal value.

Scientists and engineers have long envied Nature's ability to design crystalline structure whose properties are often superior to those of similar synthetic materials, thanks to the huge timeframe Nature has had to optimize and perfect functional materials.

Through a process called biomineralization, proteins orchestrate the growth processes of many natural minerals into designs that confer them exceptional properties. The biological control to determine the size, shape, and properties of crystals is a key to addressing challenges as diverse as synthesizing nanostructures, characterizing climate change, treating disease, and designing new materials for national security applications.

It follows that to mimic biological materials is a powerful approach for the synthesis of advanced materials with complex shape, hierarchical organization and controlled size, shape and polymorphism under ambient conditions in aqueous environments. Increased understanding of biomineralization mechanisms has greatly enhanced the possibilities of biomimetic mineralization approaches.

Biomaterials are promising materials because they combine complex morphology over several hierarchy levels with superior materials properties and environmentally friendly synthesis and biocompatibility. This makes them very attractive archetypes for materials chemists. When studying these materials, the main aim is not to simply emulate a particular biological architecture or system, but to abstract the guiding principles and ideas and use such knowledge for the preparation of new synthetic materials and devices. Based on these ideas a rapidly developing research field has evolved, which can be summarized as bio-inspired or biomimetic materials chemistry. The creation of superstructures resembling naturally existing biomaterials with their unusual shapes and complexity, is meanwhile already an important branch in the broad area of biomimetics. During the past decade, exploration as well as application of these bio-inspired synthesis strategies has resulted in the generation of complex materials with specific

size, shape, orientation, composition, and hierarchical organization [2], influenced also by organic molecules.

Organisms have been producing mineralized skeletons for the past 550 million years. The mineral phases are often not pure but are made as composites because they contain of an organic part too. This is the one which takes part in and controls the biomineralization. Morphosynthesis consist of the chemical construction and patterning of inorganic materials with unusual and complex architecture [3 - 5]. The complex inorganic architectural replication is constructed hierarchically on a length scale from the nanometre to the millimetre level. The controlled synthesis of inorganic materials with specific morphology is an important aspect in the development of new materials in many fields such as catalysis, electronics, nanocomposites, etc. From a materials perspective, biomimetic syntheses have permitted the replication of a range of organized inorganic forms using, as templates, bacterial colonies [4], insect wings [5], spider silk [6] and pollen grains [7], for example. Most of the morphosynthesis routes or biomimetic syntheses involve precipitation reactions in self-assembly organic media, such as micelles, surfactants and microemulsions [5, 8, 9].

During the past 30-40 years there has been a major advance in the development of medical materials for biomedical applications, in particular in the innovation of ceramic materials for skeletal repair and reconstruction. The materials within this class are often referred to as “Bioceramics” and the expansion in their range of medical applications has been characterised by a significant increase in the number of patents and publications in the field and an ever increasing number of major international conferences and themed meetings. Bioceramics are now used in a number of different applications throughout the body. According to the type of bioceramics used and their interaction with the host tissue, they can be categorised as either “bioinert” or “bioactive”, and the bioactive ceramics may be resorbable or non-resorbable. The materials used include: polycrystalline materials; glasses, glass ceramics and ceramic-filled bioactive composites, and all these may be manufactured either in porous or in dense form in bulk, as granules or in the form of coatings [10].

Biomaterials for Hard Tissue Repair

The development of advanced materials for biomedical applications is among the most important problems facing modern materials engineering [11]. In recent times, problems like osseous tumours, trauma and other debilitating diseases created the need to fill defects in the skeleton. Most bone tissue engineering strategies rely on the use of temporary scaffolds that can be seeded with cells prior to implantation, or designed to induce the formation of bone from the surrounding tissue after implantation. The effectiveness of such materials can be highly improved if they can simultaneously act as drug delivery systems. Depending on the specificity of the illness, bioactive agents (e.g. growth factors or other protein-drugs) can be locally released and potentially accelerate the process of bone regeneration. Increasing efforts have been also devoted to the development of improved injectable materials aimed at providing an alternative for the filling of bone defects with less patient discomfort, as they can be applied through minimally invasive surgical procedures. Most injectable materials described in the literature consist of pastes, gels or liquid precursors that solidify in situ in response to some stimulus. Micro- or nano-particles have also been described, but they must be suspended in either autologous blood or other appropriate vehicle prior to injection. A variety of injectable materials, both ceramic- and polymer-based, have been developed for use in multiple orthopaedic applications. The combination of ceramic particles with polymeric matrices has also been extensively investigated in an attempt to mimic bone tissue, which may itself be seen as a complex composite material made of organic and inorganic components. Different ceramic phases have been used, hydroxyapatite and tricalcium phosphate being the most common, as well as several polymeric matrices, both of synthetic or natural origin, the latter including collagen, chitosan, gelatin and alginate, among others [12]. Calcium phosphate (CaPs) materials are already widely used as bone substitutes due to their excellent biological behaviour [13]. Hydroxyapatite (HA), for example, forms the main mineral constituent of human hard tissues and ceramics constituted by this compound have proved to be biocompatible and bioactive materials, which can chemically bond with bone, and have been successfully used clinically for repair of bone defects and augmentation of osseous tissues [14]. As a matter of fact, the greatest potential for bone substitution is shown by materials based on hydroxyapatite, which can develop tight bonding with bone tissue, exhibits osteoconductive behaviour, is stable toward bio-resorption, and has no adverse effects

on the human organism [15, 16]. Synthetic hydroxyapatite precursors are produced by a variety of ceramic processing routes including precipitation, sol-gel and hydrothermal processing [17]. Many biological materials are known to have unusual mechanical properties, some of which are surprisingly advantageous, especially when taking into account the fact that they are formed at ambient temperatures and pressures. This observation has inspired many studies of these materials over the last several decades aimed at discovering some of their structural ‘secrets’. The mineralized biological materials represent an interesting subgroup within this vast world. Clearly the presence of the mineral phase and the manner in which the mineral and the organic material are organized are among the key factors that contribute to their unique mechanical properties. Understanding just how this occurs is, however, not a trivial task, as the scale of ordered structures can vary from Angstroms to millimetres. Furthermore, one level of structural organization is often nested into another larger-scaled structural type, to produce a very complicated overall structure. In order to reveal the design strategies of these natural materials we not only have to understand their structural features in great detail, but we also need to identify the specific benefits that a particular aspect of the structure contributes to the bulk material. With all these difficulties, it is therefore not surprising that we still really know very little about the strategies used by organisms to form their superior materials. Minerals, macromolecules and water are the major components of these materials. More than 60 different minerals are known to be formed biologically, but only a small subset of these are common components of endo- and exo-skeleton types based on the organization of their mineral constituents. The one type is composed of multicrystalline arrays, in which the individual crystals are generally all aligned at least in one direction, and often in all three directions. The best known examples of such materials are bones, teeth and shells of various types [18].

1.1 Bone Tissue

Hard tissues are in general ceramic/organic composites with complex microstructure. Bone is a complex living tissue which has an elegant structure at a range of different hierarchical scales. It is basically a composite comprising an organic and an inorganic phases. Water (9 wt. %) is the third major component but its importance for the

mechanical functioning of bone has not to be underestimated as demonstrated by the results showed by the difference of the mechanical properties of dry and wet bone [19]. In fact, the mechanical properties of bone depend largely on the humidity along with other parameters such as mode of applied load, direction of the applied load, and kind of bone.

The organic component (ca. 20 wt. %) is based on collagen which regulates nucleation and growth of the mineral crystals. Collagen constitutes the main component of a three-dimensional matrix into which the mineral forms. The inorganic component (ca. 69 wt. %) is constituted by numerous isolated and small calcium phosphate crystals of nonstoichiometric carbonated apatite [20] embedded in and held together by collagen matrix.

Strength and the other mechanical properties of bone depend also upon these main components. Orientation of the collagen fibers, bone density, and porosity, and the molecular structure and arrangement of its constituent apatite crystals within their collagen matrix are critical parameters to be considered.

Collagen is in the form of small microfibers. The collagen arrangement with hole zones is *necessary* for the controlled mineral nucleation and growth, but it may not be *sufficient* [21]. Additionally, other organic materials, such as proteins, polysaccharides, and lipids are also present in small quantities and are an integral part of the nucleation site being implicated in the mechanism of nucleation. Several studies have clearly demonstrated that phosphoproteins, in particular, are either limited or concentrated mainly at the site of initial mineralization, in close relationship with the collagen fibrils [22]. The phosphoproteins appear to become enzymatically phosphorylated [23], prior to mineralization.

At the molecular level, the triple helices of collagen molecules, secreted by osteoblasts, are assembled into microfibrils, with a specific tertiary structure having 67 nm periodicity and 40 nm gaps, or holes, between the end of the molecules (*Figure 1*). The holes localize a microenvironment containing free mineral ions and bound side chain groups, with a molecular periodicity that serves to nucleate the mineral phase heterogeneously [24].

The diameter of the collagen microfibers varies from 100 to 2000 nm. Calcium phosphate in the form of crystallized HA and/or amorphous calcium phosphate provides stiffness to the bone.

The inorganic phase is present in the form of plates or needles, about 40-60 nm long, 20 nm wide, and 1.5 - 5 nm thick. They grow with a specific crystalline orientation parallel to the collagen fibrils, such that the larger dimension of crystals is along the long axis of the fiber. It is worth mentioning that the mineral phase present in the bone is not a discrete aggregation of the HA crystals. It is rather made of a continuous phase which is evidenced by a very good strength of the bone after a complete removal of the organic phase.

The basic building block of bone material is the mineralized collagen fibril (*Figure 2*) that is the combination of collagen's triple helix with carbonate hydroxyapatite crystals.

At the next hierarchical level, a conspicuous diversity in structure occurs, with fibril arrays organized in a variety of patterns, which can lead to very organized structures such as *osteons* (*Figure 3*) [25].

The result is that bone is usually composed of a relatively dense outer layer (*cortical bone*) surrounding a less dense, porous tissue (*cancellous bone*) (*Figure 4*), which is filled with a gel-like tissue (*bone marrow*). This complex tissue is the body's repository for the undifferentiated stem cells that are the precursors to most of the reparative or regenerative cells produced after the embryonic organism has formed.

Cross sections of the compact bone, showing cylindrical osteons (also called Haversian system) with blood vessels running along Haversian canals (in the center of each osteon) are shown in *Figure 5*. The metabolic substances can be transported by the intercommunicating systems of canaliculi, lacunae, and Volkmann's canals, which are connected with the marrow cavity. The various interconnecting systems are filled with body fluids and their volume can be as high as 19%. Cancellous bone (also called trabecular or spongy bone) is a cellular material consisting of a connected network of rods or plates. Low density, open cell, rod-like structures develop in regions of low stress while high density, closed cell, plate-like structures occur in regions of higher stress [26]

Adult human bone maintains a dynamic state, which continually undergoes a process termed remodelling through the coordinated actions of bone resorption and synthesis, through osteoclasts and osteoblasts, respectively. Osteoclasts originate from haematopoietic precursor cells, which are possibly present in bone marrow, and differentiate into multinucleated cells by the fusion of mononuclear progenitors.

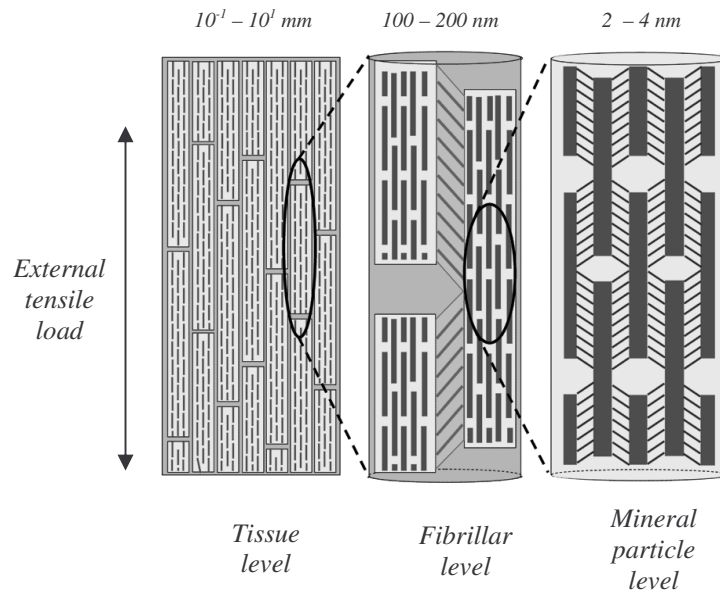


Fig. 1 - Representation of bone's organization.

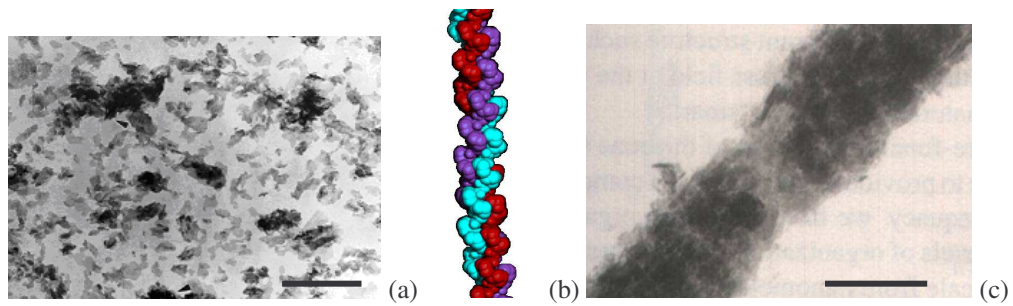


Fig. 2 - Bone's hierarchical levels: isolated carbonate apatite from human bone (a), collagen structure (triple helix) (b), and the mineralized collagen fibril (c) (scale bars = 200 nm).

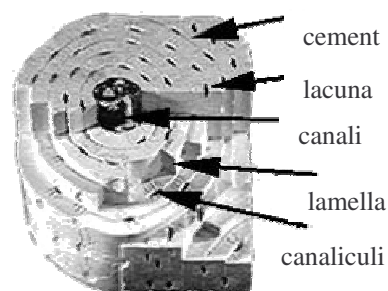


Fig. 3 - Single osteon representation, cylindrical motif.

The developing multinuclear cells are responsible for the resorption of bone matrix (a process involving attachment to the bone surface), establishment of cell polarity, migration and subsequent degradation of bone matrix components. Calcium phosphate resorption depends on the ability of the osteoclasts to generate an acidic extracellular compartment between the cell and the bone surface. An acidic pH value is essential for bone mineral dissolution. The primary cellular mechanism responsible for this acidification is the active release of protons into the extracellular space. These protons allow the solubilization of hydroxyapatite (HA) crystals. The other component of bone, the organic bone matrix, which consists of substances such as collagen, is digested by acid lysosomal enzymes secreted by osteoclasts. The activity of bone-resorbing cells is highly regulated and stimulated by hormones and cytokines. Steroid hormones act on various cell types to regulate development, cell proliferation and cell differentiation.

So, bone is a dynamic tissue that undergoes remodelling even after growth and modelling of the skeleton have been completed.

The remodelling involves the coupled processes of bone resorption and formation.

The resorption behaviour of osteoclast cells is fundamental to integration of bone substitute material [27].

In addition, bone has two essential functions: structural material and ion reservoir. Both functions depend on a significant extent on the exact size, shape, chemical composition and crystal structure of the mineral crystallites and their arrangement within the organic matrix [21].

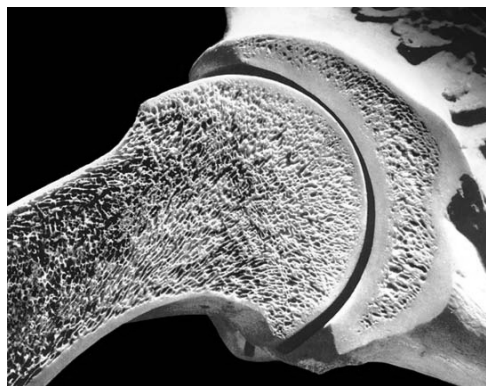


Fig. 4 – Vertical section of a human bone and its density's difference: cortical (compact) bone surrounds cancellous (spongy) bone.

However, although the skeleton plays a vital role in the mammalian body both in terms of support and locomotion and also the protection of vital organs, it is susceptible to fractures as a result of injury and degenerative diseases which are often associated with ageing. Therefore there has always been a need, since the earliest time, for the repair of damaged hard tissue. The earliest attempts to replace hard tissue with biomaterials aimed to restore basic functions by repairing the defects caused by injury and disease with minimal biological response from the physiological environment. The materials fulfilling these requirements are now largely classed as “bioinert”. “Bioinert” is a term that should be used with care, since it is clear that any material introduced into the physiological environment will induce a response. However for the purposes of biomedical implants, the term can be defined as a minimal level of response from the host tissue in which the implant becomes covered in a thin fibrous layer which is non-adherent.

On the contrary, bioactive materials are supposed to stimulate a positive response from the host tissue. In this area, calcium phosphates play a fundamental role.

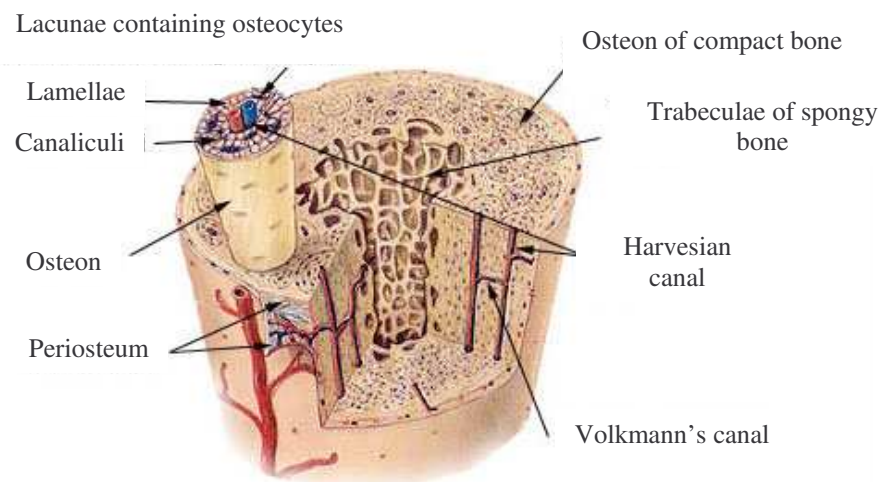


Fig. 5 - Global bone's organization: compact and cancellous bone.

(www.web-books.com/eLibrary/Medicine/physiology/Skeletal/skeletal.htm)

1.2 CaPs of Biological Interest

Calcium phosphates exhibit a wide range of possible applications, which span from their use as catalysts, as starting materials in the preparation of phosphatic fertilizers, as columns in chromatographic separation, and as stabilizers for plastics, to the biomedical field, where they are applied in the form of nutrient supplements, dentrifice additives, and biomaterials. The inorganic phase deposited in mineralized tissues, such as bone and dentine, is a poor crystalline carbonated apatite characterized by nanometric dimensions of crystals, a low crystallinity and defective stechiometry due to the presence of numerous extrinsic ions [28], which, however, could be just the final phase of a process involving other calcium phosphates as precursor phases. In particular, octacalcium phosphate is thought to be involved in the first stages of mineralization of bone and tooth tissues, on the basis of its similarity with hydroxyapatite structure, its significantly higher solubility, as well as its reported involvement in the formation of several calcified tissues. The interest towards the chemical nature of the possible products of α -tricalcium phosphate hydrolysis justifies its increasing employment in calcium phosphate bioactive bone cements.

As already discussed, calcium phosphates in general form the mineral component of bones and teeth, occur in pathological calcification, and provide bones, teeth and tendons their hardness and stability. Furthermore they are widely distributed minerals [29, 30].

A number of features make calcium phosphates ideal biomaterials including the ability to form strong interfacial bonds with bone tissue without fibrous encapsulation; facilitate the growth of bone tissue so as to achieve early mechanical bone fixation; and act as scaffolds on which bone-forming cells (osteoblasts) can attach, grow, divide and form new bone [31].

Accordingly, apatites and other calcium phosphates are increasingly used as biocompatible and bioactive materials in orthopaedic and dental applications.

During the last forty years, important progress has been made in the understanding of the structure and chemistry of the apatites and related calcium phosphates. Although the basic apatite structure had been determined in 1930, at the beginning of this period substantial aspects of the structures of the other calcium orthophosphates were unclear. The existence of one of them, octacalcium phosphate, had not been universally accepted and little was known about the amorphous calcium phosphate. As regards the apatites,

there were still disputes about the location of carbonate in biological and many mineral apatites. Another matter of investigation was that apatites could be precipitates from solutions with Ca/P molar ratios from the stoichiometric value of 1.67 to about 1.5, without any apparent changes in the X-ray diffraction powder pattern.

The calcium orthophosphates are salts of the tribasic phosphoric acid, H_3PO_4 , and thus can form compounds that contain H_2PO_4^- , HPO_4^{2-} , PO_4^{3-} ions (their list is reported in *Table 1*). Those with H_2PO_4^- ions only form under rather acidic conditions, therefore are not normally found in biological systems. However, both HPO_4^{2-} and PO_4^{3-} ions occur in the mineral of bones and teeth and in various pathological calcifications. Some calcium phosphates are hydrated, and those that belong to the basic apatitic calcium phosphate family contain OH^- ions.

The calcium phosphates are all white solids, unless doped with a coloured ion. Most are sparingly soluble in water and some are very insoluble, but all dissolve in acids.

The crystallization of complex and lightly soluble apatitic structures evolves through the formation of intermediate products which are thermodynamically metastable but cinetically favourite.

In vitro, amorphous calcium phosphate converts into octacalcium phosphate (OCP) which on its turn converts into carbonate hydroxyapatite; at lower pH values the intermediate phase seems to be dicalcium phosphate dehydrate (DCPD).

Calcium phosphates with their relative abbreviation, formula and Ca/P ratio can be found in *Table 1*.

1.2.1 Hydroxyapatite

Hydroxyapatite [HA, chemical formula $\text{Ca}_{10}(\text{PO}_4)_6(\text{OH})_2$] is widely studied as an artificial bone and teeth replacement material in dental and orthopaedic implants, as coating of hard tissue implants, bone fillers, and for drug delivery, due to its chemical and crystallographic resemblance to bone and tooth minerals. HA is known to have an appropriate biological activity when implanted in living organisms and this property has attracted growing interest in the last decades. The goal of the biomaterials synthesis and processing nowadays is to mimic the way materials have been created in nature.

Organisms in nature create perfect fine mineralized structures with diverse biological functions and very often from simple salt solutions through interactions between inorganic and organic substances. Stimulated by fascinating natural examples, such as

bones, teeth, cartilage, shells and corals, attempts are being made to develop synthetic, biomimetic nanocomposites by simulating the basic principles of biomineralization [32].

HA is well suited for its use as a bioactive coating for medical and dental implants. HA coatings have been proven to promote rapid osseointegration which results in earlier and superior implant stabilization. The degree of integration between bone and implant material results from the material's ability to mimic the natural properties of bone such as chemical composition, surface and mechanical properties, as well as grain size structure.

Table 1 - Calcium orthophosphates.

COMPOUND	ABBREVIATION	FORMULA	Ca/P
Dihydrogen calcium phosphate monohydrate	MCPM	$\text{Ca}(\text{H}_2\text{PO}_4)_2 \cdot \text{H}_2\text{O}$	0.5
Dihydrogen anhydrous calcium phosphate	MCPA	$\text{Ca}(\text{H}_2\text{PO}_4)_2$	0.5
Dihydrate calcium hydrogen phosphate	DCPD	$\text{CaHPO}_4 \cdot 2\text{H}_2\text{O}$	1.0
Anhydrous calcium hydrogen phosphate	DCP	CaHPO_4	1.0
Octacalcium phosphate	OCP	$\text{Ca}_8\text{H}_2(\text{PO}_4)_6 \cdot 5\text{H}_2\text{O}$	1.33
α -Tricalcium phosphate	α -TCP	$\alpha\text{-Ca}_3(\text{PO}_4)_2$	1.5
β -Tricalcium phosphate	β -TCP	$\beta\text{-Ca}_3(\text{PO}_4)_2$	1.5
Hydroxyapatite	HA	$\text{Ca}_{10}(\text{PO}_4)_6\text{OH}_2$	1.67
Tetracalciumphosphate	TTCP	$\text{Ca}_4(\text{PO}_4)_2^\circ$	2.0
Amorphous calcium phosphate	ACP	—	—

The plate-like HA crystals that make up the inorganic phase of bone are 20 to 80 nm long and 2 to 5 nm thick and can be categorized as a nanophase material because they

have grain sizes less than 100 nm in at least one direction. Studies have shown that ceramic biomaterials, including HA, with a nanophase crystalline structure more readily promote cellular activity related to bone growth than ceramic biomaterials with conventional crystal structures.

The crystallinity of an hydroxyapatite coating, which is typically dependent on the processing method and whether the coating is subject to a heat treatment, determines the dissolution rate of the coating in vivo. Poor crystalline HA is readily dissolved in the body and promotes cell growth while crystalline HA dissolves slower or not at all, thus allowing more time for bone formation and bone ingrowth [33].

Apatites, in general, have the formula $\text{Ca}_5(\text{PO}_4)_3\text{X}$, where X can be an OH^- ion (hydroxyapatite), a F^- ion (fluoroapatite) or a Cl^- ion (chlorapatite), for example. The apatite structure is very tolerant for ionic substitutions, so Ca^{2+} ions can be partly or completely replaced by Ba^{2+} , Sr^{2+} or Pb^{2+} ions and PO_4^{3-} by AsO_4^{3-} ions. Thus, there are lead minerals with apatitic structure such as $\text{Pb}_5(\text{PO}_4)_3\text{Cl}$ (pyromorphite), $\text{Pb}_5(\text{VO}_4)_3\text{Cl}$ (vanadite) and $\text{Pb}_5(\text{AsO}_4)_3\text{Cl}$ (mimetite). Coupled substitutions frequently occur in apatites, where one ion is replaced by another of the same sign, but different charge, and neutrality is maintained by substitutions of ions with dissimilar charge or vacancies elsewhere.

The carbonate apatites have been the subject of many studies. These include the minerals francolite, dahllite and the rock-phosphates, and the biological apatites. Nonstoichiometry, with vacant lattice sites, occurs in biological apatites and frequently in synthetic ones, which considerably complicates their crystal chemistry.

Pure HA crystallizes in the monoclinic space group $\text{P}2_1/\text{b}$. However, the presence of impurities stabilizes the hexagonal structure at room temperature. The basic apatite hexagonal structure, space group $\text{P}6_3/\text{m}$, exhibits approximate lattice parameters $\underline{a} = 9.43 \text{ \AA}$ and $\underline{c} = 6.88 \text{ \AA}$ with two formula units per cell. This is the reason why a double formula is often used $[\text{Ca}_{10}(\text{PO}_4)_6\text{X}_2]$. The values often depend on the mode of preparation because of the frequent nonstoichiometry.

The $\text{P}6_3/\text{m}$ space group has three kinds of vertical symmetry elements (*Figure 6*): (1) six-fold screw axes passing through the corners of the unit cells marked by dashed lines in the figure. These symmetry elements are equivalent to a three-fold rotation axis with a superimposed two-fold screw axes; (2) three-fold rotation axes passing through $2/3, 1/3, 0$ and $1/3, 2/3, 0$; and (3) two fold screw axes passing through the mid points of the cell

edges and its centre. There are also mirror planes perpendicular to the c -axis at $z = \frac{1}{4}$ and $\frac{3}{4}$, and numerous centres of symmetry.

There are columns of Ca^{2+} ions spaced by one-half of the c -axis parameter along the three-fold axes at $\frac{2}{3}, \frac{1}{3}, 0$ and $\frac{1}{3}, \frac{2}{3}, 0$ which account for two-fifths of the Ca^{2+} ions in the structure. These ions are given the designation Ca(1) or Ca(I) or Ca_1 .

The site they occupy is often called *columnar site*. Each of these Ca^{2+} ions is connected to its neighbouring Ca^{2+} ions above and below by three shared oxygen atoms that lie in the mirror plane (*Figure 6*). On one side, there are three O(1) atoms at 2.397(1) Å, and on the other side three O(2) atoms at 2.453(1) Å. Each Ca(1) ion is also coordinated by three further oxygen atoms, O(3), at a greater distance (2.801 (1) Å) at approximately the same z parameter as the Ca^{2+} ion. Thus the columnar Ca^{2+} ions are nine-fold coordinated by oxygen atoms. These columns of Ca^{2+} ions and their coordinated oxygen atoms are linked together by PO_4 tetrahedra in which three oxygen atoms come from one column, and the fourth from the adjacent column.

The result is a three-dimensional network of PO_4 tetrahedra with enmeshed columnar Ca^{2+} ions and with channels passing through it.

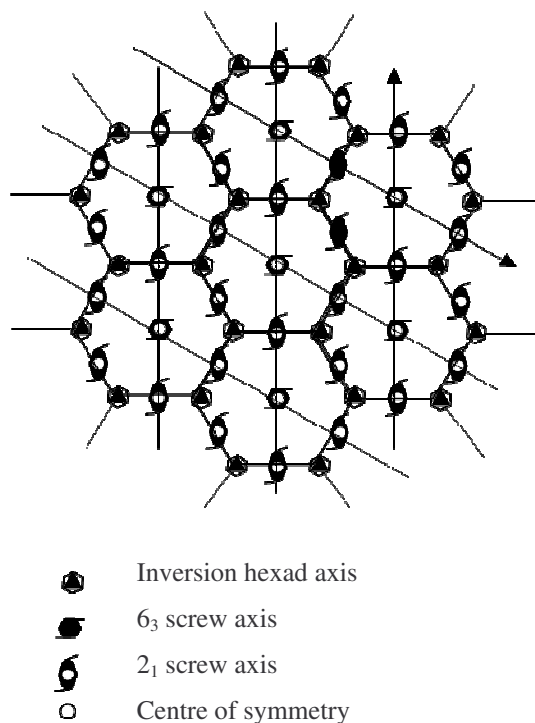


Fig. 6 – Vertical symmetry elements of the space group $P6_3/m$. The dashed lines indicate the apatite unit cells with the c – axis out of the diagram. There are also horizontal mirror planes at $z = \frac{1}{4}$ and $\frac{3}{4}$ and numerous centers of symmetry.

The axes of these channels coincide with the six-fold screw axes and the corners of the unit cells, and one forms the c -axis.

The remaining ions, OH^- and their adjacent $\text{Ca}(2)$ ions that are required to complete the structure are located in the channels. These channels have six cavities per c -axis repeat of the unit cell, centred on the mirror planes at $z = 1/4$ and $3/4$, into which $\text{Ca}(2)$ ions can fit. These ions form two triangles of Ca^{2+} ions rotated by 60° from each other about the c -axis (*Figure 7*) at whose centres the OH^- are located. Thus the OH^- ions are three-fold coordinated by Ca^{2+} ions, with all four ions lying on a mirror plane. The $\text{Ca}(2)$ ions occupy the so-called triangular site.

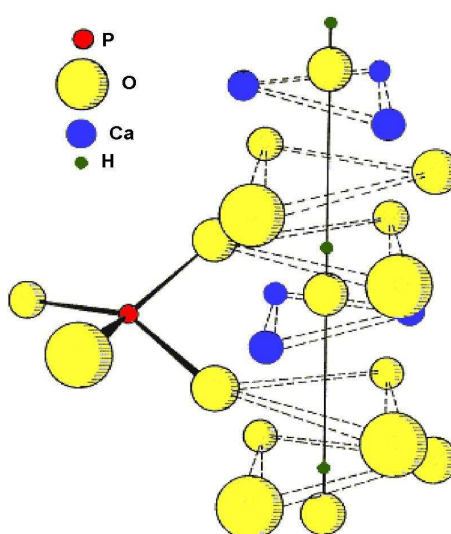


Fig. 7 - Parallel canals to c -axis constituted of Ca^{2+} (2) ions that occupy equilateral triangles' vertexes (in blue) and inside this triangles OH^- ions take place.

1.2.2 Octacalcium Phosphate

OCP has been supposed to be a precursor of biological apatite. Generally, OCP is observed in pathological biomineralization such as dental calculus [34]. In addition to this roles in the formation kinetics and composition of apatites, OCP has been found as a constituent in dental calculus and other pathological calcifications [35]. Furthermore, it has been reported in X-ray powder diffraction of bone from the distal metaphysis of rabbit [36] and it was found in a crystal of calcifying dentine together with apatite [37].

By X-ray diffraction it is possible to follow new bone formation. The implanted OCP has been shown to convert to the apatitic phase, through hydrolysis of the OCP to apatitic crystal and/or re-mineralization of the OCP after dissolution [38].

So, understanding the growth of OCP and its hydrolysis to HA is important in order to understand the processes of mineralization in human tissues. The close structural relationship between OCP and HA can explain the incorporation via hydrolysis of impurities (especially Mg^{2+} and CO_3^{2-}) and so the frequent non-stoichiometry of precipitated apatites.

Octacalcium phosphate [OCP, $\text{Ca}_8\text{H}_2(\text{PO}_4)_6 \cdot 5\text{H}_2\text{O}$] is also referred to as octacalcium bis(hydrogenphosphate) tetrakis(phosphate) pentahydrate or tetracalcium hydrogen triphosphate trihydrate.

A calcium phosphate with the composition of OCP was first described in 1836 [39], but its existence was not universally accepted until the middle of 20th century, and its importance unrecognized until the early 1960s.

OCP crystallizes in a triclinic structure [40, 41], space group $\text{P}\bar{1}$ and unit cell $a = 19.692(4) \text{ \AA}$, $b = 9.523(2) \text{ \AA}$, $c = 6.835(2) \text{ \AA}$, $\alpha = 90.15(2)^\circ$, $\beta = 92.54(2)^\circ$ and $\gamma = 108.65(1)^\circ$. The asymmetric unit is $\text{Ca}_8\text{H}_2(\text{PO}_4)_6 \cdot 5\text{H}_2\text{O}$ with two units per unit cell.

OCP crystals are {100} blades of triclinic pinacoidal symmetry, elongated along the c -axis. It is a layered structure parallel to (100) where *apatitic layers* about 1.1 nm thick alternate with a *hydrated layers* about 0.8 nm thick (*Figure 8*).

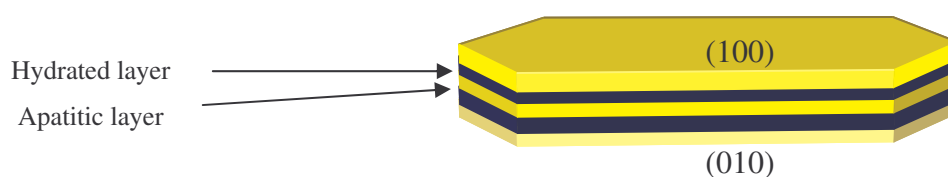


Fig. 8 - Layered structure of Octacalcium phosphate.

The presence of the *apatitic layer* explains the similarity of lattice parameters with those of HA ($a = 9.4176 \text{ \AA}$ and $c = 6.8814 \text{ \AA}$), since that layer consist of phosphate ions interdispersed with Ca^{2+} ions resembling the ions positions in the structure of apatite

The *hydrated layer* consists of more widely spaced phosphate and calcium ions with a slightly variable number of water molecules between them. Six of the Ca^{2+} ions and two

of the phosphate ion are in the *apatitic layer*, the other two Ca^{2+} ions and one phosphate ion are in the *hydrated layer* and the remaining three phosphate ions lie at the junction of the *apatitic* and *hydrated layers*. The phosphate ion in the *hydrated layer* and one at the junction between the layers are protonated (*Figure 9*).

1.2.3 α -TriCalcium Phosphate

Increasing attention has been paid in recent years to alpha-tricalcium phosphate [α -TCP, $\alpha\text{-Ca}_3(\text{PO}_4)_2$], which is used as the main constituent of calcium phosphate bioactive bone cements and biphasic calcium phosphate ceramics. Its hydrolysis and conversion into apatite phase may play an important role in new bone formation in vivo. These bone cements can be easily moulded during operation and simply implanted or injected into the bone defects, and will turn into apatite after setting and hardening. Bonding with bone will finally be realized through the converted apatite phase. This distinguishing feature of the bone cements can be attributed to the hydrolysis of α -TCP to a large extent [14].

The adjective *anhydrous* is used to distinguish it from hydrated apatitic precipitates that have similar Ca/P molar ratio of 1.5. It was first reported in 1932 [42].

α -TCP is highly reactive in aqueous systems and can be easily hydrolyzed to a mixture of other calcium phosphates. α -TCP crystallizes in a monoclinic structure, space group $\text{P}2_1/\text{a}$ and unit cell $a = 12.887(2) \text{ \AA}$, $b = 27.280(4) \text{ \AA}$, $c = 15.219(2) \text{ \AA}$ and $\beta = 126.20(1)^\circ$, with 24 formula units per unit cell [43]. There is an approximate subcell with a \underline{b} -axis parameter of $\underline{b}/3$ (9.09 \AA) that contains 8 formula units, which corresponds to the unit cell reported earlier [44].

The structure of α -TCP is constituted of columns of Ca^{2+} and PO_4^{3-} ions which run parallel to the \underline{c} -axis.

The section of the structure of α -TCP that corresponds to a unit cell of apatite is marked with dotted lines in *Figure 10*.

The correspondence can also be seen from a consideration of the dimensions of the unit cell of α -TCP with those of apatite: the α -TCP approximate subcell \underline{b} -axis parameter of 9.09 \AA corresponds to the apatite \underline{a} -axis parameter, whilst half the \underline{c} -axis parameter of α -TCP (7.6 \AA) corresponds to the \underline{c} -axis parameter of apatite. The apatite structure can so be derived from α -TCP by replacing the cation-cation columns at the

corners of the apatite cell by anion columns (OH^- in hydroxyapatite, F^- in fluoroapatite...).

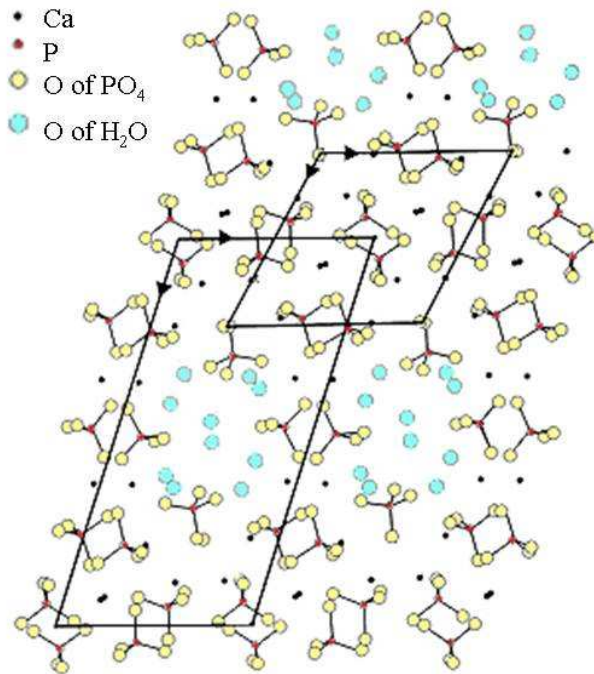


Fig. 9 – Structure of octacalcium phosphate projected onto the (001) plane, showing the relationship with the structure of apatite. The unit cell of OCP (lower left one) and of HA (upper right one) have been drawn. The c – axis is out of the plane of the diagram for OCP and into the plane for HA.

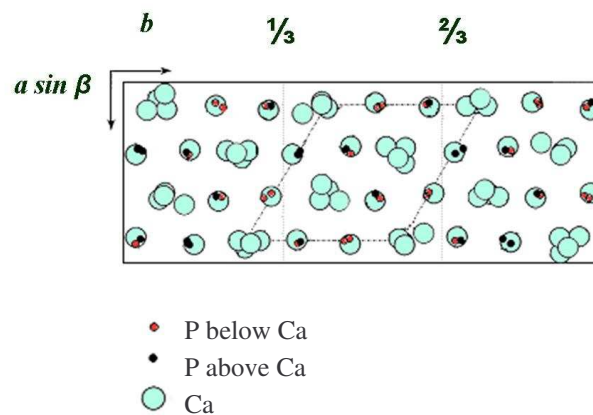


Fig. 10 - Projection of α -TCP structure onto the (001) plane. The dotted lines outline the apatite unit cell

The remaining cation columns in α -TCP become the columnar Ca(1) ions in apatite, whilst the PO_4^{3-} and Ca^{2+} ions that form the cation-anion columns in α -TCP have very approximately the same position as the PO_4^{3-} and Ca(2) ions in apatite.

1.2.4 DiCalcium Phosphate Dihydrate

Dicalcium phosphate dihydrate [DCPD, $\text{CaHPO}_4 \cdot 2\text{H}_2\text{O}$] is also referred to as calcium monohydrogen phosphate dehydrate or dibasic calcium phosphate dihydrate or calcium hydrogen orthophosphate 2-hydrate.

Its mineral (brushite) was discovered in 1865 and named by the mineralogist G.J. Brush [45]. Brushite occurs as a component of rock-phosphate deposits and in dental calculus [35] and other pathological calcifications [46]. DCPD can occur as an intermediate in the apatitic mineralization and dissolution processes [47, 48]. It can be easily crystallized from aqueous solutions. At temperatures above 80°C , it transforms into the anhydrous form DCPA.

The first structure proposed for DCPD consisted in a centrosymmetric space group [49], but this was inconsistent with the subsequent finding of piezoelectricity characteristics, which means a non-centrosymmetric structure. The absence of a centre of symmetry has been confirmed later [50] by refining the first measurements. DCPD crystallizes in a monoclinic structure, space group Ia and unit cell $a = 5.812(2) \text{ \AA}$, $b = 15.180(3) \text{ \AA}$, $c = 6.239(2) \text{ \AA}$, and $\beta = 116.25(2)^\circ$.

The asymmetric unit is $\text{CaHPO}_4 \cdot 2\text{H}_2\text{O}$ with four formula units per unit cell.

The structure contains columns of alternating Ca^{2+} and HPO_4^{2-} ions, which run parallel to the short diagonal of the (010) face of the unit cell.

A striking feature of this structure is that these columns are joint together to form corrugates sheets (*Figure 11*). The sheets, that result to have a composition of CaHPO_4 , are normal to the \underline{b} -axis and are linked together by water molecules.

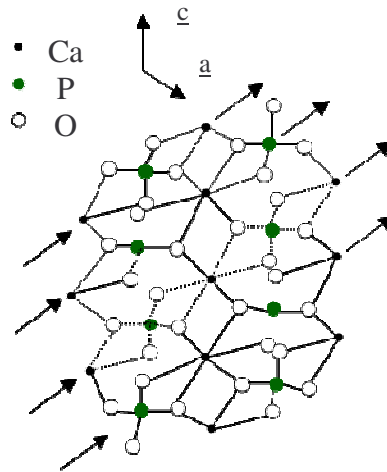


Fig. 11 – Structure of one of the corrugated sheets that characterize DCPD. The \underline{b} – axis is into the plane. The arrows indicate the directions of four CaHPO_4 chains (the bonds in the 3rd one are dotted for emphasis).

1.3 CaPs for Hard Tissue Repair

Reconstruction of large bone defects that are resulting from trauma, neoplasms, or infection is a substantial biomedical burden in oral and maxillofacial surgery. Autogeneous bone grafting is commonly used to repair the critical sized bone defect, whereas it has disadvantages of limited availability and morbidity that is associated with harvesting bone from a second operative site. In the case of allograft, it has the potential for adverse immunological reaction and/or disease transmission. Therefore, it has been expected to develop synthetic biomaterials that overcame the disadvantages of autogeneous and allogeneous bone grafting.

Today, it has been accepted that main components for bone regeneration are stem cells or osteoprogenitors, an appropriate biological scaffold, and cytokines. Newly developed synthetic biomaterial should be a substitute for extracellular matrix, which could be resorbed and replaced by the host tissue, activates osteoprogenitors, and sustain and deliver cytokines appropriately.

Calcium phosphates, in the form of powders, dense and porous ceramics, composites and cements, attract great interest as biomaterials because of their good biocompatibility

and bioactivity, which make these compounds particularly suitable for hard tissue replacement.

There is, in fact, a necessity for replacing bone substance which has been lost due to traumatic or non-traumatic events. The lost bone can be replaced by endogenous or exogenous bone tissues, which is connected with several problems. The use of endogenous bone substance involves additional surgery: moreover, the endogenous bone is available only in limited quantities. The major disadvantage of exogenous bone implants is that they may be rejected by the human body, diseases may be transmitted together with the implant, also the clinical performance of exogenous bone is considerably inferior to fresh endogenous graft material. For these reasons, there is a growing need for fabrication of artificial hard tissue replacement implants. The biomaterials industry worldwide has an annual turnover of 2.3 billion of dollars in the field of hard tissue repair and replacement. There is currently a projected growth rate of 7-12% per annum for biomaterials in clinical applications. Although the biomaterials sector is expanding, it is expected that the volume of materials required will never exceed tens of tons, as compared with thousands of tons for other developing engineering markets. Reconstructive orthopaedic surgery methods involving autogenous and allogeneous bone grafting are currently used to treat large bone defects. Due to their serious limitations, severe clinical problems have arisen and new approaches for bone tissue repair are essential. The main advantage of using bone allografts or autografts is their osteoconduction. However, allografts can lead to an immune response, which requires long-term medication. Another major problem is the risk of transferring diseases (e.g. AIDS or hepatitis). Currently, autografts are better alternatives for repairing bone defects caused by tumours and serious trauma. However, the use of these substitutes is also restrictive. In the autograft procedure not only is the operation time increased, but morbidity at the donor site is more frequent, which poses a high risk to the patient's health. Therefore, synthetic calcium phosphate ceramics are becoming more widely used as bone substitutes in orthopaedic and oral surgery. Synthetic bone substitutes can solve certain problems associated with bone transplantation. An ideal synthetic material should provide a framework for continuous bone resorption and bone deposition [51].

The surface properties of calcium phosphate constituted biomaterials, such as hydroxyapatite (HA), fundamentally govern their overall interface function, which includes biological processes such as adsorption of biomolecules, apatite crystal

dissolution, nucleation and growth, thereby modulating the biomineralization process. The prototype for minerals in bones and teeth is usually considered to be basic calcium phosphate HA, with impurities such as carbonate and acid phosphate. Biological apatites display better crystallinity and a higher Ca/P molar ratio with mineral development. Several precursor phases have been proposed to explain the non-stoichiometric composition of biominerals. These precursors are dicalcium phosphate dihydrate (DCPD), octacalcium phosphate (OCP) and amorphous calcium phosphate (ACP). OCP was first proposed by Brown et al. [41] to participate as the initial mineral crystals in bones and teeth that subsequently hydrolyze into HA. Debates continue relating to the chemical nature of the first mineral crystals formed in biomineralization. Based on in vitro crystal growth studies that ACP and DCPD can be hydrolyzed to HA via OCP, OCP has been suggested as the direct precursor to HA. Several lines of evidence support the involvement of OCP as the initial crystal formation in dentin, enamel and bone minerals. Previous studies showed that implantation of OCP enhanced bone formation accompanied by in situ conversion of the OCP into an apatite structure [52].

1.3.1 Modified CaPs

Apatites are a family of inorganic crystalline compounds, of general formula $M_{10}(XO_4)_6Y_2$. M is usually a bivalent cation, such as Ca^{2+} , Sr^{2+} , Ba^{2+} , Cd^{2+} , Pb^{2+} , but monovalent and trivalent cations, such as Na^+ , K^+ and Al^{3+} , can be hosted as well; XO_4 is usually PO_4^{3-} ; VO_4^{3-} or AsO_4^{3-} , but the possible substitutions also include SiO_4^{4-} ; CO_3^{2-} and SO_4^{2-} ; Y is a monovalent anion, OH^- , F^- , Cl^- , Br^- . Apatites are widely spread in nature; in particular, the inorganic phase of the hard tissues of vertebrates is assimilated to the synthetic hydroxyapatite $Ca_{10}(PO_4)_6(OH)_2$, CaHA. The similarity with biological apatites accounts for the high biocompatibility of synthetic CaHA, which displays many other properties and exhibits a wide range of potential practical applications as a bioceramic, catalyst, liquid-chromatographic column, lighting material, chemical sensor. The size and morphology of the individual particles, as well as the kind and extent of isomorphous substitutions greatly affect many of the physico-chemical properties of the apatites.

The great variety of possible cationic and anionic substitutions is justified by the high stability and flexibility of the apatite structure

1.3.1.1 Strontium

Among the bivalent cations that can replace calcium in CaHA, strontium has attracted a remarkable interest for its possible biological role.

Strontium is one of the alkaline earth metals. It never occurs free in nature, because metallic Sr oxidises easily forming strontium oxide, which has a yellowish colour. Strontium is well known from the minerals celestite (SrSO_4) and strontianite (SrCO_3). Natural Sr is a mixture of four stable isotopes: ^{84}Sr (0.56%), ^{86}Sr (9.86%), ^{87}Sr (7.02%), and ^{88}Sr (82.56%). The elements of group 2 of the periodic system, to which Sr belongs along with Ca and Mg, form divalent cations in biological fluids, and have varying degrees of protein binding in biological fluids like serum or plasma.

Radioactive Sr isotopes are dealt with only when they are used for physiological or diagnostic purposes. Some of the Sr radioisotopes can be used in medicine. They have been used as excellent tools for kinetic studies, substituting for Ca in kinetic investigations because the two metals behave very much alike in the human body, both having strong bone-seeking properties.

However, biological differences between the two elements exist, explicable in part by the larger size of the Sr molecule.

Toxic symptoms due to overdosing of Sr have not been reported in man. However, intravenous administration of high doses of Sr induces hypocalcaemia due to increased renal excretion of Ca.

The only stable Sr-containing chemical that is considered to be harmful to humans in small amounts is strontium chromate, the toxicity being caused by the chromium which is a genotoxic carcinogen.

The amount of Sr in the skeleton is only 0.035 of its Ca content. Radiostrontium is cleared from the blood almost immediately after injection [53].

It is present in the mineral phase of the bone, especially at the regions of high metabolic turn-over, and its beneficial effect in the treatment of osteoporosis is well known. In vitro, strontium increases the number of osteoblasts and decreases the number and the activity of osteoclasts, whereas strontium administration reduces bone resorption and stimulates bone formation. Strontium can replace calcium in the HA

structure in the whole range of composition. The solid solutions, which have been obtained by hydrothermal methods or by treatment at high temperatures, display a linear variation in the lattice parameters with composition, whereas different data are reported on the preferential substitution site of Sr for Ca in CaHA. A better understanding of the interaction of Sr with hydroxyapatite structure could provide useful information also for clarifying the biological role of Sr in the process of biomineralization of bone and related pathologies [54] even though the role of strontium in human pathology had attracted less attention than the other two important divalent metals, calcium and magnesium. However, there has been an increasing awareness of the biological role of strontium since the development of the drug strontium ranelate, which has recently been shown to reduce incidence of fractures in osteoporotic patients. In fact, strontium is a trace element that is found in calcareous rocks and ocean water; it is also a natural component of food and beverages but there is growing evidence that strontium has a beneficial effect on bone because of its ability to enhance bone volume and prevent bone loss. In line with its chemical analogy to calcium, strontium is a one seeking element and 98% of the total body Sr content can be found in the skeleton. Sr has become increasingly popular in the prevention and treatment of osteoporosis as a ranelate compound. Sr has been associated with improving postmenopausal osteoporosis by reducing bone resorption and increasing bone formation with an eventual effect of decreasing the risk of fractures. The currently available data indicate that strontium administration at low dose reduces bone resorption and increases bone formation, resulting in increased bone mass in normal ovariectomized animals. In vitro studies revealed that strontium ranelate (SR) has an anabolic and antiresorptive activity which leads to an increase in both the collagen and non-collagen protein synthesis, an enhancement in pre-osteoblast differentiation, an inhibition in osteoclast differentiation, and a reduction in osteoclast function [55, 56].

1.3.1.2 Magnesium

Another interesting ion from a biological point of view is magnesium. Magnesium deficiency in humans was first described in the medical literature in 1934. The adult human daily nutritional requirement, which is affected by various factors including gender, weight and size, is 300-400 mg/day. Inadequate magnesium intake frequently

causes muscle spasms, and has been associated with cardiovascular disease, diabetes, high blood pressure, anxiety disorders, migraines, osteoporosis and cerebral infarction. Acute deficiency (see hypomagnesemia) is rare, and is more common as a drug side effect (such as chronic alcohol or diuretic use) than from low food intake per se, but it can also occur within people fed intravenously for extended periods of time. The incidence of chronic deficiency resulting in less than optimal health is debated. A balance of magnesium is vital to the well being of all organisms. Magnesium is a relatively abundant ion in the lithosphere and is highly bioavailable in the hydrosphere. This ready availability, in combination with a useful and very unusual chemistry, may have led to its usefulness in evolution as an ion for signalling enzyme activation and catalysis. However, the unusual nature of ionic magnesium has also led to a major challenge in the use of the ion in biological systems. Biological membranes are impermeable to Mg^{2+} (and other ions) so transport proteins must facilitate the flow of Mg^{2+} , both into and out of cells and intracellular compartments [57]. Magnesium ions appreciably retard the rate of OCP growth, probably by adsorption at active growth site and this property could be useful to obtain better and better biomaterials [58].

1.3.1.3 Manganese

The insufficiency of manganese in human body is a probable cause of osteoporosis. Its induced lack in animals retards bone growth and provokes skeletal deformities. In fact, manganese is an essential trace nutrient in all forms of life. The classes of enzymes that have manganese cofactors are very broad and include oxidoreductases, transferases, hydrolases, lyases, isomerases, ligases, lectins, and integrins. The reverse transcriptases of many retroviruses (though not lentiviruses such as HIV) contain manganese. The best known manganese-containing polypeptides may be arginase, the diphtheria toxin, and Mn-containing superoxide dismutase (Mn-SOD). The human body contains about 10 mg of manganese, which is stored mainly in the liver and kidneys. 70% of Manganese present in the human organism is contained in the skeletal structure. It is essential for bone and teeth enamel growth. It has also a very important role in the glycolysis process. Although the biological effects of manganese deficiency are well established in several animal species, no role in human nutrition has yet been described. Animals rendered manganese deficient show retardation of growth, skeletal and muscular

abnormalities, and neurological signs. The human requirement for manganese is very low and even during prolonged therapies no clear evidence of deficiency has emerged. However, because of the potential importance of manganese, additives containing the element have been included in therapy regimens. Earlier, some trace element additives contained too much manganese leading to brain abnormalities shown on magnetic resonance imaging and, in a few cases, Parkinson's Disease-like symptoms. Current additives contain less manganese but children with liver problems can still accumulate this element. For whole blood where the normal concentrations are about ten-fold higher than in serum, the manganese from contamination is proportionally less significant and so no special precautions are necessary in sampling. Manganese toxicity is a known problem in metal refining and manganese ore production. Respiratory illness and eventually neurological effects are seen after years of heavy exposure. No guidelines for biological monitoring are available. It was shown that the presence of small amounts of Mn^{2+} in the apatitic structure leads to better osteoconductive properties of metallic prosthesis coatings [59]. This ion is able to activate a receptors family, the integrins, that control the interactions between the cellular surface and the extracellular matrix [60, 61].

1.3.1.4 Bisphosphonates

Bisphosphonates (BPs) were introduced in the 1970s for the management of disorders of bone metabolism, associated to bone loss. In particular, they are widely used for the treatment of tumor-induced hypercalcemia, Paget's disease and osteoporosis [61 - 63].

These chemical compounds are synthetic analogues of pyrophosphate in which the P-O-P group is replaced by the P-C-P bridge. Individual BPs are characterized by the two covalently bonded side-chains attached to the central carbon atom, termed R1 and R2, which determine the efficiency of the compound. Binding to bone is enhanced when R1 is a hydroxyl group, whereas the R2 side group has some effect on binding but predominantly it determines the antiresorptive potency of the bisphosphonates [61, 64 - 66].

The presence of nitrogen groups within the R2 side group is associated with the ability of an individual BP to inhibit farnesyl pyrophosphate (FPP) synthase, a major enzyme in the mevalonate pathway. This results in the disruption of many of the activities of the

osteoclasts, including migration, attachment, and resorption. Ultimately, cell death can occur via apoptosis [67].

Prolonged use of bisphosphonates, especially through intravenous preparations, has been recently associated to over suppression of bone metabolism and to possible osteonecrosis of the jaws [65]. Local administration might be helpful against the potential negative effects of their prolonged use. However, the great affinity of BPs for calcium hinders the direct synthesis of hybrid calcium phosphate crystals, as shown by the sudden precipitation of amorphous calcium alendronate that occurs when alendronate is introduced in the synthesis medium of hydroxyapatite [68].

Composite HA nanocrystals at different alendronate content, up to 7.1 %wt, were synthesized in aqueous solution thanks to a strategy based on a slight modification of a classical method of synthesis of HA [69]. The results of the structural refinements carried out on the composite nanocrystals were interpreted as suggesting that alendronate interacts with calcium ions through a bidentate chelation of deprotonated oxygen atoms of the bisphosphonate anion without greatly affecting the crystal structure of HA [70]. *In-vitro* tests demonstrated that alendronate is able to promote osteoblast activation and extra-cellular matrix mineralization processes, and to inhibit osteoclast proliferation even if incorporated in the composite nanocrystals [71].

1.3.2 Coatings

Several non-metallic materials have been proposed as candidates for artificial bones and/or teeth, but none has found wide applications.

Clinical success of the implant requires the simultaneous achievement of a stable interface with connective tissue and a match of a mechanical behaviour of the implant with the tissue to be replaced.

Moreover, the material biocompatibility is very important in medical applications and therefore the interactions of the cells with the materials have been intensively investigated. Cells are highly sensitive to topography, roughness, chemistry, surface charge, and hardness. Cell–material interactions *in vitro* may be approximated by the process of cell adhesion and spreading, which is a convenient way to determine the biocompatibility of a material [32].

Pure etched titanium is already widely used in the orthopaedic field (*Figure 12*) on the basis of its innocuousness, resistance to corrosion, very low allergic problems and

satisfying biocompatibility. Moreover, it provides and grants stable chemistry performances.

However, metallic implants, such as those necessary in total hip-joint replacements and artificial tooth sockets, meet mechanical stability requirements, but do not form mechanically stable bonds to bone tissue. The high incidence of bone implant failures is mainly blamed on incomplete osteointegration and stress shielding due to significant differences in mechanical properties between the implant and surrounding bone [70, 71].

Improved implant fixation to hard tissues can be achieved by coating the metallic surface with a thin film of calcium phosphates. The deposition of calcium phosphates films on medical implants enable to combine the high mechanical strength of metallic implant with excellent bioactivity of the calcium phosphates surface layers.

Therefore it is important to develop calcium phosphate coatings characterised by the proper chemical composition and physical characteristics [72 - 74].



Fig. 12 - Examples of titanium bone prostheses.

(www.colognesurgicale.com)

1.3.2.1 Pulsed Laser Deposition

Coatings can be deposited by several physical and chemical methods, including plasma spray, pulsed laser deposition, sputtering, electrodeposition, anodic deposition and anodic spark deposition, sol-gel dipping and biomimetic deposition [75 - 90].

Among these numerous techniques, pulsed laser deposition is commonly used to produce calcium phosphate coatings. This method is characterized by high deposition rate as well as possibility of precise controlling of thickness and composition of a

growing layer. The physical and chemical properties of deposited layers can be controlled by changing conditions of PLD process. The basic parameters of the above method are pressure of ambient gas, laser fluence, substrate temperature, wavelength and repetition of laser pulses [81].

PLD allow to produce coated metallic prosthetic devices which bond strongly to the bone material that surrounds the bone intended to be replaced by the device by encouraging bone ingrowth into the coating, while retaining immunity from delamination and separation of the coating from the metal. PLD, so, gives ideal coatings with an intermediate metal–ceramic region with a compositionally gradient interface which reduce interfacial problems and enhance in vivo lifetime [77 - 87].

PLD has proved to be a successful technique for growing thin calcium phosphate structures on metallic substrates. PLD uses short, mostly UV, pulsed laser beams to expel the species and then focus them onto a target that rotates under a controlled atmosphere in a reaction chamber. The stoichiometry and crystallinity of the deposited material that forms the coating can be selected by a proper choice of the ablation and deposition parameters [88 – 91].

In PLD (*Figure 13*), a pulsed laser beam strikes the surface of the source material, also called the target, and the energy from the laser evaporates the target's surface.

In most materials, the ultraviolet radiation is absorbed by only the outermost layers of the target to a depth of about 1 Å. The extremely short laser pulses, each lasting less than 50 ns, cause the temperature of the surface to rise rapidly to thousands of degrees Celsius, but the bottom of the target remains virtually unheated, close to room temperature. Such non-equilibrium heating produces a flash of evaporants that deposit on the substrate, producing a film with composition identical to that of the target surface. Several aspects make PLD a great technique. It produces a highly forward-directed and confined plume of materials, which can be deposited with less contamination than the unconfined plasma in a sputter process. In addition, PLD is incredibly precise.

PLD does not require any monitoring, because the composition of the film replicates the composition of the target. With PLD, the background gas pressure does not affect the passage or absorption of the laser, and the same system can be used to fabricate thin films composed of many materials by simply changing the background gas pressure.

Making multilayer materials can also be done rather easily with PLD, because different targets can be positioned under the laser beam. This is generally done with a computer-controlled target holder or carousel.

PLD is a good technique for depositing extremely pure films while in most processes the film includes contaminants. For example, thermal and electron-beam evaporation use a container for the source material, and the fairly high temperatures needed to evaporate the source materials can also evaporate parts of the container, thereby contaminating the deposition process.

The variety of coatings that can be deposited provides a range of solubilities with known consequences on the physico-chemical characteristics of the coatings.

The species that were ejected in each laser pulse conformed the coating as they reached the substrate, which can also be heated to a fixed temperature. The X-ray diffractogram of the pure HA coating substantiated its high crystallinity. Its surface had a compact crystalline morphology with droplets [87, 92].

Polymer and organic coatings have a wide range of pharmaceutical, bioengineering, and sensing applications. In fact, thin films of polymers and biomaterials are the basis of the chemoselective or biospecific layers that make possible the operation of most types of chemical and biochemical sensor systems, and gene and protein recognition microarrays.

In the biomedical field, thin films of numerous types of biomaterials are essential in diverse areas such as tissue engineering, spatial patterning of cells, time-release drug delivery systems, antiinflammatory coatings for medical implants and implantable devices, and novel biocompatible adhesives for wound closure, eye repair, and nerve reconstruction.

Attempts to deposit thin films of organic and polymeric materials by pulsed laser deposition (PLD) date back to the first report by Mith and Turner [96] who demonstrated the growth of thin films of fuchsine (an organic dye) and Ni-dimethyl glyoxime (a pigment used in paints and cosmetics).

Despite this early report, little additional work was performed in PLD of organics and polymers for the next 20 years until Hansen and Robitaille demonstrated the use of pulsed ultraviolet (UV) lasers for depositing films of several polymers such as polyethylene, polycarbonate, polyimide, and poly(methylmethacrylate), or PMMA [93].

Their results showed an improvement of the laser ablation behaviour and film morphology with decreasing laser wavelengths. Indications were also observed that the

film quality is enhanced by working at laser energies near the ablation threshold of the polymers. However, they also noted a decrease in the molecular weight of all the films that they prepared. Since then, there has been a large number of reports on the use of PLD for growing thin films of many types of polymeric and organic materials.

Despite the extensive list reported in the literature of polymer and biomaterials deposited by PLD, fundamentally the use of PLD for the deposition of organic and polymeric materials has provided, at best, mixed results.

Despite the large number of variables explored in deposition parameter space by numerous research groups, the quality of the films produced by PLD has only been adequate for a very small number of systems. By using a pulsed UV laser to ablate the various organic and polymeric targets, it is not surprising that the resulting films will tend to show some degree of irreversible decomposition or damage.

In fact, the question from early studies of polymer laser ablation has been whether the ablative decomposition takes place primarily through photochemical or photothermal pathways. Upon absorption of the UV pulse, the organic molecules are excited into high-energy electronic states that might result in direct bond dissociation, that is, photochemical, or instead decay through lattice vibrations with considerable heating of the surrounding molecules, that is, photothermal effects.

Given the fact that in most organic materials the chemical bonds have energies well below the UV photon energies, some degree of photochemistry is expected to occur during the PLD process. However, the decomposition pathways are mainly determined by the chemical structure of the organic molecule itself. As a result, the products of the interaction between the UV photons and the organic or polymeric molecule tend to be extremely difficult to predict and thus control.

Only for a small group of addition polymers such as poly(tetrafluoroethylene) (PTFE) and PMMA, the absorbed UV radiation causes the simple photothermal depolymerization of the starting material into its monomer building blocks, resulting in the reversible unzipping of the polymer chains. Blanchet's work showed that under the appropriate conditions it is possible to deposit high-quality PTFE and poly(vinyl fluoride) (PVF) thin films by PLD [94].

More often than not, however, the interaction of the UV photons with the polymeric or organic molecules causes the loss or decomposition of functional groups, or in the case of condensation polymers the resulting photochemistry is responsible for the substantial modification of the starting material.

Such modifications might be acceptable for some applications, but in general, the use of lasers for depositing thin films of polymeric biomaterials requires more subtle approaches than those offered by PLD alone.

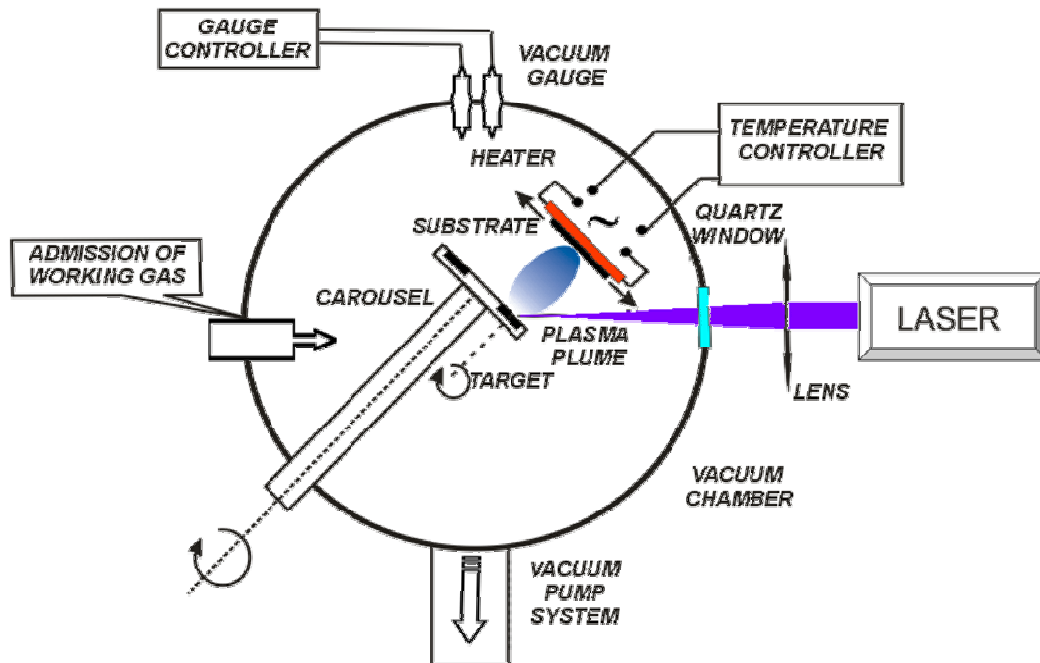


Fig. 13 - PLD apparatus.

1.3.2.2 Matrix Assisted Pulsed Laser Evaporation

Laser processing of polymer and biomaterial thin films using traditional PLD is not a viable option for depositing organic coatings that faithfully replicate the properties and functionality of the starting materials. One approach that has shown great promise is known as matrix-assisted pulsed laser evaporation, or MAPLE.

MAPLE is a recently developed thin film deposition technique, slightly different from PLD, particularly well suited for organic/polymer thin film deposition. In PLD, largely applied for inorganic thin film deposition, a pulsed laser beam is focused onto a solid target whose material is ablated from target and deposited on a nearby substrate. Although some addition polymers were successfully deposited, the PLD of addition polymers seems to proceed via a “depolymerisation-ablation of monomers-

repolymerization” mechanism. This is clearly not possible in general for condensation polymers or other organic molecules.

In MAPLE deposition technique the pulsed laser beam is focused on a target obtained as a frozen solution in a relatively volatile solvent of the molecules to be deposited. The advantage of MAPLE with respect to PLD technique is that a great part of the laser beam energy is transferred to the solvent and molecules to be deposited are ejected from the target mainly due to solvent vaporization. Such technique is therefore especially well suited for deposition of large molecules as in organic or polymeric compounds, whose structure may be damaged by direct laser irradiation (*Figure 14*) [95, 96]. The MAPLE process was developed in the late 1990s at the U.S. Naval Research Laboratory to provide a gentler pulsed laser evaporation process for functionalized polymers [94].

The MAPLE technique has been used successfully for depositing thin and uniform layers of chemoselective polymers, as well as organic compounds such as simple carbohydrates and their polymers [97].

MAPLE is a variation of conventional PLD. It provides, however, a less damaging approach for transferring many different organic and polymeric compounds that include small and large molecular weight species, from the condensed phase into the vapour phase. In MAPLE, a frozen matrix consisting of a solution of a polymeric compound dissolved in a relatively volatile solvent is used as the laser target. The solvent and solution concentration are selected so that the material of interest can dissolve to form a dilute, particulate-free solution and also so that the majority of the laser energy is initially absorbed by the solvent molecules and not by the solute molecules but is also very useful if the sample is suspended into the solvent.

In MAPLE, the target usually contains 55 wt% of solute material, that is, polymer or biomaterial to be deposited. Thus, each polymer or biomaterial molecule is surrounded or shielded by a large amount of solvent or matrix. This configuration reduces both thermal and photonic damage to the polymer or biomaterial in solution during their laser-induced volatilization. Instead, the matrix molecules absorb the laser radiation and rapidly leave the surface as showed in the scheme reported below.

Ideally, the solute molecules are entrained in the plume of matrix molecules leaving the frozen target due to collisions between the matrix and the embedded polymer or biomaterial molecules.

Molecular dynamics simulations of the laser ablation of large molecules embedded into a low-molecular-weight matrix show in fact that as a result of the laser excitation,

clusters containing polymer molecules surrounded by matrix molecules are ejected together with the matrix material [98].

By careful optimization of the MAPLE deposition conditions, this process can occur without any significant polymer or biomaterial decomposition. The MAPLE process depletes the target of solvent and polymer in the same concentration as the starting matrix.

The substrates are typically at room temperature during the MAPLE deposition process, but they can be heated slightly to anneal the growing film. Typically, an excimer laser is used (KrF at 248 nm or ArF at 193 nm) with 10- to 30-ns pulse width, at repetition rates between 1 and 20 Hz, focused to a 1 to 10 mm² spot size on the target, although other types of lasers with wavelengths ranging from the visible to the infrared (IR) can be employed as well. The laser fluence at the target is typically set between 0.01 and 0.5 J/cm², depending on the solute material and solvent used. The depositions can be carried out at pressures ranging from vacuum to a few hundred millitorr and in the presence of inert or reactive background gases, in the same manner as conventional PLD.

The matrix solution is prepared by dissolving the organic or polymeric material to be deposited in a solvent such as water, various types of alcohols, acetone, toluene, and so forth. To make a target, a few milliliters of the solution are flash frozen in a target die by submerging it in liquid nitrogen (LN₂). Once frozen, the MAPLE target is mounted on a cryogenically cooled rotating target holder with the open die end facing the laser. In short, the MAPLE processing parameters are: composition of the target matrix, target and substrate temperature, target-to-substrate distance, type of background gas and pressure, laser wavelength, laser fluence, and laser repetition rate.

When a substrate is positioned directly in the path of the plume, a coating starts to form from the evaporated solute molecules, while the volatile solvent molecules, which have very low sticking coefficients, are evacuated by the pump in the deposition chamber.

One advantage of the MAPLE process is that it can easily be combined with noncontact shadow masks to limit the deposition to only those required areas on a substrate.

This is important for fragile substrates and is much less time-consuming than subsequent removal by patterning and etching. Furthermore, many polymer and organic coatings will not survive the solvents used to wash off the resists making them incompatible with standard lithographic processes. In such cases, MAPLE deposition of

the polymer or organic through a shadow mask might be the only way to deposit discrete thin-film structures of these materials.

The MAPLE process has been used successfully to deposit polymer films through masks with features in the micron. This capability is very important for the manufacture of sensor arrays and electronic devices.

Despite the great success achieved with the MAPLE technique for the deposition of polymers and biomaterials, this process is not without certain important drawbacks. First, the typical deposition rates that can be achieved with MAPLE are about an order of magnitude lower than those for conventional PLD.

Given that most of the organic compounds to be deposited have a very large UV absorption cross section, it is necessary for the matrix solution to contain low concentrations (2-5 wt%) of the polymer or biomaterial solute molecules in order to minimize their interaction with the UV photons.

Finally, the solvent molecules might be subject to photochemical reactions during their interaction with the laser pulse, which in some cases can result in the generation of highly reactive radicals that can alter the chemical structure and functionality of the solute polymer or biomaterial being deposited.

Another aspect that must be taken into consideration when using MAPLE is the resulting film surface morphology.

Under certain conditions, that is, low laser fluence, low laser repetition rate, low solute concentration in the matrix, and/or lower temperature of the target matrix, it is possible to produce very smooth and uniform coatings with MAPLE. More often than not, however, the surface morphology of the films tends to be rough and in some cases large droplets are present as well.

The film roughness not only depends on processing conditions but also on the type of polymer or organic being deposited and in the case of many biomaterials might not be modifiable due to the characteristic intrinsic arrangements of the molecular chains. For some applications, such as in biosensors, higher surface areas resulting from the rough film morphology might be desirable since they increase the area for analyte binding.

The rough protein films that can be generated by MAPLE can potentially increase the detection capability of a biosensor by increasing the active protein area exposed to a particular analyte.

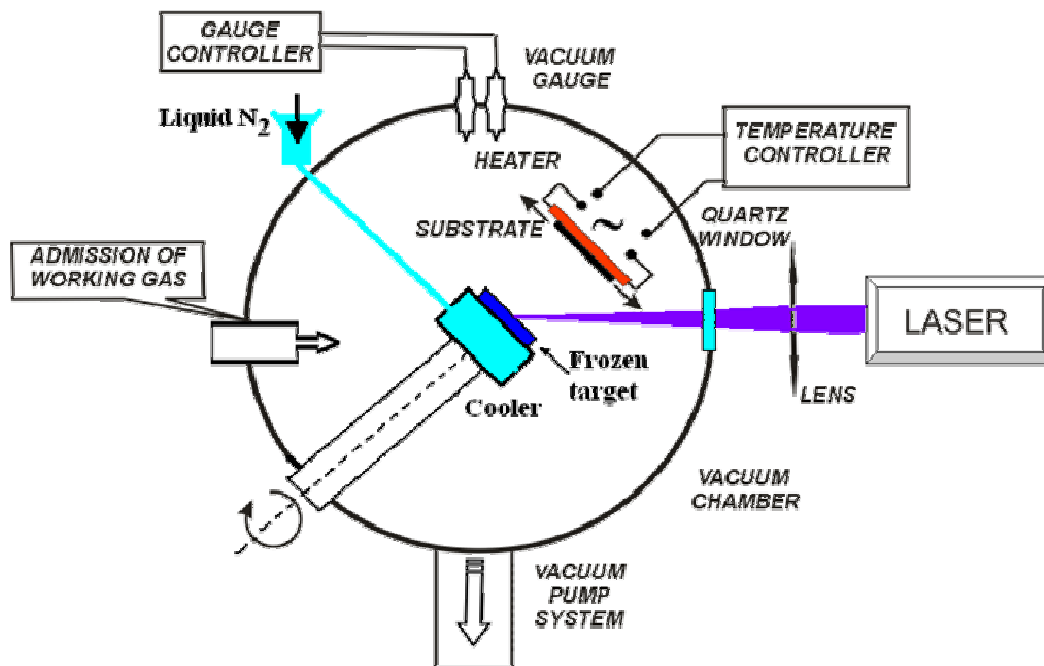


Fig. 14 - MAPLE apparatus.

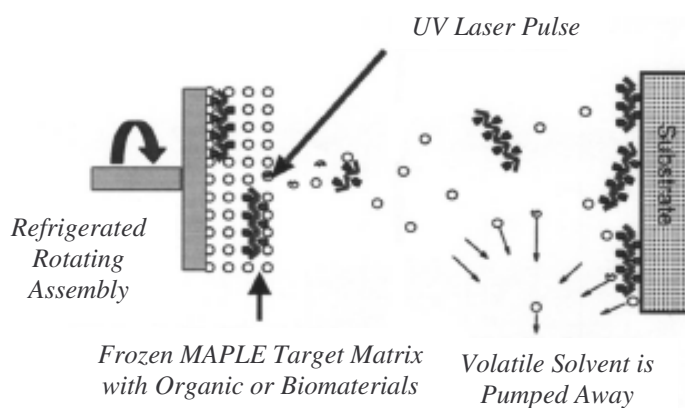


Fig. 15 - Scheme of MAPLE process.

1.3.3 Bone Cements

Calcium phosphate bone cements first appeared in the literature during the 1980s and these materials offer the potential for in situ moulding and injectability. There are a variety of different combinations of calcium compounds which are used in the formulation of these bone cements but the end product is normally based on a calcium deficient HA.

The development of calcium phosphate cements as a class of viable biomaterials has increased interest in their use as artificial hard tissues. One of the earliest CaPs investigated was based on the hydrolysis of α -tricalcium phosphate. α -TCP was shown to hydrate to a calcium-deficient hydroxyapatite (CDHA) in dilute aqueous solutions. This calcium phosphate is unique because it can hydrolyze to form a cement. The rate of α -TCP hydrolysis has been observed to increase with temperature and decrease with increasing pH. Hydrolysis of α -TCP to CDHA occurs by a mechanism involving two steps. The first step occurred within the first hour and resulted in high initial pH values commensurate with a spike in the calcium concentration. This initial step was a result of slight compositional non-homogeneities attributable to synthesis conditions initially employed. The elevated pH also resulted in a reduction of the rate of hydrolysis. The second reaction step resulted in the bulk of hydrolysis. The activation energies for these steps were determined; they indicate a nucleation and growth mechanism. The microstructure of the resulting CDHA differed greatly from that produced by the DCPD-TetCP reaction at equivalent temperatures. In particular, crystallites are much larger, resulting in lower surface areas, and the hydroxyapatite formed is more crystalline than that produced by reaction of DCPD with TetCP at equivalent temperatures. This difference is attributable to the slower rate of TCP hydrolysis combined with the absence of the formation of ACP as an intermediate. The CDHA crystallites grew perpendicular to the α -TCP surface, thus minimizing the formation of a diffusion barrier. Understanding the factors influencing the hydrolysis of calcium phosphate salts to apatites by cement reactions is essential in controlling the setting times and times to complete reaction. The properties must be understood and controlled if these types of materials are to be used in vivo applications. The crystallite size, morphology, and the crystallinity of CDHA from α -TCP hydration should change its resorption characteristics when compared with HA formed by other techniques [99, 100].

1.3.4 Scaffolds

Scaffolding is a temporary framework used to support living matters in the construction or repair of large structures.

Scaffolds are largely used for tissue engineering and regenerative medicine. In particular, scaffolds for osteogenesis should mimic bone morphology, structure and function in order to optimize integration into surrounding tissue.

The development of the new technologies of bone tissue engineering required the production of bioresorbable macroporous scaffolds.

One of the most promising approaches to the problem of bone regeneration and repair is bone tissue engineering (BTE). To guide *in vitro* or *in vivo* tissue regeneration, it is necessary to obtain appropriate scaffold materials, which satisfy all the goals required: osteoconductivity, controlled degradation, mechanical properties, formability, etc. Moreover, one of the main characteristics that is required in a BTE scaffold is a high interconnected macroporosity, to ensure cell colonisation and flow transport of nutrients and metabolic waste. In general, it is accepted that the pore size should range between 100 and 400 μm . To this end, several porous ceramic manufacturing techniques have been proposed, such as hydrothermal exchange from corals, the inclusion of porogenic volatile or soluble substances, impregnation and gel-casting of foams, dual phase mixing, or solid free-form fabrication among others. However, the majority of these methods are based on the production of high temperature apatites, which are known to be hardly resorbable in normal physiological conditions, and some of the routes presented required complex processes of preparation, or the addition of second phases, which need to be eliminated to create the porosity even by sintering [97, 98].

An alternative route was recently presented to develop macroporous scaffolds at low temperature from calcium phosphate cements (CPCs). In this case, the consolidation of the porous structures is expected to be attained not by sintering, but through a low temperature setting reaction, and specifically through the entanglement of the crystals produced as a result of a dissolution-precipitation reaction.

This approach has several advantages: first of all, the cementing reaction takes place at low temperature and therefore the final product is a low temperature precipitated hydroxyapatite, chemically more similar to the biological apatites, and with a much higher specific surface than that of a sintered hydroxyapatite. All these factors contribute to bring this material a higher reactivity, as compared to a ceramic

hydroxyapatite. In addition, the low temperature processing allows the introduction of proteins or different kinds of drugs into the material (for example, antibiotics, antiinflammatory or anticancer drugs). In second place: combination of intrinsic microporosity and introduced macroporosity, guarantees the interconnectivity between the macropores introduced into the cement, at least in a higher amount than that obtained in high temperature sintered materials. Finally, the processing techniques are simpler, and less expensive than those involved in the fabrication of high temperature porous ceramics.

Moreover, as bone is a complex material composed of nanocrystals of a basic calcium phosphate deposited within an organic matrix which is mainly type I collagen, it is not surprising that a lot of research has been performed on collagen, and on its derivative, gelatin. Gelatin is obtained by thermal denaturation or physical and chemical degradation of collagen through the breaking of the triple- helix structure into random coils. With respect to collagen, gelatin does not express antigenicity under physiological conditions, it is completely resorbable in vivo and its physicochemical properties can be suitably modulated; furthermore it is much cheaper and easier to obtain in concentrated solutions. The functional properties of gelatin are related to its chemical characteristics. In particular, the gel strength, viscosity, setting behaviour and melting point of gelatin depend on its molecular weight distribution and amino acid composition. Bone tissue formation is enhanced by scaffolds because of the presence of pores, which allow migration and proliferation of osteoblasts and mesenchymal cells, as well as vascularization. In addition, a porous surface improves mechanical interlocking between the implant biomaterial and the surrounding natural bone, providing greater mechanical stability at this critical interface.

Porosity can be produced with the same methods as those used for polymeric scaffolds, which have been intensively studied for decades to provide implantable devices for tissue regeneration. The methods include fiber bonding, melt molding, solvent casting/particulate leaching, gas foaming/particulate leaching, phase separation, high-pressure processing, electrospinning and rapid prototyping. The formulations proposed for porous gelatin scaffolds with ceramic particles include β -tricalcium phosphate (β -TCP) and HA. These porous scaffolds usually exhibit poor mechanical properties and are easily degraded, due to the high solubility of gelatin in aqueous solution. Mechanical, as well as biological stability is increased by gelatin crosslinking,

though this can also decrease biocompatibility because of the cytotoxic reaction of crosslinking agents such as glutaraldehyde.

Lately, a relatively soluble and easily hydrolysable calcium phosphate, α -tricalcium phosphate [α -Ca₃(PO₄)₂, α -TCP], has been used to prepare porous scaffolds based on gelatin. The composite scaffolds were obtained by freeze-drying gelatin foams at different α -TCP contents and it's possible to vary the composition in order to modulate their morphological and mechanical properties [101].

1.3.4.1 Drug Delivery

Another way to treat bone disorders is by using local drug delivery devices. The local delivery of drugs should greatly reduce any systemic toxicities and side effects of parenteral administration. A higher drug concentration in relevant tissues can be administered by these local drug delivery devices, therefore an improved efficacy can be expected [102].

There has been considerable interest in recent years in developing controlled or sustained drug delivery systems by using biopolymers. Controlled or sustained release drugs provide many advantages in comparison with conventional forms including reduced side effects, drug concentration kept at effective levels in plasma, improved utilization of drug and decrease the dosing times.

Targeted drug delivery is essential to modern medicine in which specifically designed and effective drugs are employed to work on selected tissues, cells, and cellular structures. The use of microspheres based therapy allows drug release to be carefully tailored to the specific treatment site through the choice of appropriate formulation variables. The design of metal oxide/polymer hybrid nanocapsules has attracted much attention in the last few years, due to their wide range of applications, from catalysis to controlled release devices. Many of these nanocomposites are designed as polymer-core/oxide-shell materials, although oxide-core/polymer-shell as well as bi-continuous structures were also described.

Preparation of core-shell particles can take place following a one-step process, based on the self-assembly of organic and inorganic components, or a two-step process, i.e. the deposition of the shell on a pre-formed core particle.

In particular, inorganic coatings of polymeric particles have been realized by reactions that utilize specific functional groups on cores' surfaces in order to induce the inorganic

phase precipitation. The inorganic shells obtained in this way include silica, basic yttrium carbonates and metal oxides [103]. Gelatin is a protein produced by partial hydrolysis of collagen extracted from the bones, connective tissues, organs, and some intestines of animals such as the domesticated cattle, and horses. The natural molecular bonds between individual collagen strands are broken down into a form that rearrange more easily. Gelatin is an irreversibly hydrolyzed form of collagen [104].

The main limitation of gelatin for the preparation of sustained release systems arises from its rapid dissolution in aqueous environments leading to fast drug release at body temperature. In order to overcome this problem, chemical cross-linking procedures giving rise to the formation of non-soluble networks have to be taken into consideration [105].

The main characteristics of gelatin involve the presence of acidic and basic functions like all biopolymers. It is also able to form triple helixes in aqueous solution at low temperature and this is not observed in synthetic polymers [106 - 108]. The rate of formation of the triple helixes depends on many factors, such as the presence of covalent bonds, the molecular weight of gelatin and its concentration in the solution, the presence of aminoacids [107 - 109].

Moreover it interacts in a specific way with water, different from that one followed by synthetic hydrophilic biopolymers. This characteristic controls the structural and physic-mechanical properties of gelatin when in solid state. The capacity to absorb water depends on pH value and it increases on increasing the ionization of those groups that can dissociate. From the comparison between a collagen film and a gelatine film with an helycoidal or disordered structure, it is possible to conclude that the higher is the rate of molecular order inside the protein, the higher is the capacity to absorb of water vapour at almost all the humidity's values of the atmosphere.

The water bonded with the protein is in part absorbed by the polar groups of the macromolecules out of the helycoidal fragments, thus improving their stabilization.

In particular conditions of temperature, pH and solvent values, gelatin macromolecules can represent sufficient flexibility to realize a great quantity of conformations, so as to vary all the gelatin properties that depends on its structure.

Gelatin is the only one hydrocolloid substances that forms thermoreversible films with a melting point similar to that of the human body.

At molecular level, the gelification of gelatin solutions is promoted by a conformational change, from coil to helix [110], where three portions of the chain can

associate by hydrogen bonds. The characteristic parameters of the triple helixes are almost the same as those of collagen fibres [111]. The main differences between the original and renatured triple helixes consist first of all in the length of the helix and also in the supramolecular arrangement of these units. Several experiments showed that collagen molecule can't be created in the gel state because the α chains hardly can perfectly interact [112].

So, in gelatin gels, the only ordered regions are the sequences with a limited length of triple helixes, randomly distributed in space: the tendency to be side by side observed in the dry state disappears when water is added. The considerable swelling of the fibres is induced by the possibility to space the triple helixes.

The supramolecular arrangement of collagen molecules in native fibres is absent in gelatin gels where portions of renatured triple helixes act like junctions and form a tridimensional structure. This structure and the physical properties of gelatin gels deeply depend from their renaturation level, that on its own is influenced by temperature, type of gelatin and the utilized solvent. Because of its ability to form transparent and resistant gels, and also flexible and thermoreversible films, gelatin finds several applications. In fact, it is used in alimental processes as base for gummy cakes, as meat and fruits preservative, in powder components and as whitening for beer and wine; its industrial applications include capsules for drugs, biomaterials, coatings of photographic plates, paper production.

2. Aim of the Research

A material for hard tissue replacement must be able to create a bond with the host living tissue [113]. This requirement is better fulfilled the more the synthetic material resembles the biological one in composition, structure, morphology, and functionality [114]. This approach is included in the biomimetics principles, which is addressed to the design and development of new synthetic materials using strategies adopted by living organisms to produce biological materials. In particular, biomineralized tissues are often sophisticated composite materials, in which the components and the interfaces between them have been defined and optimized, and that present unusual and optimal chemical-physical, morphological and mechanical properties. Moreover, biominerals are generally produced by easily traceable raw materials, in aqueous media and room pressure and temperature, that is with cheap process and materials. Thus, it is not surprising that the idea to mimic those strategies proper of Nature has been applied to several areas of applied sciences, in particular to the synthesis of new materials for the substitution and repair of skeletal tissue.

Due to its similarity with bone mineral and to its high biocompatibility and bioactivity, synthetic HA has generated a great deal of interest in relation to hard tissue applications. However, bone apatite differs from synthetic stoichiometric HA for several aspects, namely small crystal dimensions, poor degree of crystallinity, and non stoichiometry due to the presence of a variety of foreign ions. Biomimetics' approach to the development of biomaterials for bone tissue repair shifted the attention from stoichiometric, highly crystalline HA, towards nanocrystalline apatite (also called biomimetic apatite), and further more resorbable calcium phosphate, such as octacalcium phosphate (OCP), α -tricalcium phosphate (α -TCP) and dicalcium phosphate dihydrate (DCPD), that can easily transform into nanocrystalline apatite [115 - 118]. The research activity of this PhD thesis is addressed to study the interaction between calcium phosphates and biologically active ions and molecules in order to obtain new materials with potential applications as biomaterials for hard tissue substitution and repair.

The research program involves the following lines:

1) Modified calcium phosphates.

a) hydroxyapatite and octacalcium phosphate, modified by the introduction of biological interesting ions or molecules, such as strontium, magnesium, manganese and bisphosphonates, have been synthesized and characterized in order to put into evidence the structural and morphological modifications induced by the additives.

b) strontium ion was also investigated in order to clarify its influence on the reaction of α -TCP which is the basis of the hardening reaction of bone cements. Strontium ion delays the reaction kinetics but it is engulfed in the powder so that the final cement results more biocompatible.

2) Deposition of modified calcium phosphates on metallic substrates.

Some of the synthesized calcium phosphates have been used to coat metallic substrates using PLD and MAPLE methods in order to improve the biological performance of the implants:

a) hydroxyapatite at increasing Sr content, up to 7 atom % has been deposited by means of Pulsed Laser Deposition on etched Titanium substrates;

b) alendronate-hydroxyapatite nanocrystals at different bisphosphonate content have been successfully deposited on Titanium substrates using Matrix Assisted Pulsed Laser Evaporation.

The chemistry, structure and morphology of the coatings have been characterized, before *in vitro* tests with bone cells.

3) Core-shell particles for drug delivery.

Scaffolds are largely used for tissue engineering and regenerative medicine, as well as for drug delivery. Integration into surrounding tissue is better achieved the more the scaffold mimics bone morphology, structure and function. As bone is a complex material composed of nanocrystals of a basic calcium phosphate deposited within an

organic matrix which is mainly constituted of type I collagen, core-shell particles based on the self-assembly of gelatin and calcium phosphates as main components could fulfil this requirement. On this basis, the preparation of gelatin microspheres stabilized with dialdehyde alginate and coated with a uniform layer of calcium phosphate has been optimized. Aspirin has been used as a model drug to test the performance of these materials as drug release devices.

3. Materials

3.1 Syntheses

3.1.1 Sr-substituted Hydroxyapatite

(Ca–Sr) hydroxyapatites (Ca–Sr–HA) with Sr/(Ca + Sr) molar ratios in the range from 0 to 1 were synthesized in N₂ atmosphere using 50 mL solutions with different Sr/(Ca + Sr) ratios prepared by dissolving the appropriate amounts of Ca(NO₃)₂ · 4H₂O and Sr(NO₃)₂ in CO₂-free deionized water and adjusting the pH to 10 with NH₄OH.

The total concentration of [Ca²⁺] + [Sr²⁺] was 1.08 M. The solution was heated at 90 °C and 50 mL of 0.65 M (NH₄)₂HPO₄ solution, pH 10 adjusted with NH₄OH, was added dropwise under stirring. The precipitate was maintained in contact with the reaction solution for 5 hours at 90 °C under stirring, then centrifuged at 10000 r.p.m. for 10 minutes and washed repeatedly with distilled water. The product was dried at 37 °C overnight [54].

3.1.2 Alendronate-Hydroxyapatite Nanocrystals

The syntheses of AL–HA nanocrystals were carried out using a method recently developed. Briefly, 50 mL of 1.08M Ca(NO₃)₂ · 4H₂O solution at pH adjusted to 10 with NH₄OH was heated at 90 °C in N₂ atmosphere and 50 mL of 0.65M (NH₄)₂HPO₄ solution, pH 10 adjusted with NH₄OH, was added dropwise under stirring. Soon after completion of the phosphate addition, the alendronate solution was dropped under stirring in the reaction vessel. The precipitate was maintained in contact with the reaction solution for 5 hours at 90 °C under stirring, then centrifuged at 10,000 r.p.m. for 10 min and repeatedly washed with CO₂-free distilled water. The product was dried at 37 °C overnight. Four series of samples (HA, HA–AL7, HA–AL14, and HA–AL28) were prepared using alendronate concentrations of 0, 7, 14 and 28 mM [119].

3.1.3 Substituted OctaCalcium Phosphate

Octacalcium phosphate was synthesized by dropwise addition of 250 mL of 0.04 M $\text{Ca}(\text{CH}_3\text{COO})_2$ (Carlo Erba) into 750 mL of a phosphate solution containing 5 mmol of Na_2HPO_4 (Carlo Erba) and 5 mmol of NaH_2PO_4 (Carlo Erba) maintained at 60°C, starting pH was 5 by adding H_3PO_4 [120].

The precipitate was stored in contact with the mother solution for 10 min, filtered, repeatedly washed with bidistilled water and dried at 37°C. The synthesis of substituted OCP was carried out by adding $\text{Sr}(\text{CH}_3\text{COO})_2$, $\text{Mn}(\text{CH}_3\text{COO})_2$, $\text{Mg}(\text{CH}_3\text{COO})_2$ to $\text{Ca}(\text{CH}_3\text{COO})_2$ in the appropriate ratios so as to maintain the right molarity.

3.1.4 α -TriCalcium Phosphate

α -TCP was obtained by solid-state reaction of a mixture of CaCO_3 and $\text{CaHPO}_4 \cdot 2\text{H}_2\text{O}$ in the molar ratio of 1:2 at 1300°C for 5 hours [121]. The solid product was ground before being submitted to hydrolysis reaction.

3.2 Thin films deposition

Disk-shaped (diameter = 15 mm, thickness = 0.5 mm) Ti substrates were mechanically polished and subsequently submitted to acid etching to obtain an extended active surface.

3.2.1 Pulsed Laser Deposition

For PLD experiments disk-shaped tablets with 1 gram of the powder were prepared simply pressing it under 15 tons for a few minutes. The tablets were then subjected to the laser beams.

3.2.2 Matrix Assisted Pulsed Laser Evaporation

For MAPLE experiments a concentrated suspension in H₂O of the sample were prepared. It was stirred for 10 minutes to reach homogeneity. Then it was frozed with liquid nitrogen and after that it was subjected to the laser beams.

3.3 Hydrolysis

Hydrolysis of α -TCP was carried out in bidistilled water at different concentrations of SrCl₂ · 6H₂O from 2 to 20% (calculated with respect to the Calcium atoms in the α -TCP powder: [Sr/(Ca + Sr)] · 100 ratios from 2 to 20). The reaction of hydrolysis was performed on 100 mg α -TCP/50 mL solution at 37 or 60°C, without stirring, for different periods of time, up to 35 days. Then the products were filtered, repeatedly washed with double distilled water and dried at 37°C.

In order to increase the phase conversion speed, the hydrolyses were also performed by adding 5 mg of DCPD to the α -TCP powder.

Alternatively, the hydrolysis of α -TCP was studied in solutions containing gelatin. Type A gelatin (280 Bloom, Italgelatine S.p.A.) from pig skin was used. α -TCP was soaked at 37°C in solutions at gelatin concentration of 0.1, 0.5 and 1% wt. The co-presence of Sr²⁺ ions was also evaluated, even in the presence of DCPD.

3.4 Microspheres

3.4.1 Alginate dialdheyde

Alginate dialdheyde (ADA) was obtained by a partial oxidation of sodium alginate (Carlo Erba) by using sodium metaperiodate (Fluka). 10 grams of sodium alginate were added to 50 mL of ethanol and then this solution was added to a metaperiodate solution characterized by 0,95 mol every sodium alginate mol in 50 mL of distilled water.

This mixture was maintained stirring at 25°C for 6 hours in a dark ambient so as to obtain dialdeide alginate (ADA) oxidate at about 50-60%. After the necessary time the

mix was dialyzed with 2,5 L of H₂O mQ for 48 hours refreshing the water repeatedly so as to obtain the complete exclusion of the oxidant agent. This was demonstrated by adding 0,5 mL of the dialysed product to 0,5 mL of silver nitrate 1% solution and verifying that no precipitate was observed. At the end the dialysed product was freeze-dried [122].

3.4.2 Gelatin microspheres cross-linked with Alginate Dialdehyde and Calcium

Cross-linking of gelatin was performed before starting the reaction of preparation of the microspheres, by addition of 5 mL of calcium acetate 0.2 M to 5 mL of aqueous solution containing gelatin 10% w/v and ADA 3% w/w [51]: after 2 minutes of magnetic stirring, 5 mL of the mixture were added to the oil phase at 40°C. The mixture was mechanically stirred at 400 r.p.m. for 5 minutes, then very rapidly made cold by using ice for 10 minutes under stirring. 50 mL of acetone at 5°C were added to dehydrate the microspheres, slowly stirring (200 r.p.m.) for a couple of minutes. The mixture was then filtered under vacuum and washed three times with cold acetone so as to remove oil residues. Then it was air dried.

3.4.3 Synthesis of the inorganic shell

The coating of gelatin microspheres with calcium phosphates was obtained by direct synthesis. After the preparation of gelatin microspheres when the reaction medium is maintained at 0°C by the use of ice, 7,5 mL of sodium phosphates solution (0.2 mmol Na₂HPO₄ · 12H₂O, 0.2 mmol NaH₂PO₄ · 2H₂O, 0,084 g sodium polyacrylate) at pH 5 for H₃PO₄ were added. The solution was slowly stirred for a couple of minutes. Then 5 mL of a calcium acetate 0.16 M were dropped in the reaction solution in 5 minutes and after 10 minutes the speed of stirring was decreased and 50 mL of cold acetone were added. The product was then filtered under vacuum and three times washed with aliquots of 25 mL of acetone at 5°C. Then it was air dried.

To make easier the precipitation of calcium phosphate on the microspheres' surfaces and form a complete and homogeneous coating several different tests have been

performed. Many parameters have been changed, such as pH value, sodium phosphates concentration NaPA concentration and temperature. A regular and homogeneous coating of amorphous calcium phosphate was obtained at pH 5.

3.4.4 Aspirin-loaded microspheres

Acetyl salicylic was chosen as a model to test the drug release from gelatin microspheres. It is, in fact, soluble in aqueous media (10 mg/L mL H₂O at 20°C) and for this reason as demonstrated by the experiments, it doesn't badly influence the gelatin microspheres preparation. 50 mg of aspirin was dissolved before starting the reaction in the same water in which gelatine was dissolved so as to be automatically contained inside the microspheres in an homogeneous way. The procedure adopted was the same optimized for the preparation of gelatin microspheres previously described.

4. Methods

4.1 X-Ray Diffraction

X-ray diffraction analysis was carried out by means of a PANalytical X'Celerator powder diffractometer equipped with a monochromator in the diffracted beam. Cu Ka radiation was used (40 mA, 40 kV). The 2θ range was from 3° to 60° at a scanning speed of $0.75^\circ/\text{min}$. In order to evaluate the coherence lengths of the crystals and to perform the line profile analysis, further X-ray powder data were collected in the 2θ range from 15° to 100° in the step scanning mode with a fixed counting time of 10 s for each $0.030^\circ/\text{step}$.

For Rietveld analysis, the diffractometers were recorded in the range of 2θ from 3° to 60° slower than before, in order to obtain as precise as possible peaks positions ($0.03^\circ/\text{step}$, 200 s/step).

X-ray diffraction analysis of thin films deposited on Ti substrates was carried out by means of a PANalytical X'Pert PRO powder diffractometer. CuKa radiation was used (40 mA, 40 kV). Data were obtained in the range of 2θ from 3° to 60° ($0.02^\circ/\text{step}$, 10 s/step).

4.1.1 Scherrer analysis

The line broadening of the 002 and 310 reflections was used to evaluate the length of the coherent domains (hkl) along the c-axis and along a direction perpendicular to it.

τ_{hkl} values were calculated from the widths at half maximum intensity ($b_{1/2}$) using the Scherrer equation [123]:

$$\tau_{hkl} = \frac{K \cdot \lambda}{\beta \cdot \cos \theta}$$

where k is the wavelength, h the diffraction angle and K a constant depending on crystal habit (chosen as 0.9). The silicon standard peak 111 was used to evaluate the instrumental broadening.

4.1.2 Rietveld refinement analysis

The DEBVIN program [124 - 126], essentially implemented on Rietveld routine [127], was used to refine the structures of the samples. The space group ($P6_3/m$, No. 176), the cell parameters, the atomic positions and the thermal parameters of CaHA are introduced as the initial structural model. For SrHA, the data of the single crystal were used [128]. The phosphate group was considered as a rigid body. The background is treated as an empirical segmented line where the heights of the six nodes are free variables. The peaks were fitted by using a Pearson VII function. The half width of the diffraction peaks as a function of 2θ was evaluated by the formulation of the Caglioti model [129].

The possibility to refine the mean crystallite size parallel to crystallographic axes was taken into account. Rietveld refinement was performed in several stages, the parameters obtained in each step being deferred in the following one.

In the first cycles the scale factor and the background were refined. The refinement of the other parameters is in the following order: zero shift, profile parameters, asymmetry parameter, cell parameters, crystallite anisotropy. The refinements of the occupancy factors and of the coordinates were tested at the latest stages of the procedure, starting with those of the two metal sites. The atomic displacement parameters in the form of Biso were refined but not simultaneously with occupancy factors, because of their correlation. The total number of variables refined was 22.

4.2 Fourier Transform Infra-Red Spectroscopy

For the IR adsorption analysis, 1 mg of the powdered samples was carefully mixed with KBr (250 mg, infrared grade) and pelletized under a pressure of 10 tons for 2 min. The pellets were analyzed using a Nicolet 380 FTIR spectrophotometer to collect 32 scans in the range $4000 - 400 \text{ cm}^{-1}$ at a resolution of 4 cm^{-1} .

4.3 Atomic Absorption Spectroscopy

Calcium and strontium contents were determined using a GBC 901 atomic absorption spectrophotometer ($\lambda(\text{Ca}) = 422.7 \text{ nm}$; $\lambda(\text{Sr}) = 460.7 \text{ nm}$). The samples were diluted to an appropriate volume with 10% lanthanum in 50% HCl, in order to suppress interferences.

4.4 Scanning Electron Microscopy

Morphological investigations of the synthesized products were conducted using a Philips XL-20 Scanning Electron Microscope. The samples were sputter coated with gold for 2 minutes and 30 seconds before examination.

4.5 Transmission Electron Microscopy

For TEM investigations, a small amount of powder was dispersed in ethanol and submitted to ultrasonication. A drop of the calcium phosphate suspension was transferred onto holey carbon foils supported on conventional copper microgrids. A Philips CM 100 transmission electron microscope operating at 80 kV was used.

4.6 Surface Area Analysis by Gas Adsorption (BET)

The surface area was measured using a Carlo Erba Sorpty 1750 BET analyzer using constant volume N_2 absorption with desorption at 100 °C [130].

4.7 Pulsed Laser Deposition

The films were pulsed-laser deposited on etched Ti substrates using an UV KrF* excimer laser source ($\lambda = 248$ nm, $\tau \sim 7.4$ ns). Prior to each deposition, the reaction chamber was evacuated down to a residual pressure of 10^{-4} Pa. Films were deposited in 50 Pa water vapour flux on substrates heated to 400 °C. The substrates were placed parallel to the targets, 4 cm away from them. Fluence was set at 2.4 J cm $^{-2}$, and 25,000 subsequent laser pulses were applied at a frequency repetition rate of 2 Hz for the deposition of each film. The as-deposited samples were submitted to annealing treatments in water vapour and ambient pressure for 6 hours at the same temperatures as those applied during deposition. The average thickness of the obtained structures, as measured by profilometry, was ~ 1 μ m.

4.8 Matrix Assisted Pulsed Laser Evaporation

The procedure just described above for PLD was adopted for MAPLE too. Only a few characteristic parameters are different. In fact, in MAPLE the fluence is deeply lower than that in PLD being only $0,75$ J cm $^{-2}$ because of the nature of compounds treated. Moreover, the temperature of the substrate is only 30 °C and the pressure inside the reaction chamber 10^{-1} torr.

4.9 UV – Phosphorous, Gelatin and Drug Release Determination

Phosphorus content in Sr-HA was determined spectrophotometrically in molybdovanadophosphoric acid using a Varian Cary50Bio instrument ($\lambda = 400$ nm).

Bicinconinic acid test allowed to determine the protein concentration of the solution by a colorimetric technique [131]. 50 mg of gelatine microspheres were immersed in 5

ml of phosphate buffer solution (PBS) pH 7.4 at 37 °C; several fractions of release solution were drawn, refreshing the PBS solution after every drawing, the gelatin concentration was analyzed. A test solution was prepared with cuprum(ii)sulfate pentahydrate and an excess of bicinconinic acid so as to obtain a final ratio of 1:50 v/v. 200 µL of the release solution were added to 2 mL of test solution and with PBS. The final volume was 5 mL. After 1 hour and 30 min at ambient temperature the absorbance of each of these solutions was measured by using a Cary 50 spectrophotometer at 562 nm. The gelatine concentration was evaluated by a calibration curve, constituted by the results of standard solutions in the concentration range of 5-100 mg of gelatine/100 mL PBS.

200 µL of the same solution were diluted in PBS to the final volume of 5 mL and analyzed by measuring the absorbance at 297 nm so as to obtain the drug released percentages.

4.10 Cell Culture

4.10.1 Osteoblast culture

MG63 human osteoblast-like cells were cultured in Dulbecco's modified Eagle's medium (DMEM, Sigma, UK), supplemented with 10% fetal bovine serum (FBS) and antibiotics (100 U mL⁻¹ penicillin, 100 mg mL⁻¹ streptomycin).

The cells were detached from culture flasks by trypsinization, and centrifuged. Their number and viability were determined by the trypan blue dye exclusion test.

MG63 osteoblast-like cells were plated at a density of $2 \cdot 10^4$ cells mL⁻¹ in 24-well plates containing sterile samples of reference sample and samples of substitutes compounds. The same concentration of cells was seeded in empty wells as a control (CTR). Plates were cultured in standard conditions at 37 °C and 95% humidity, and 5% CO₂. After 24 hours, the medium was replaced with DMEM supplemented with β-glycerophosphate (10⁻⁸ nM) and ascorbic acid (50 µg mL⁻¹) to activate the osteoblasts. To stimulate the production of osteocalcin, the culture medium was enriched with 1,25(OH)₂D₃ 48 hours before the end of the experiment.

After 1 hour of culture, phalloidin staining was performed to assess cell adhesion and colonization of the samples. The cultures were washed in PBS and fixed in a solution of 4% formaldehyde in PBS for 15 min at 37 °C. The samples were then permeabilized in 0.5% Triton X-100 for 15 min and washed in PBS. A FITC-conjugate phalloidin solution (1:100 in PBS) was added for 30 minutes at 37 °C.

After washing, the samples were examined by fluorescence microscopy.

The Cell Proliferation Reagent WST-1 test was carried out to assess cell proliferation and viability at fixed experimental times (7, 14 and 21 days): 100 µL of WST-1 solution and 900 µL of medium (final dilution: 1:10) were added to the cell monolayer, and the multiwell plates were incubated at 37 °C for the next 4 hours. Supernatants were quantified spectrophotometrically at 450 nm using a reference wavelength of 625 nm. The results of WST-1 were reported as optical density (OD).

Finally, at the end of experimental times the supernatant was collected from all wells and centrifuged to remove particulates, if any. Aliquots were dispensed in Eppendorf tubes for storage at -70 °C and assayed for type I collagen (CICP, Procollagen-C Enzyme Immunoassay Kit, Metra Biosystem, CA), osteocalcin (OC, Enzyme Immunoassay Kit, Bender MedSystems, Vienna), osteoprotegerin (OPG, Immunoassay Kit, Bender MedSystems, Vienna), TNF-related activation-induced cytokine receptor (TRANCE, Immunoassay kit, Bender MedSystems, Vienna). Alkaline phosphatase activity (ALP, kinetic assay, Biosystems SA, Barcelona), was checked on supernatants immediately after collection. All the measured concentrations and activities were normalized by cell number to take cell growth differences into account.

4.10.2 Isolation of mononuclear cells for osteoclast culture

Peripheral human blood was obtained from healthy adult volunteers and collected in heparinated tubes, to prevent clotting. Density gradient centrifugation was used to separate mononuclear cells from the other elements of blood. Briefly, a volume of peripheral blood was diluted 1:1 with pre-warmed PBS and carefully layered on an equal volume of Histopaque 1077 in a 50 mL tube. The tube was centrifuged with 400g at 20 °C for 30 min. After centrifugation, the mononuclear cells accumulating at the interface between PBS and Histopaque were collected and transferred to another tube; 10 mL of PBS were added, and the tube was centrifuged with 250 grams at 20 °C for 10

min. The pellet was resuspended in 1 mL of culture medium (DMEM + 10% FBS). The trypan blue method was used to assess cell viability and counting was done in a Neubauer chamber. After that, the cells were plated on thin slides (diameter = 10 mm) of bone (CTR), and samples of considered compounds were placed in 24-well culture plates and incubated at 37 °C in 5% CO₂ for 90 minutes.

Twenty-four hours later, the non-adherent cells were washed off, to rid the culture of contaminating lymphocytes, so that adherent monocytes alone were used for culture, and the medium was replaced with osteoclast differentiation medium (DMEM + 10% FBS + 10⁻⁷ M PTH, 25 ng mL⁻¹ M-CSF, 3 ng mL⁻¹ RANKL). The cells were cultivated for up to 21 days.

After 1 week, cells cultured on the CTR bone slides were TRAP-stained exactly according to the manufacturer's instructions (Sigma, Buchs, Switzerland). The positive cells stained red in different intensities. To measure the resorbed area in the pit-assay, bone slides with cultured cells were washed with PBS at the end of the experimental time, incubated in 5% sodium hypochlorite for 10 min, washed twice with water, and stained with 0.1% toluidine blue, as a result of which the pits turned blue to purple. Phalloidin staining and WST-1 test were performed on the experimental samples.

Samples of each material were processed for scanning electron microscopy investigation at the end of the experiment. Osteoblasts grown on the materials were fixed in 2.5% glutaraldehyde, in pH 7.4 phosphate buffer 0.01 M for 1 hour and dehydrated in a graded ethanol series. After a passage in hexamethyldisilazane, the samples were air dried and sputter-coated with Pd/Pt prior to examination with a Philips XL-20 scanning electron microscope operating at 15 kV.

Statistical evaluation of data was performed using the software package SPSS/PC+ Statistics™ 10.1 (SPSS Inc., Chicago, IL). The experiment was repeated three times and the results presented are the mean of the triplicate values. Data are reported as mean ± SD at a significance level of P < 0.05. After having verified normal distribution and homogeneity of variance, a one-way ANOVA was done for comparison between groups. Finally, Scheffé's post hoc multiple comparison tests were performed to detect significant differences between groups [132].

5. Results and Discussion

5.1 Strontium-Substituted Hydroxyapatite

Among the bivalent cations that can replace calcium in CaHA, strontium has attracted remarkable interest for its possible biological role. Strontium is present in the mineral phase of bone, especially at the regions of high metabolic turn-over [133], and its beneficial effect in the treatment of osteoporosis is well known [134]. In vitro, strontium increases the number of osteoblasts and decreases the number and the activity of osteoclasts [134, 135], whereas strontium administration reduces bone resorption and stimulate bone formation [136 - 138]. Strontium can replace calcium in the HA structure in the whole range of composition. The solid solutions, which have been obtained by hydrothermal methods or by treatment at high temperatures, display a linear variation of the lattice parameters with composition, whereas different data are reported on the preferential substitution site of Sr for Ca in CaHA [139]. A better understanding of the interaction of Sr with hydroxyapatite structure could provide useful information also for clarifying the biological role of Sr on the process of biomineralization of bone and related pathologies. With this aim, we have carried out a chemical, morphological and structural analysis of calcium-strontium-hydroxyapatite solid solutions prepared by direct synthesis in aqueous medium.

The X-ray diffraction patterns of the solid products synthesized with different Sr/(Ca+Sr) molar ratios are shown in *Figure 16*. All the patterns indicate the presence of hydroxyapatite as a unique crystalline phase. The patterns of the samples corresponding to CaHA (Sr0) and to SrHA (Sr100) display well-defined and sharp peaks in agreement with a high degree of crystallinity of the two end members. On the other hand, the patterns of the samples containing both Ca and Sr generally exhibit broader diffraction peaks, in agreement with a reduced degree of crystallinity of the mixed Ca-Sr-HA. The broadening is more evident for the samples with smaller Sr content, suggesting a greater difficulty for CaHA to host the greater strontium ion than for SrHA to host the smaller calcium ion (Ca^{2+} ionic radius = 0.100 nm; Sr^{2+} ionic radius = 0.118 nm).

Strontium relative amount in the solid products, χ_{Sr} , evaluated through atomic absorption spectrometry is reported in *Table 2* as a function of strontium content in solution. The values of χ_{Sr} increase on increasing Sr/(Ca+Sr) in the starting solution, in agreement with a quantitative incorporation of strontium in the solid phase. The ratio

between the two cations in the solid phase is very close to that in the synthesis solution. Just the samples obtained from solutions with Sr/(Ca + Sr) molar ratios smaller than 0.5 exhibit χ_{Sr} lower than Sr/(Ca + Sr) indicating a slight preference of CaHA for Ca^{2+} ions.

The isomorphous substitution does not significantly affect the stoichiometry of HA as it can be deduced from the (Ca+Sr)/P molar ratio which assumes a mean value of 1.68 ± 0.03 , very close to the stoichiometric value of 1.67, independently from the Ca and Sr content.

The FT-IR spectra of the solid solutions show a decrease of the relative intensity of the absorption bands due to OH⁻ stretching and libration modes respectively, on increasing χ_{Sr} (Figure 17).

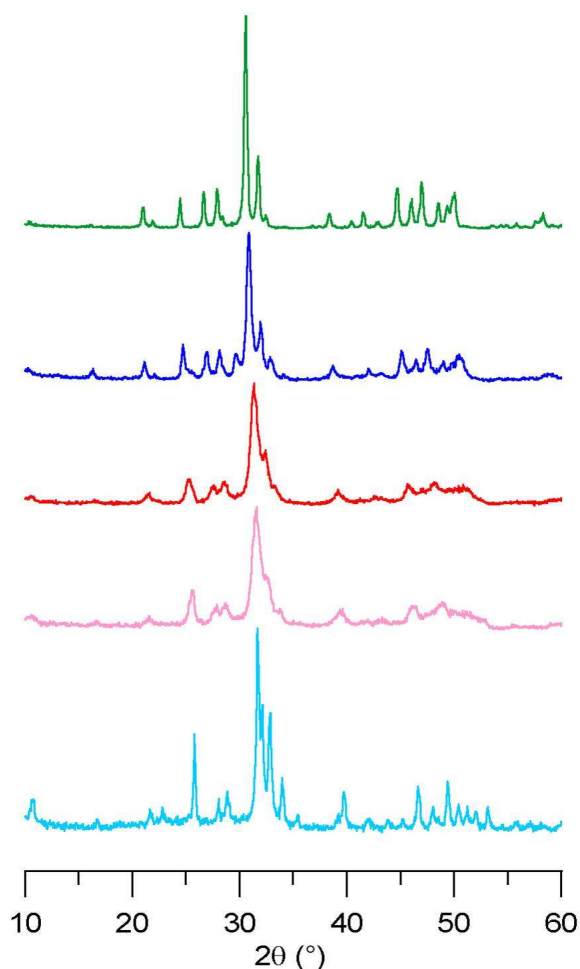


Fig. 16 - Powder X-ray diffraction patterns of: Sr0 (azure line); Sr30 (pink line); Sr50 (red line); Sr70 (blue line); Sr100 (green line).

Furthermore, the OH⁻ stretching band, which is at 3572 cm⁻¹ in Ca-HA, progressively shifts to higher wave numbers on increasing strontium content, up to 3590 cm⁻¹ for Sr-HA, whereas the OH⁻ libration band shifts from 630 cm⁻¹ to 537 cm⁻¹, in agreement with the results previously reported for Ca-HA and Sr-HA. The infrared absorption bands due to phosphate groups shift to lower wave numbers on increasing strontium relative content. *Figure 18* shows how the bands due to the symmetric stretching (ν_1) and bending (ν_4) modes of phosphate groups move respectively ν_1 from 962 (Ca-HA) to 947 cm⁻¹ (Sr-HA) and ν_4 from 603 (Ca-HA) to 592 cm⁻¹ (Sr-HA). Both shifts proceed in a linear way as a function of χ_{Sr} .

The approximately linear decrease in frequencies of the internal phosphate modes on going from CaHA to SrHA, to BaHA, was interpreted by Fowler [140] as indicating that the predominant factor causing shifts in the internal PO₄ frequencies to lower energies is decreased anion-anion repulsion concomitant with increased anion-anion separation on increasing cation radius. In agreement, the shift of the infrared absorption bands due to phosphate groups with increasing χ_{Sr} can be ascribed to the increasing mean dimensions of the cation.

The results of TEM investigation indicate that the morphology of the apatitic crystals is affected by the chemical composition.

Table 2 – Strontium relative amount in the solid products, evaluated through atomic absorption spectrometry reported as a function of Strontium content in solution.

Sample	Sr/(Ca + Sr) sample molar ratio in the solution	Sr/(Ca + Sr) sample molar ratio in the solid product
Sr0	0	0
Sr3	0.03	0.01
Sr5	0.05	0.03
Sr10	0.10	0.07
Sr20	0.20	0.18
Sr30	0.30	0.27
Sr50	0.50	0.49
Sr70	0.70	0.71
Sr90	0.90	0.93
Sr100	1.00	1.00

Figure 19 compares the TEM micrograph of Ca-HA crystals with those of apatitic crystals with different χ_{Sr} . Ca-HA is constituted of plate shaped crystals, with mean dimensions up to about $200 \cdot 40$ nm (*Figure 19(a)*). Ca-Sr-HA nanocrystals at small Sr content ($0 < \chi_{\text{Sr}} \leq 0.5$) display more perturbed shapes and ill-defined edges (*Figure 19(b)*), in agreement with the lower degree of crystallinity put into evidence by the broadening of the X-ray diffraction peaks. At relatively greater Sr content ($\chi_{\text{Sr}} \geq 0.7$), the crystals dimensions increase on increasing χ_{Sr} (*Figure 19(c)*). Sr-HA crystals display mean dimensions of about $500 \cdot 100$ nm and very well defined shape elongated in a direction parallel to the crystallographic *c*-axis (*Figure 19(d)*).

The values of specific surface area measured on HA samples applying the BET method are reported in *Table 3*. In accordance with TEM results, the surface area, which assumes a value of $60 \text{ m}^2/\text{g}$ for CaHA, increases slightly on increasing χ_{Sr} up to about 0.3, and then decreases for samples containing $\chi_{\text{Sr}} > 0.5$, reaching the minimum value of $26 \text{ m}^2/\text{g}$ for SrHA.

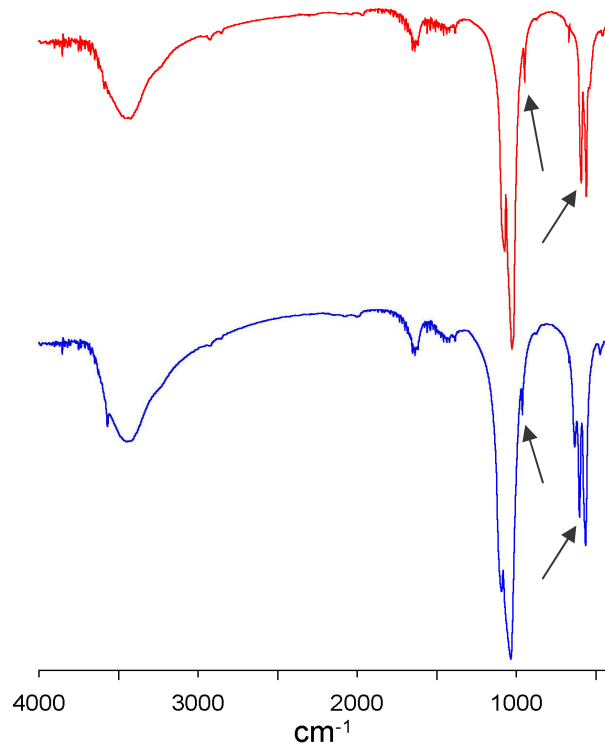


Fig. 17 - FT-IR adsorption spectra of Sr0 (blue line) and Sr100 (red line), the arrows on the left stand for phosphate stretching (ν_4), those on the right for the phosphate bending (ν_1).

Line profile analysis has been applied in order to investigate the line broadening increase and the peaks shifts observed in the XRD patterns of the samples (*Figure 20*). A qualitative estimation of the size of coherently scattering domain (i.e. the crystallite size) as derived from the Scherrer equation, on the hypothesis of negligible microstrain, is reported in *Table 4*.

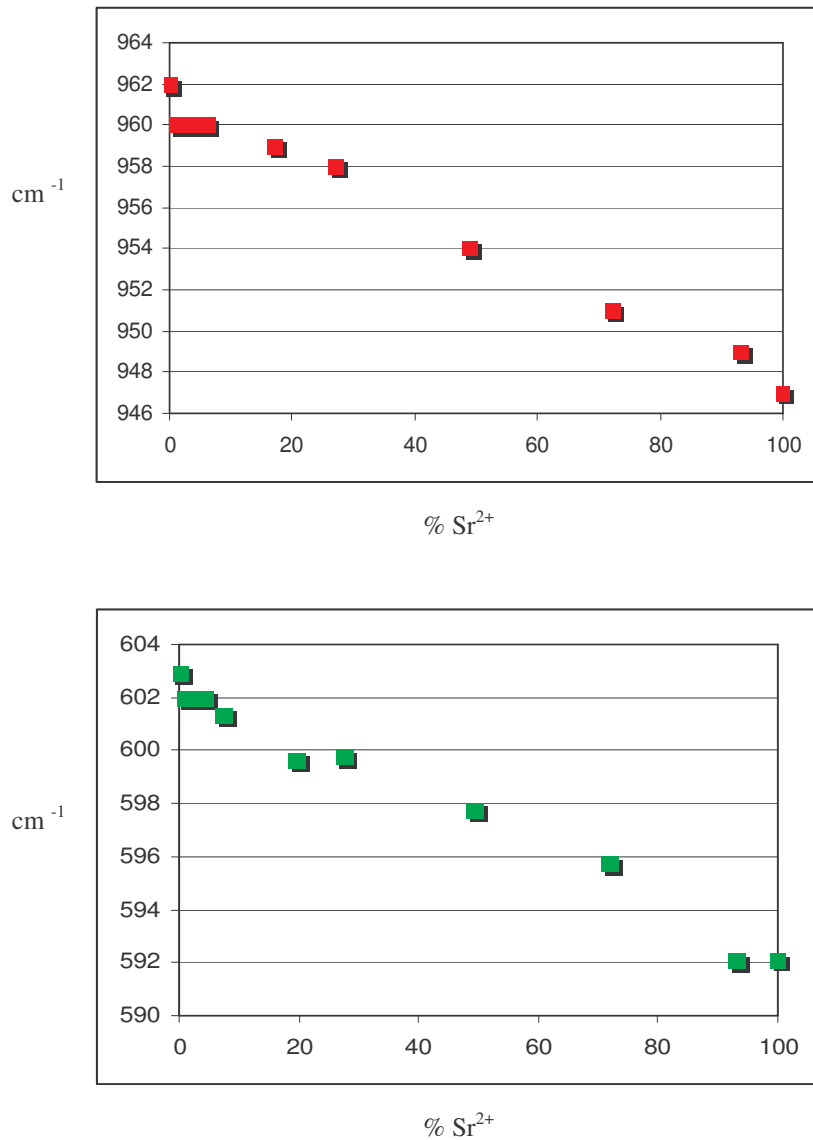


Fig. 18 - Shifts of the infrared absorption bands due to phosphate groups stretching (red squares) and bending (green squares) plotted as a function of χ_{Sr} .

τ_{002} is related to the mean crystallite size along the c-axis whereas τ_{310} refers to the mean crystal size along a direction perpendicular to it. At strontium content smaller than

50% the crystallite sizes decrease as χ_{Sr} increases. However, both τ_{002} and τ_{310} decrease, but the contraction appears to be slightly greater along the c-axis direction. As a matter of fact, the observed maximum contraction is of about 75% along the 002 direction, and of about 60% along the 310 direction.

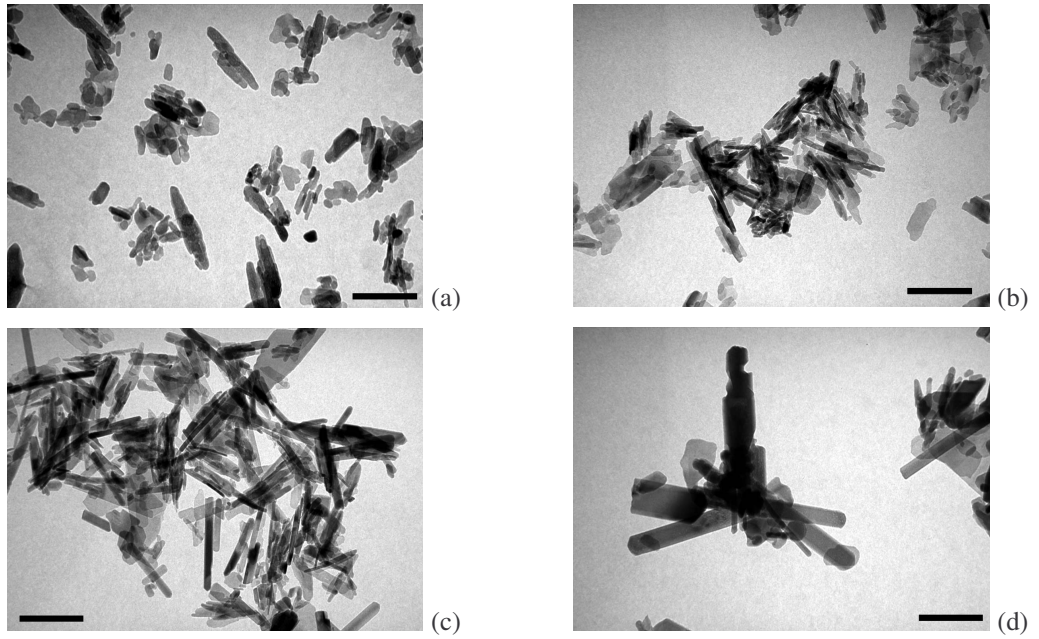


Fig. 19 - TEM micrographs of (a) Sr0; (b) Sr20; (c) Sr70; (d) Sr100 crystals. Scale bars = 200 nm.

Table 3 – Specific surface area measured on hydroxyapatite samples applying the BET method.

Samples	Surface Area (m ² /g)
Sr0	60
Sr10	60
Sr20	66
Sr30	72
Sr50	66
Sr70	44
Sr90	40
Sr100	26

For higher strontium contents, crystallite sizes progressively increase up to reach the maximum values in Sr-HA.

In order to acquire further information on the modifications of hydroxyapatite structure induced by strontium substitution for calcium, the samples were submitted to whole pattern fitting minimization procedure. The results of the structural parameters refinements are reported in *Table 5* for three selected samples.

Table 6 shows the relative data concerning metal cation distribution. The value of the overall strontium content of these samples, as obtained from the refinements without any constrain, is close to the results of the chemical analysis with the exception of sample Sr50 which exhibits a slightly lower value.

The comparisons between the observed and calculated profiles of Sr5, Sr10, Sr50 and Sr100 are displayed in *Figure 20*.

The structural refinements reveal that strontium atoms occupy both the M(1) and M(2) sites of the apatitic structure.

As regards the debated topic of strontium distribution, the results of *Table 6* show that at very low strontium content the occupancy of M(1) is higher than the statistical one, but when the strontium content increases the situation is reversed.

This result explains both the data of Kikuchi et al. that in hydrothermally grown single crystal containing 1.9 Sr atom % found a preferential substitution of Sr for Ca at M(1) site, and the data of other authors that in samples containing > 10 Sr atom % found a preferential Sr occupancy of M(2) sites [141].

Table 4 – Coherent lengths (τ_{hkl}) of the perfect crystalline domains in the direction normal to 002 and to 310 planes calculated using the Scherrer method.

Samples	τ 002 (Å)	τ 310 (Å)
Sr0	469 (5)	224 (6)
Sr3	408 (1)	222 (4)
Sr5	396 (1)	217 (4)
Sr10	385 (5)	153 (6)
Sr20	212 (7)	92 (7)
Sr30	168 (4)	86 (8)
Sr50	113 (4)	93 (5)
Sr70	293 (3)	190 (3)
Sr90	391 (6)	230 (2)
Sr100	490 (5)	305 (3)

The strontium replacement of the calcium at M(2) sites allows a better accommodation of the bigger strontium atoms because in this position metals atoms form “staggered” equilateral triangles centered on the apatitic channel, whereas in the M(1) site metals are strictly aligned in columns parallel to the c axis. At very low strontium content it is present only in a limited number of unit cells, and it is in M(1) site only in a fraction of them. As an example, in Sr5 which contains 3.5 Sr atom %, strontium is present only in one cell out of three, and it is in M(1) only in one cell out of five.

This suggests that the driving force in the distribution process is the optimization of metal-oxygen interaction: M(1) site allows to accommodate a larger cation because of the longer M(1)-O mean distances.

However, when the number of the bigger ions increases, the repulsion between atoms in M(1) position would cause an enlargement of the c-axis that is partially restrained by accommodating Sr atoms in site M(2).

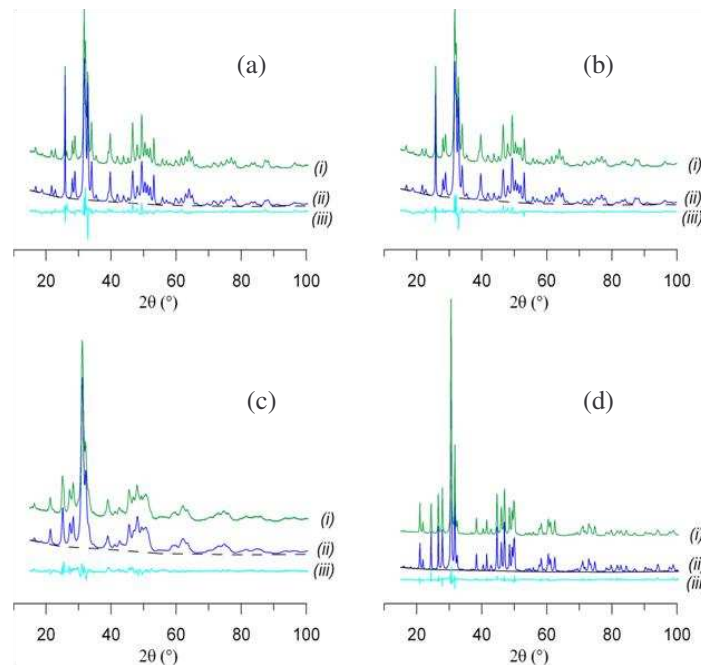


Fig. 20 - Comparison between (i) the observed, (ii) calculated and (iii) difference powder diffraction patterns of (a) Sr5, (b) Sr10, (c) Sr50 and (d) Sr100 samples. The dotted line represents the calculated background.

Although a preferential distribution for the cation is detected, the cell parameters plot exhibits a good linearity as a function of composition (*Figure 21*), likely because of the moderate difference from the statistic distribution in the two sites. In the case of mixed calcium-lead hydroxyapatite solid solutions the larger amount of preferential distribution provokes a significant discontinuity in the cell parameters variation [54].

Table 5 - Cell parameters, fractional atomic coordinates (nm), occupancy factors, atomic displacement parameters for mixed Ca-Sr-HA (e.s.d. in parentheses).

	x	Y	z	O.F.	Biso [Å ²]
Sr5	a=0.94437(3)	c=0.68918(2)	Rp=4.8	Rwp=6.2	
M(1)	0.3333	0.6667	0.0018(6)	0.016(1)*	2.81
M(2)	0.2442(5)	0.9929(6)	0.2500	0.013(1)*	2.81
P	0.4000	0.3690	0.2500	0.5000	2.0
O(1)	0.3318(4)	0.4846(5)	0.2500	0.5000	3.0
O(2)	0.5857(5)	0.4676(7)	0.2500	0.5000	3.0
O(3)	0.3411(5)	0.2617(6)	0.070(2)	1.0000	3.0
O(H)	0.0000	0.0000	0.1897(8)	0.1667	3.0
Sr10	a=0.94511(3)	c=0.69017(2)	Rp=3.6	Rwp=4.7	
M(1)	0.3333	0.6667	0.0029(5)	0.016(1)*	2.91
M(2)	0.2430(6)	0.9929(5)	0.2500	0.034(1)*	2.91
P	0.4000	0.3690	0.2500	0.5000	2.0
O(1)	0.3307(5)	0.4835(7)	0.2500	0.5000	3.0
O(2)	0.5855(7)	0.4685(5)	0.2500	0.5000	3.0
O(3)	0.3418(6)	0.2617(6)	0.070(1)	1.0000	3.0
O(H)	0.0000	0.0000	0.186(1)	0.1667	3.0
Sr50	a=0.96300(4)	c=0.71026(2)	Rp=2.6	Rwp=3.4	
M(1)	0.3333	0.6667	-0.0028(5)	0.122(2) *	2.86
M(2)	0.2415(7)	0.9879(7)	0.2500	0.256(3) *	2.86
P	0.4000	0.3690	0.2500	0.5000	2.0
O(1)	0.3352(7)	0.4842(6)	0.2500	0.5000	3.0
O(2)	0.5822(6)	0.4637(6)	0.2500	0.5000	3.0
O(3)	0.3411(6)	0.2638(6)	0.075(1)	1.0000	3.0
O(H)	0.0000	0.0000	0.1890(9)	0.1667	3.0

* Relative to strontium atoms

The pattern R-factor Rp is defined as $R_p = 100 \{ \sum |Y_{oi} - Y_{ci}| / \sum Y_{oi} \}$

The weighted pattern R-factor Rwp is defined as $R_{wp} = 100 \{ \sum w_i (Y_{oi} - Y_{ci})^2 / \sum w_i (Y_{oi})^2 \}^{1/2}$.

The refinement of the SrHA sample was performed only with the idea to compare and validate the procedure. The single crystal data perfectly fitted the experimental ones and gave non-crystallographic parameters very similar to those found for the other samples. The atomic coordinates of the Ca-Sr-HA solid solutions are very similar and no significant variation in the atom positions is appreciated [142].

Cell proliferation and markers of osteoblast synthetic activity were tested to evaluate osteoblasts behavior when cultured on Sr-HA at different Sr contents. The tests were carried out on samples Sr0%, Sr3%, Sr5% and Sr10%, which contain strontium amount in a biologically relevant range (0, 1, 3, 7% respectively).

Table 6 – Strontium distribution over metal sites.

Sample	Sr/cell	Refinement distribution (A)		Statistic distribution (B)		(A-B / B)	
		M(1)	M(2)	M(1)	M(2)	M(1)	M(2)
Sr5	0.35	0.20	0.15	0.14	0.21	+0.41	-0.27
Sr10	0.59	0.19	0.41	0.24	0.35	-0.21	+0.15
Sr50	4.54	1.46	3.07	1.82	2.72	-0.20	+0.13

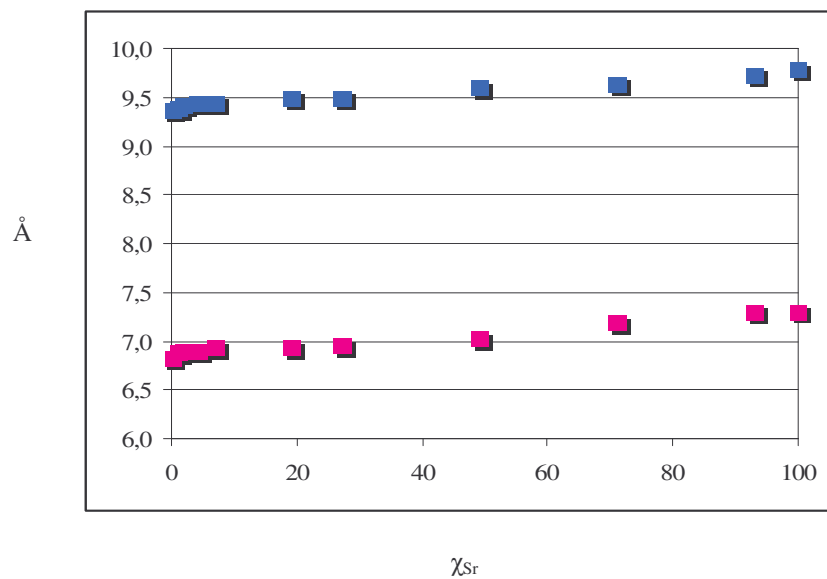


Fig. 21 – Plot of the hydroxyapatite cell parameters a (pink squares) and c (azure squares) as a function of Sr amount (χ_{Sr}).

Osteoblast proliferation increases up to 14 days, and then it decreases. No significant difference was found among all groups at 7 and 21 days, whereas in the other experimental times osteoblasts cultured on Sr10 showed significantly greater proliferation when compared to Sr0. In brief, cells grow on Sr0 reference samples as well as on Sr3 and Sr5, whereas on Sr10 they reach statistically higher values (*Figure 22(a)*).

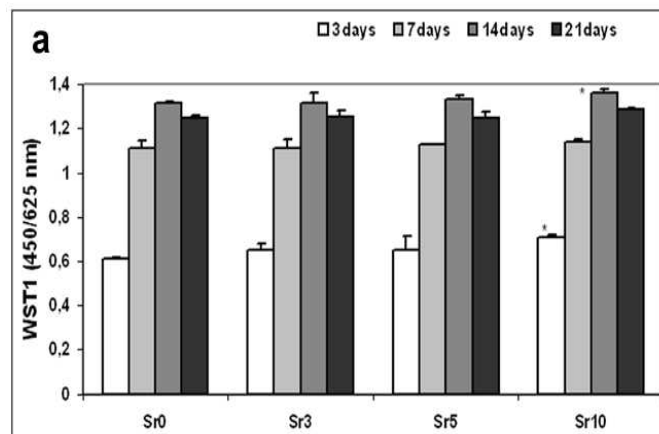
ALP activity is generally higher in Sr5 and Sr10 groups than in Sr3 and Sr0 groups.

In particular, the highest value of ALP activity was recorded for Sr10 at 14 days, whereas it decreases at 21 days (*Figure 22(b)*). The production of CICP was not influenced at 3 days, whereas at 7, 14, and 21 days CICP level was significantly higher in Sr5 and Sr10 groups when compared to Sr0 and Sr3 (*Figure 22(c)*). No differences were found for OC at 3 and 7 days among groups, but at 14 and 21 days OC was significantly higher in Sr5 and Sr10 in comparison with Sr0 and Sr3 groups (*Figure 22(d)*). These results are consistent with the different properties of the examined parameters.

ALP is an early expression of a more differentiated state, osteoblast phenotype and differentiation, with the production of CICP, while OC is late marker of osteoblast differentiation. Furthermore, they indicate that the presence of strontium in the samples promotes osteoblast differentiation and activity.

Strontium also affects osteoclast culture, as shown by the significant reduction of cell proliferation on Sr3, Sr5, and Sr10 samples in comparison with Sr0 (*Figure 23*).

SEM images show cells with the typical features of functional osteoclasts. Osteoclasts grown on Sr0 are large, flat cells with a ruffled border (characteristic morphology of osteoclasts grown in vitro), as shown in *Figure 23(a)*.



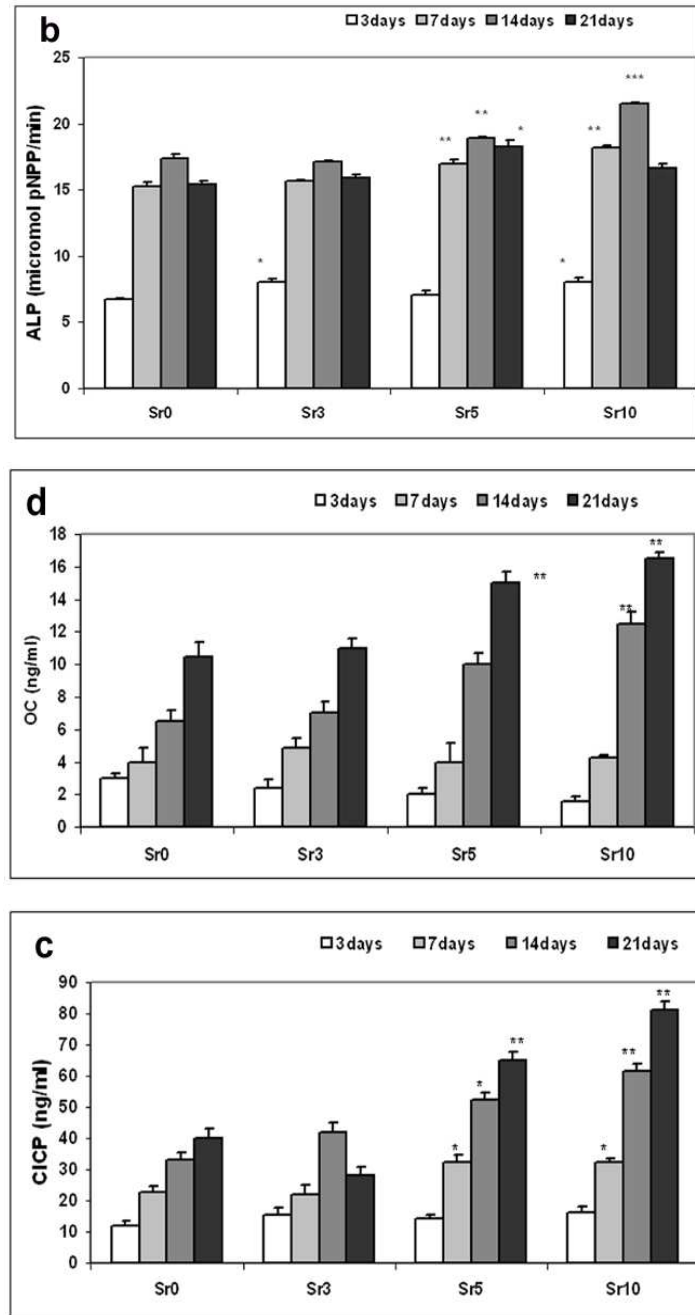


Fig. 22 - Proliferation, differentiation, and synthetic activity of MG63 after 3, 7, 14, and 21 days of culture on samples of Sr0, Sr3, Sr5, and Sr10. Mean, n 5 6 triplicates (* $p < 0.05$; ** $p < 0.005$; *** $p < 0.0005$). (a) WST1: 3 and 14 days, pp*Sr10 versus Sr0; 7 and 21 days, n.s. (b) ALP: 3 days, *Sr3, Sr10 versus Sr0; 7 days, **Sr5, Sr10 versus Sr0, Sr3; 14 days, **Sr5 versus Sr0, Sr3; ***Sr10 versus Sr0, Sr3; 21 days, *Sr5 versus Sr0, Sr3, Sr10. (c) CICP: 3 days, n.s.; 7 days, *Sr5, Sr10 versus Sr0, Sr3; 14 days, *Sr5 versus Sr0, Sr3 and **Sr10 versus Sr0, Sr3; 21 days, **Sr5, Sr10 versus Sr0, Sr3. (d) OC: 3 and 7 days, n.s.; 14 days, ** Sr10 versus Sr0, Sr3, Sr5; 21 days, ** Sr5, Sr10 versus Sr0, Sr3.

These cells are polymorphic, suggesting active motility, and have some vesicles associated with the ruffled border. Osteoclast grown on Sr containing samples generally show less filopodia and develop less ruffled borders, suggesting an inhibitory effect of Sr on the bone-resorbing activity, as it can be observed in *Figures 23(b)* and *23(c)* for Sr5 and Sr10, respectively.

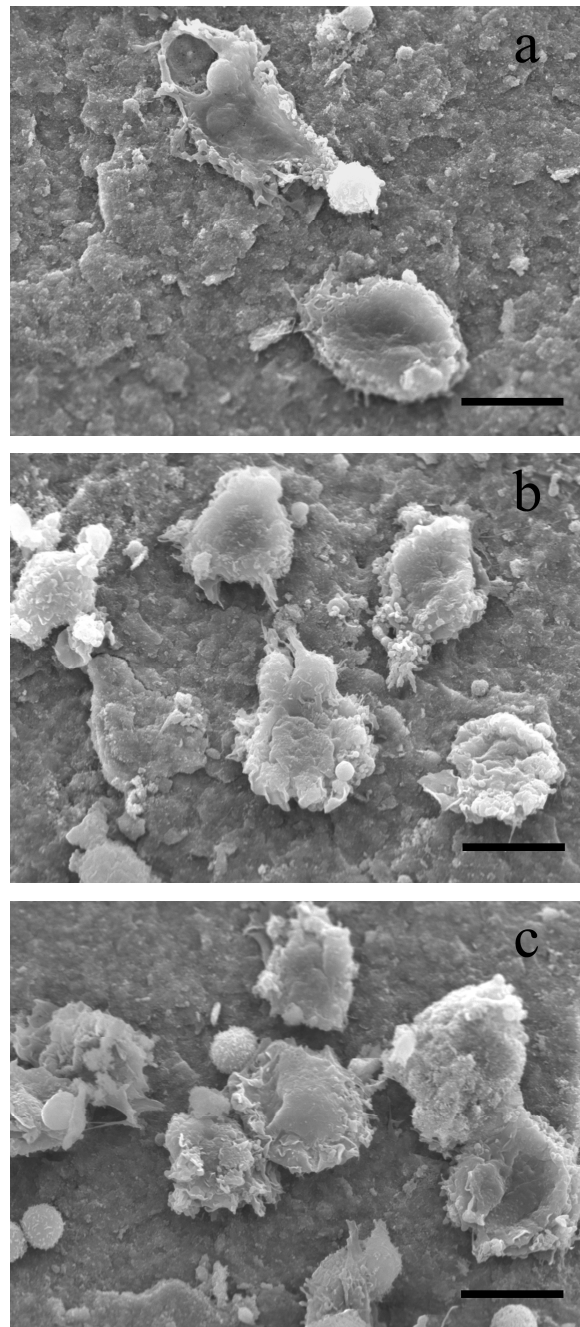


Fig. 23 – SEM images of osteoclasts growth on Sr0 (a), Sr5 (b) and Sr10 (c) substrates (scale bars = 10 μm).

Previous results showed that Sr salts enhance bone cell replication and bone formation in vitro, with a dose dependent effect, both when directly administered in cell culture, and when associated to calcium-phosphate scaffolds. Moreover the significant effect of Sr on osteoclast culture is in agreement with its inhibiting role on bone resorption through reduction of osteoclast activity and viability [112].

5.2 Pulsed Laser Deposited Sr-Hydroxyapatite

Sr-hydroxyapatite, in the same range of strontium content, were used to coat titanium substrates by means of Pulsed Laser Deposition in order to improve the bioactivity of titanium.

The XRD patterns of the PLD thin films are shown in *Figure 24*. All the patterns are consistent with the presence of HA as the sole crystalline phase. In agreement with the data obtained from the powders, patterns in *Figure 24* show a slight broadening of the diffraction peaks, consistent with a shortening of the perfect crystalline domains, where strontium concentration was increased. However, the resolution of the patterns was quite good, indicating a relatively high degree of crystallinity of the coatings, at variance with what was recently reported on plasma-sprayed strontium-substituted HA.

SEM images in *Figure 25* show that the thin films displayed granular surfaces, with grains smaller than 1 μ m on average. The presence of Sr²⁺ had no significant effect on the morphology of the coatings, which remained very similar to those previously obtained from apatites of different compositions.

Nevertheless, EDS investigation results clearly indicated the presence of increasing amounts of strontium in the coatings deposited from Sr1 (Sr content: 0.5%), Sr5 (Sr content: 3%) and Sr10 (Sr content: 7%), as can be seen in *Figure 26*.

This confirmed that PLD was able to produce thin films with a composition close to that of the initial powders. Furthermore, the EDS maps in *Figure 26* are consistent with a homogeneous strontium distribution on the surface of the thin films. The presence of strontium significantly improved osteoblast adhesion in early culture phases. In fact, cell adhesion increased with increasing strontium content in the coating, as illustrated in *Figure 27(a-d)*.

Furthermore, strontium influenced cell proliferation and viability (WST-1 test). Significant differences were found at all experimental times (*Figure 28(a)*). In particular, values recorded for TiSr5 and TiSr10 were significantly higher than those in other groups, and those obtained for TiSr1 were also significantly higher as compared with TiHA both after 14 days ($P < 0.001$) and 21 days ($P < 0.0001$).

Osteoblast activity and differentiation were tested through the analysis of selected markers, namely ALP, OC and CICP, after 7, 14 and 21 days of culture. The results indicated that all markers of osteoblast activation and differentiation were improved in proportion to the concentration of strontium in the coating.

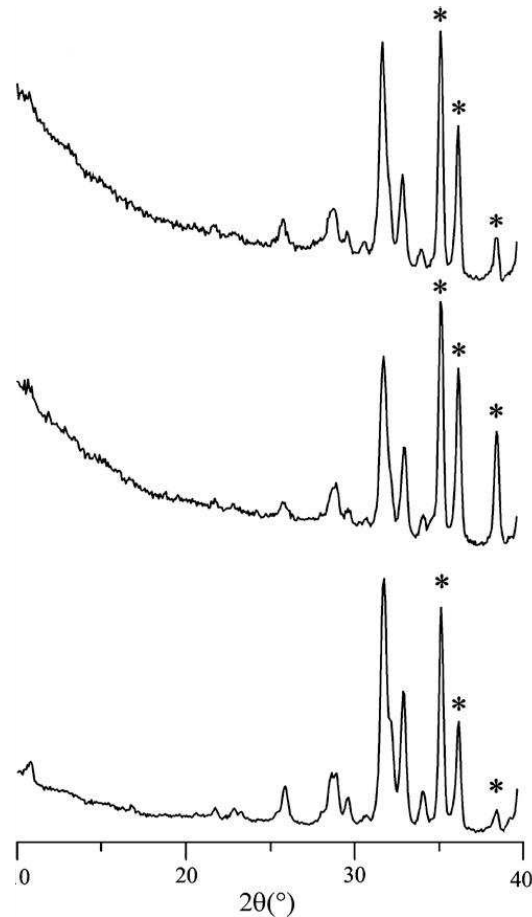


Fig. 24 - Thin film XRD patterns of the coatings deposited from Sr0 (the first on the bottom), Sr5 (in the middle) and Sr10 (on the top) samples on Ti substrates. Asterisks indicate the reflections due to Ti.

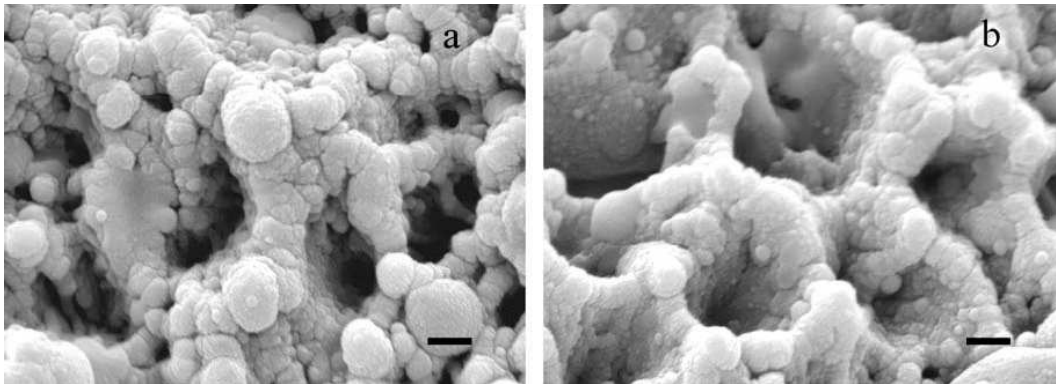


Fig. 25 - SEM micrographs of thin films deposited from (a) Sr0 and (b) Sr10 samples. Scale bars = 1µm.

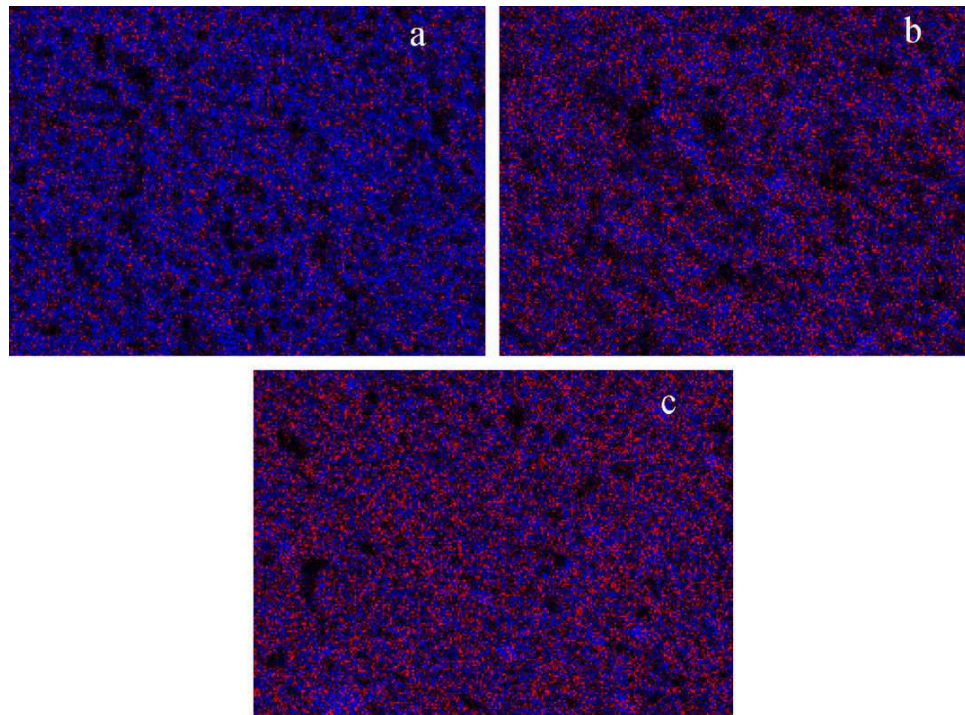


Fig. 26 - EDS maps recorded from the coatings: (a) TiSr1; (b) TiSr5; (c) TiSr10. Blue: Ca; red: Sr.

ALP showed no differences among the groups after 7 days, but both the TiSr5 ($P < 0.005$ and 0.05) and TiSr10 ($P < 0.0001$) groups revealed significantly high values of ALP activity after 14 and 21 days (*Figure 28(b)*).

A similar trend was observed for osteocalcin production (*Figure 28(c)*), which showed significant increases in the TiSr5 and TiSr10 groups as compared with TiHA. In

this case, the highest level of OC production was reached after 21 days of culture, whereas the highest values of ALP activity were recorded after 14 days. This is in agreement with earlier reports of an increased expression of ALP as compared with OC production during osteoblast differentiation. Also, the production of CICP, as one of the major components forming the extracellular matrix, usually occurred later than ALP during differentiation. Accordingly, all the samples showed the highest values of CICP production after 21 days, with TiSr10 displaying a value significantly higher than those recorded in the other samples (*Figure 28(d)*).

SEM analyses were performed to evaluate the morphology of cells grown on the different materials after 21 days of culture. Osteoblast cell morphologies on TiHA, and on the strontium-containing coatings are shown in *Figures 29(a–c)*.

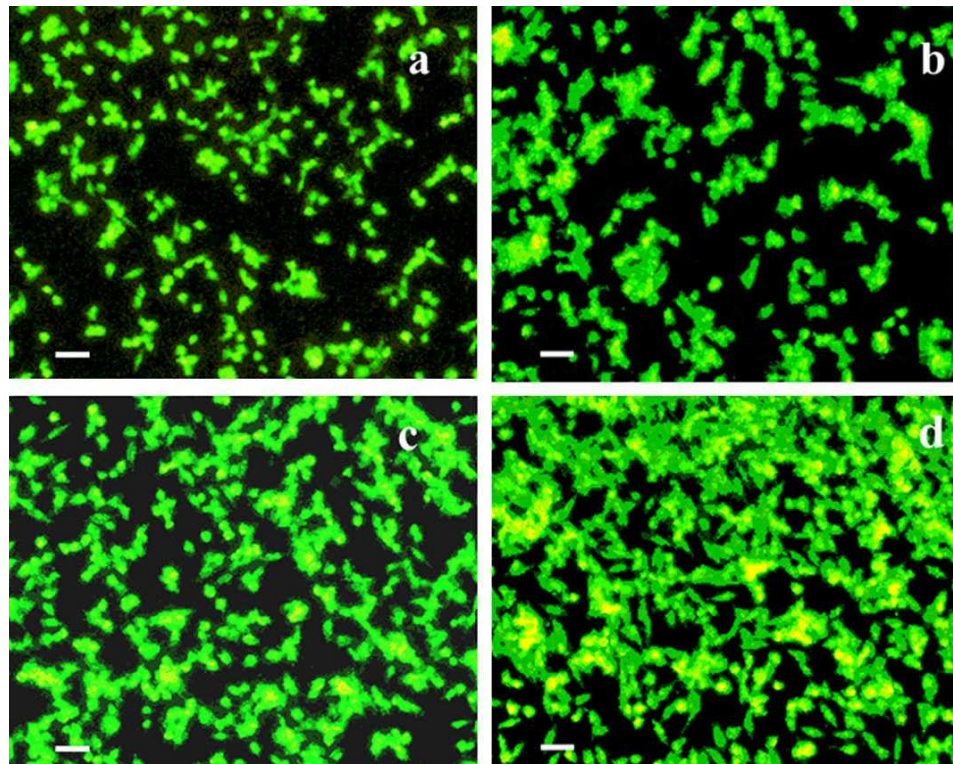


Fig. 27 - Phalloidin staining and percentage of osteoblast adhesion to biomaterial surfaces of culture (percent of examined area) 1 hour after seeding on (a) TiHA, ($42 \pm 4\%$); (b) TiSr1, ($48 \pm 8\%$); (c) TiSr5, ($58 \pm 5\%$); and (d) TiSr10, ($71 \pm 13\%$). TiSr5, TiSr10 vs. TiHA ($P < 0.05$). Bars = 50 μm .

The osteoblasts were observed to attach and spread on the various coatings. On TiHA substrates (*Figure 29(a)*), most of the cells exhibited their phenotypic morphology: the

osteoblasts were flattened, had polygonal configuration and dorsal ruffles, and were well attached to the substrate by cellular extension.

Cells grown on strontium-doped HA coatings, however, appeared much more flattened and better spread across the surface. The positive effect of strontium on osteoblast spreading and proliferation is evident even at the smallest concentration of strontium on the coating.

However, the expressions of the differentiation markers on TiSr1 sample (0.5 at.% Sr) were never statistically greater than those recorded on TiHA.

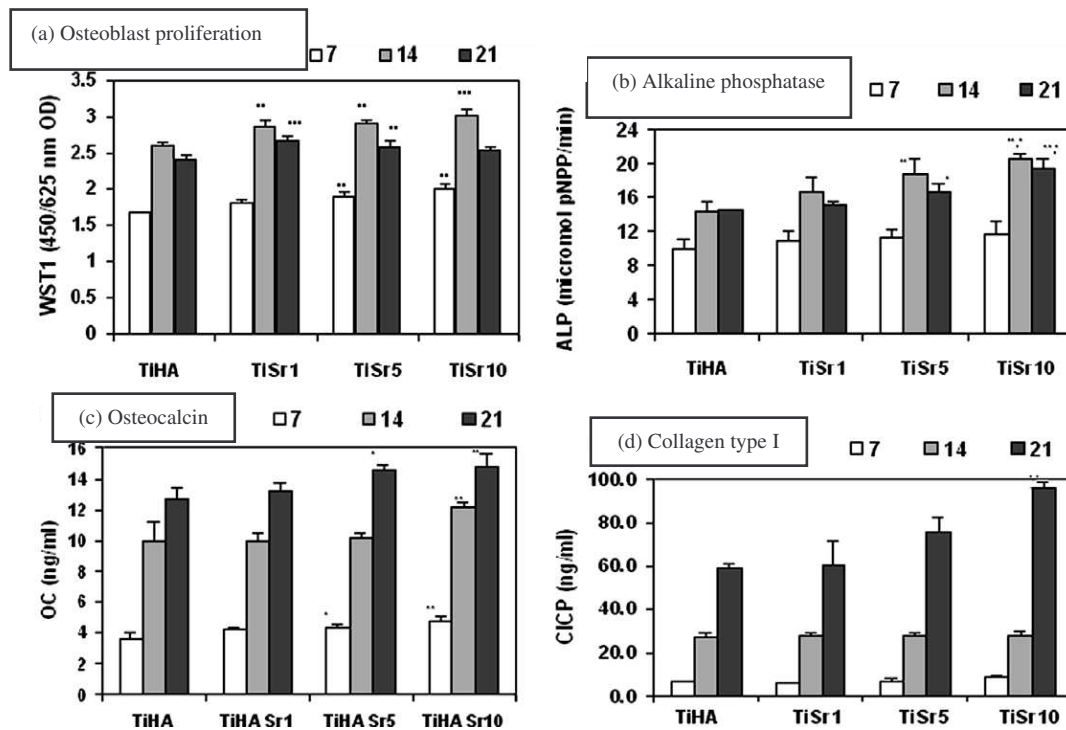


Fig. 28 - Osteoblast proliferation and activity after 7, 14 and 21 days of culture on biomaterials. Mean, n = 6 triplicates (*P < 0.05; **P < 0.005; ***P < 0.0005): (a) WST1. 7 days: **TiSr5 vs. TiHA, ***TiSr10 vs. TiHA, TiSr1; 14 days: **TiSr1, TiSr5 vs. TiHA, ***TiSr10 vs. TiHA; 21 days: ***TiSr1 vs. TiHA, **TiSr5 vs. TiHA. (b) ALP. 7 days: NS; 14 days: **TiSr5 vs. TiHA; **TiSr10 vs. TiSr1, ***TiSr10 vs. TiHA; 21 days: *TiSr5 vs. TiHA, **TiSr10 vs. TiHA, TiSr1. (c) OC. 7 days: *TiSr5 vs. TiHA, **TiSr10 vs. TiHA; 14 days: **TiSr10 vs. TiHA, TiSr1, TiSr5; 21 days: *TiSr5 vs. TiHA, **TiSr10 vs. TiHA, TiSr1. (d) CICP. 7 days: *TiSr10 vs. TiHA, TiSr1; 14 days: n.s.; 21 days: *TiSr5 vs. TiHA, TiSr1, *TiSr10 vs. TiSr5, ***TiSr10 vs. TiHA, TiSr1.

At variance, the values of ALP, OC and CACP on TiSr5 (3 at.% Sr) and TiSr10 (7 at.% Sr) were significantly greater than those recorded on TiHA for most of the experimental times. At 21 days the highest expressions of the differentiation markers were obtained on TiSr10, with values of ALP, OC and CACP significantly greater than those obtained for TiHA and TiSr1. A significant enhancement of osteoblast response has been recently reported also for silicon-substituted HA coatings deposited by magnetron co-sputtering. High cell growth, well-organized cytoskeletal architecture and enhanced osteoblast biomineralisation observed on Si-HA indicated that Si promotes osteoblast metabolism. The cellular actions of strontium have not been fully identified, although several mechanisms of action, including activation of the calcium-sensing receptor in some cell types, have been postulated.

However, it is evident that Sr inhibits bone resorption and promotes bone formation, and it acts both on osteoblast and osteoclast.

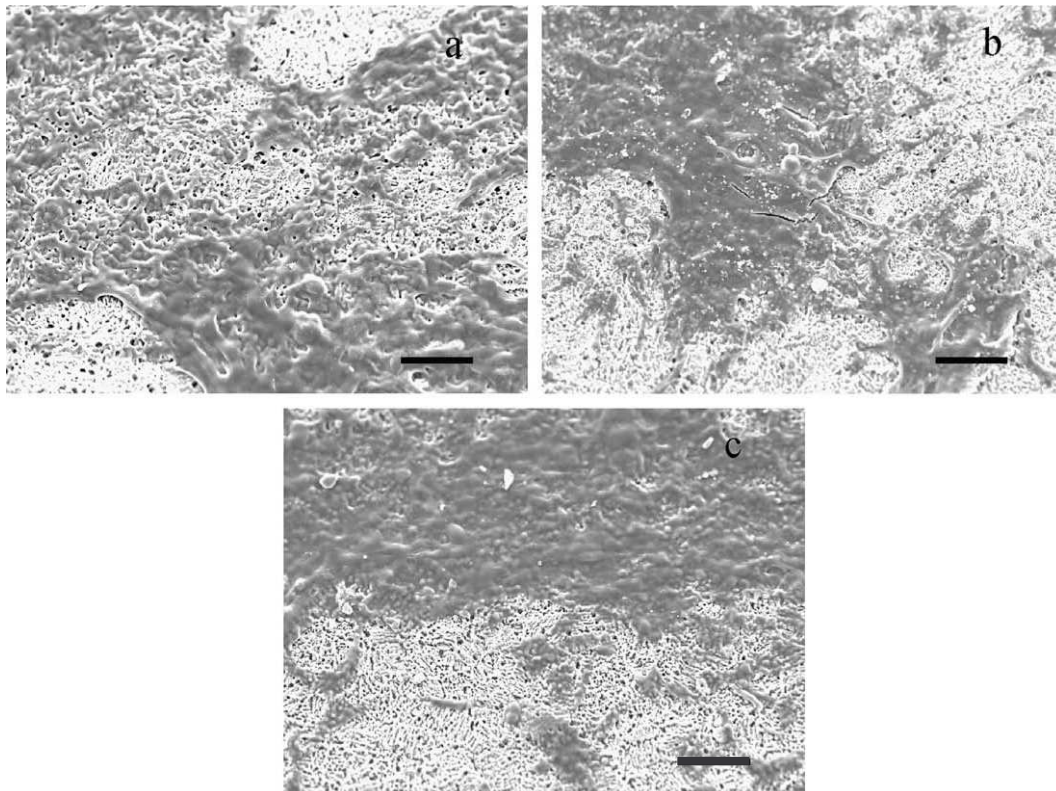


Fig. 29 - SEM micrographs of osteoblasts after 21 days of culture on (a) TiHA, (b) TiSr5 and (c) TiSr10. Scale bars = 50 μm .

Accordingly, the OPG/TRANCE ratio produced by osteoblasts cultured up to 21 days on tested biomaterials showed significantly higher values in TiSr5 (1.41 ± 0.03 , $P < 0.0001$) and TiSr10 (1.24 ± 0.04 , $P < 0.05$) as compared with TiSr1 (1.14 ± 0.05) and TiHA (1.19 ± 0.03), as shown in *Figure 30*.

OPG is a member of the TNF receptor family expressed by osteoblasts. It is a regulator of bone metabolism and has been shown to act as a potent inhibitor of osteoclast differentiation and activation. Its role is linked to Trance, which induces osteoclastogenesis and osteoclast activation. Thus, the increased values of the OPG/Trance ratio found for the TiSr5 and TiSr10 coatings indicated that strontium concentrations greater than 3 at. % inhibit osteoclast production and differentiation. Accordingly, the results of osteoclast proliferation 21 days after seeding on biomaterials indicated a significant reduction in cell numbers (TiSr5, TiSr10 vs. TiHA, $P < 0.05$) in correlation with the Sr increase in the HA coatings, as shown also by the images of fluorescent staining reported in *Figures 31(a-d)*.

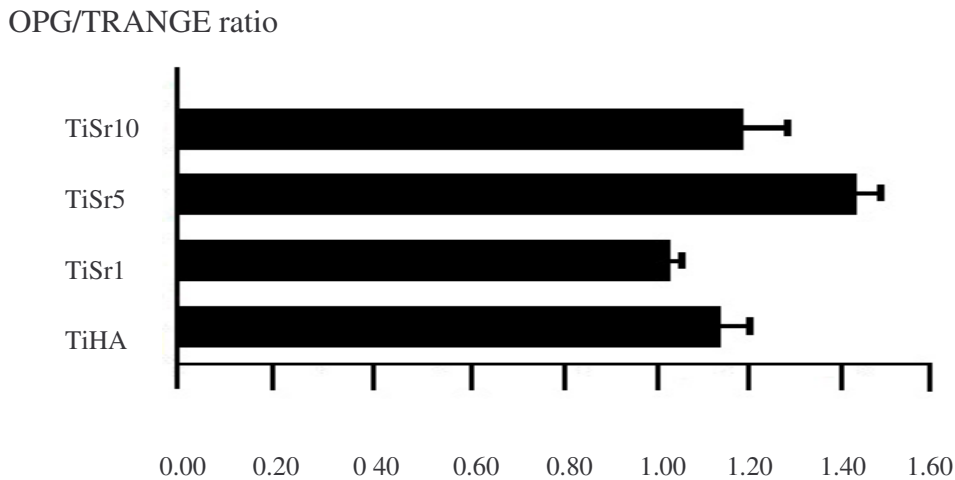


Fig. 30 - Evaluation of osteoprotegerin and Trance production by cells cultured for 21 days on tested biomaterials.

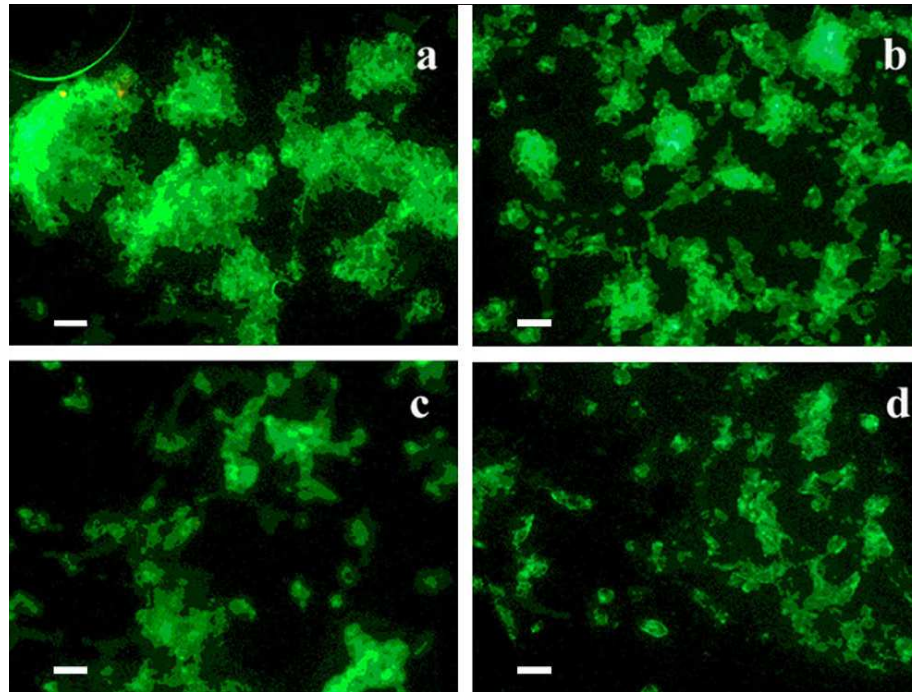


Fig. 31 - Phalloidin staining and proliferation (WST1 test) of osteoclast culture 21 days after seeding on (a) TiHA (3.285 ± 0.021); (b) TiSr1 (3.252 ± 0.047); (c) TiSr5 ($3.211 \pm 0.008^*$); and (d) TiSr10 ($3.193 \pm 0.019^*$). *TiSr5, TiSr10 vs. TiHA ($P < 0.05$). Scale bars = 50 μm .

5.3 Alendronate-Hydroxyapatite Nanocrystals

In-vitro tests demonstrated that alendronate is able to promote osteoblast activation and extra-cellular matrix mineralization processes, and to inhibit osteoclast proliferation even if incorporated in the composite nanocrystals. On the basis of these promising results, MAPLE technique was applied to deposit thin films of alendronate-HA nanocrystals on Ti substrates. MAPLE to the difference of PLD, in fact, is expected to avoid possible damage of alendronate. Sets of thin structures such as simple HA, HA doped with 3% alendronate and HA doped with 7% alendronate, were deposited by MAPLE on chemically etched Ti substrates.

The X-ray analysis carried of the thin films obtained by MAPLE technique reveal that the degree of crystallinity of the coatings deposited onto Ti substrates appears rather low (*Figure 32*). However, the pattern clearly exhibits the peaks characteristic to HA, besides to those characteristic to Ti around 35° of 2θ .

The results of the structural refinements carried out on the composite nanocrystals were interpreted as suggesting that alendronate interacts with calcium ions through a bidentate chelation of deprotonated oxygen atoms of the bisphosphonate anion without greatly affecting the crystal structure of HA [117].

SEM images of the coatings (*Figure 33 (a, b)*) show that the deposits consist of grains smaller and less defined with respect to those usually obtained through PLD.

After evaluation of the synthesized nanostructures, the optimal deposition conditions were established as described in *Table 7*.

These data are of high biological relevance since they indicate that it is possible to use MAPLE to synthesize a coating that combines the bioactivity of HA with the local availability of alendronate.

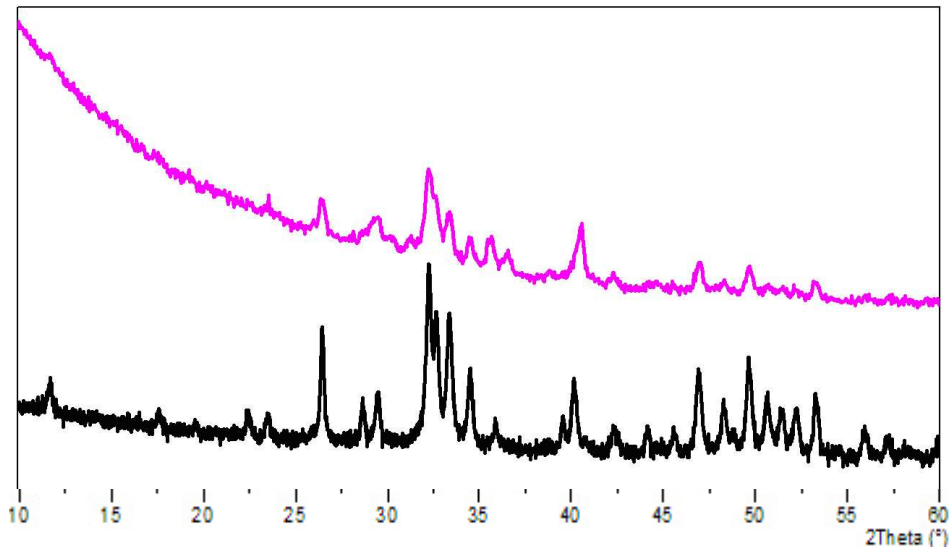


Fig. 32 - The powder X-ray diffraction patterns of HA nanocrystals containing 7 % wt of alendronate (black line); and MAPLE coating synthesized from the same alendronate-doped HA (pink line).

Table 7 - Deposition conditions of Al-HA coatings obtained by MAPLE.

Sample	Target	Substrate	Substrate T(°C)	Pressure (torr)	Distance target-substrate (cm)	Fluence (J/cm ²)	No. of pulses
HA	HA	Ti	30	10 ⁻¹	4	0.75	20.000
HA-AL7	HA-AL7	Ti	30	10 ⁻¹	4	0.75	20.000
HA-AL28	HA-AL28	Ti	30	10 ⁻¹	4	0.75	20.000

The results of *in vitro* tests indicated that alendronate promotes osteoblast proliferation and viability.

At 1, 7 and 14 days osteoblast proliferation was assessed by WST1 test (*Figure 34*). Recorded values showed that osteoblasts grew regularly on all substrates when compared to control (cells on culture plates without biomaterials), but at all experimental times HA-AL7 and HA-AL28 groups were significantly higher than HA (1, 7 and 14 days) and Ti (1 and 7 days) groups.

On culture supernatant the following parameters were evaluated at 7 and 14 days: ALP and CICP as early differentiation markers, OC as later mineralization marker, and OPG and RANKL as index of bone formation/resorption balance during the last stage of differentiation.

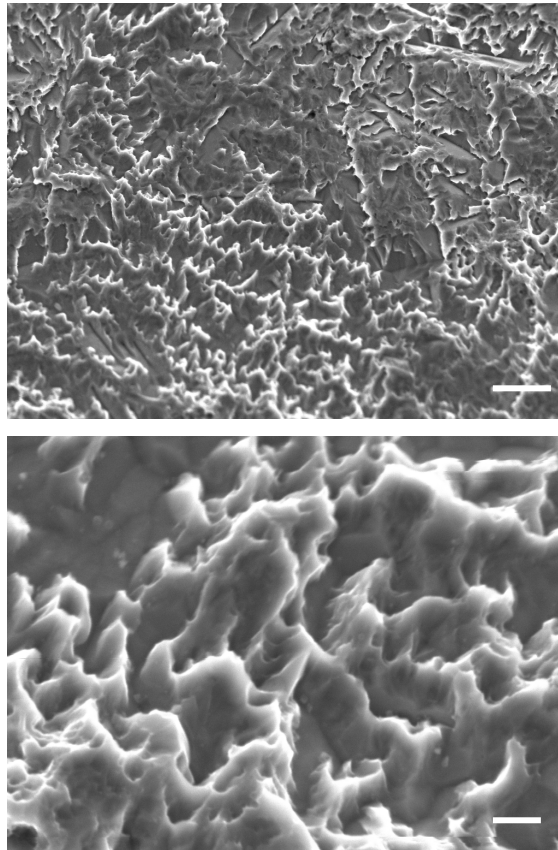


Fig. 33(a, b) - SEM micrographs of thin films deposited from HA containing 7 % wt of alendronate at two different enlargements. Scales bar = 2 μm (a) and 10 μm (b).

The evaluation of ALP activity showed no differences among groups at 7 days, while at 14 days Ti group showed significant lower values than other groups (*Figure 35(a)*).

The production of CICP was significantly higher in both HA-AL7 and HA-AL28 when compared to HA (7 and 14 days) and Ti (7 days) (*Figure 35(b)*).

The level of OC also at 7 days was significantly higher in both HA-AL7 and HA-AL28 when compared to HA and Ti groups, even if at 14 days no differences were found among groups (*Figure 35(c)*).

The results demonstrated that in the presence of alendronate osteoblasts seem to show an higher rate of proliferation and earlier differentiation when compared to other groups.

OPG and RANKL have been also implicated in bone metabolism. Specifically, the balance of these factors is believed to be key in determining the rate of osteoclastogenesis and the net outcome of bone formation/resorption. Alendronate not only significantly improves the OPG production (HA-AL28 at 14 days when compared to other groups, $p < 0.05$), but also led to a reduction of RANKL expression (HA-AL7 and HA-AL28 at 14 days when compared to other groups, $p < 0.05$).

The results of OPG/RANKL ratio (*Figure 35(d)*) were significantly higher in alendronate groups both at 7 and 14 days, demonstrating that alendronate influences osteoblast metabolism, increasing the release of soluble OPG relative to RANKL and favouring a bone-forming (and resorption-inhibiting) event. Therefore, an increased OPG/RANKL ratio could favour bone formation and contribute to successful osseointegration.

SEM analyses were performed to evaluate the morphology of cells grown on the different materials after 14 days of culture. *Figures 36(a–d)* show that the osteoblasts attach and spread on the various coatings. Most of the cells exhibit their phenotypic morphology: the osteoblasts are flattened, display polygonal configuration and dorsal ruffles, and are well attached to the substrate by cellular extensions.

Cells grown on HA coatings, and even more on HA-AL7 and HA-AL28 coatings, appear more flattened and better spread across the surface than those on bare Ti.

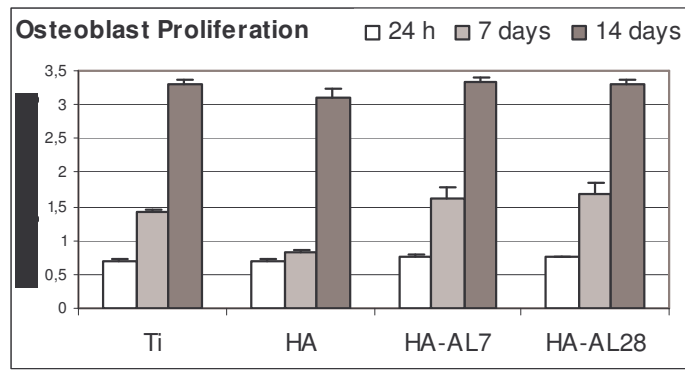


Fig. 34 - Proliferation of MG63 (WST1 tests) after 1, 7 and 14 days of culture on samples of Ti, HA, HA-AL7 and HA-AL28. Mean \pm sd, n = 3. (* = $p < 0.05$; ** = $p < 0.005$; *** = $p < 0.0001$); 1 day: *HA-AL7 versus Ti, HA; *HA-AL28 versus HA; 7 days: ***HA versus Ti, HA-AL7, HA-AL28; 14 days: *HA versus HA-AL7, HA-AL28.

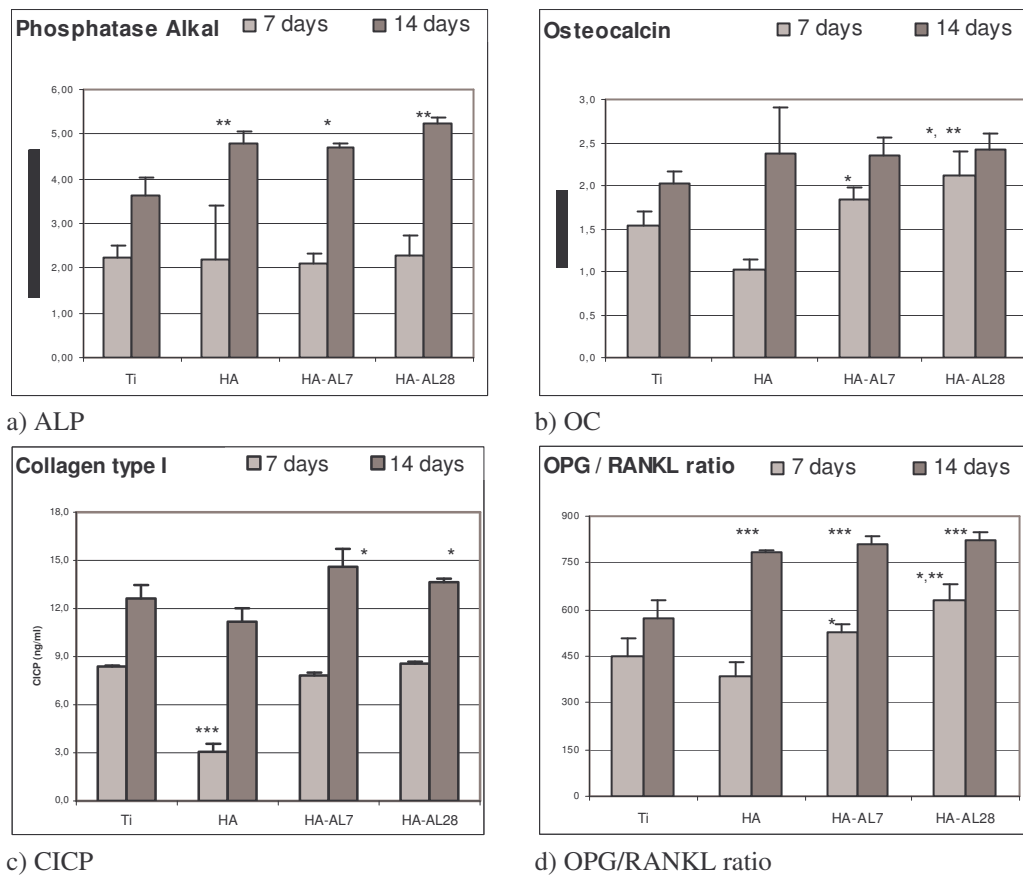


Fig. 35(a-d) - Differentiation and synthetic activity of MG63 after 7 and 14 days of culture on samples of Ti, HA, HA-AL7 and HA-AL28. Mean \pm sd, n = 3. (* = $p < 0.05$; ** = $p < 0.005$; *** = $p < 0.0001$):

(a) ALP. 7 days: ns; 14 days: **HA, HA-AL28 versus Ti; *HA-AL7 versus Ti.

(b) OC. 7 days: *HA-AL7 versus HA; *HA-AL28 versus Ti; **HA-AL28 versus HA; 14 days: ns.

(c) C1CP. 7 days: ***HA versus Ti, HA-AL7, HA-AL28; 14 days: * HA-AL7, HA-AL28 versus HA.

(d) OPG/RANKL ratio. 7 days: *HA-AL7 versus HA; *HA-AL28 versus Ti; **HA-AL28 versus HA; 14 days: ***Ti versus HA, HA-AL7, HA-AL28.

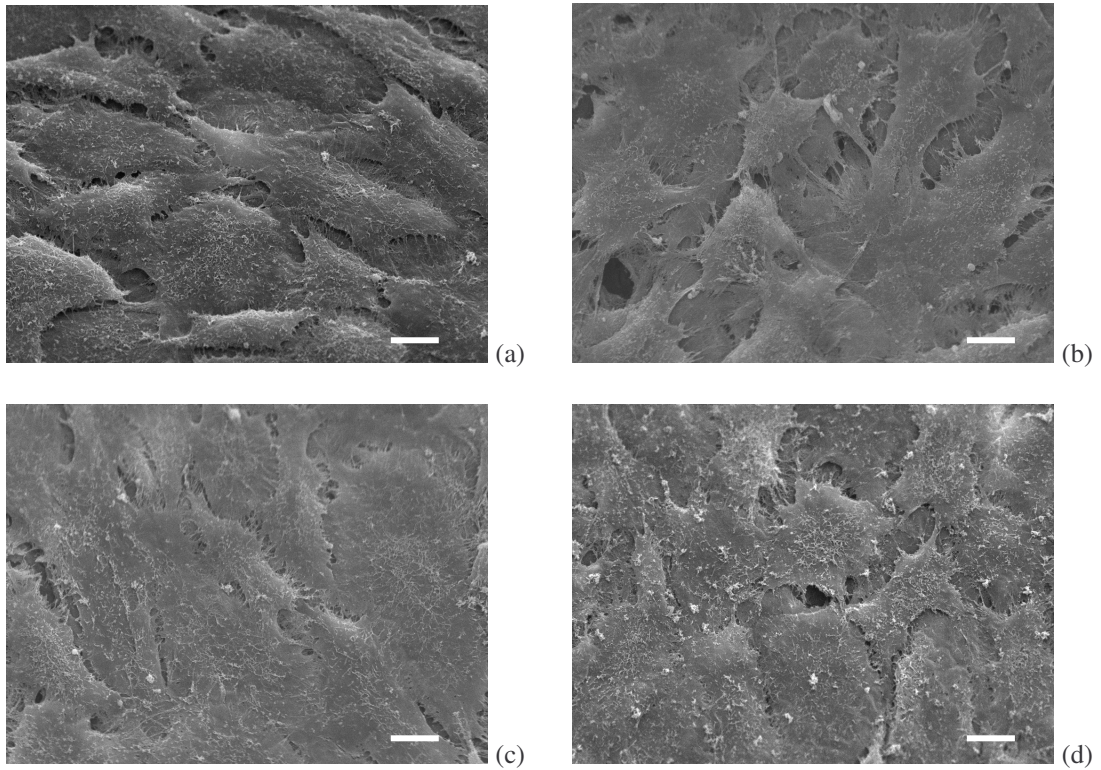


Fig. 36(a-d) - SEM micrographs of osteoblasts after 14 days of culture on Ti (a), HA (b), HA-AL7 (c) and HA-AL28(d).

5.4 Bivalent Ions Modified OCP

OCP was synthesized in the presence of increasing amounts of Sr, Mg and Mn ions.

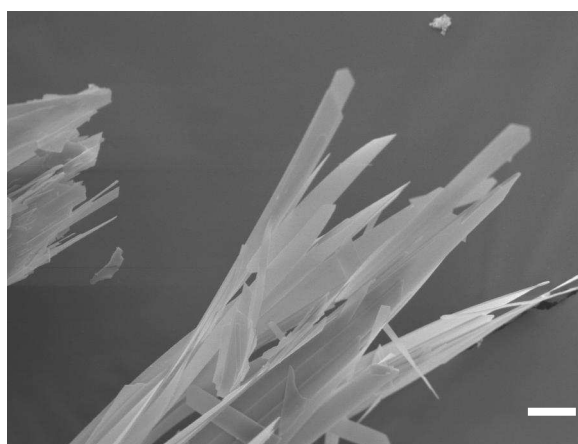
The first step of this study consisted in the optimization of OCP synthesis aimed to obtain separated crystals. The following parameters were considered: the temperature (60 or 70°C), the total time used to drop $\text{Ca}(\text{COO})_2 \cdot \text{H}_2\text{O}$ into the phosphates solution, that is 1 hour, 40 or 20 minutes, and the speed of mechanical stirring (1 round every 2 seconds, 2 rounds per second, 5 rounds per second). The results of these optimization tests are resumed in the following tables (*Tables 8 and 9*). It is interesting to mention that only at 70 °C, with 2 circles per second and in one hour dropping it is possible to obtain separate OCP crystals (*Figure 37*).

Table 8 - Morphology of OCP crystals obtained by varying dropping and stirring speeds at 60°C.

T = 60°C	1 h dropping	40 min dropping	20 min dropping
1 round / 2 seconds	separate crystals + spherules	aggregate crystals	aggregate crystals
2 rounds / 1 seconds	spherules	spherules	spherules+DCPD
5 rounds / 1 seconds	spherules	aggregate crystals	aggregate crystals

Table 9 - Morphology of OCP crystals obtained by varying dropping and stirring speeds at 70°C.

T = 70°C	1 h dropping	40 min dropping	20 min dropping
1 circle / 2 seconds	separate and aggregate crystals	aggregate crystals	aggregate crystals
2 circle / 1 second	separate crystals	separate but disordered crystals	aggregate crystals
5 circle / 1 second	Separate but disordered crystals	spherules	spherules

**Fig. 37** - SEM image of separated OCP crystals obtained at 70°C, with 1 hour dropping phosphates solution, with a speed of stirring = 2 circles/1 sec (scale bar = 10 μm).

5.4.1 Strontium Substitution

Increasing amounts of $\text{Sr}(\text{COO})_2 \cdot \text{H}_2\text{O}$, covering all the range of percentages, were added along with $\text{Ca}(\text{COO})_2 \cdot \text{H}_2\text{O}$ in the reaction solutions.

The XRPD patterns demonstrated that OCP phase was obtained at 70°C (Figure 39). Anyway, the introduction of even small amounts of a different ion deeply affects the resulting crystal morphology (Figure 40). Just a little amount of strontium ions provokes the aggregation of single crystals (Sr 5%) to form a spherule (Sr 10%), while at relatively higher Sr concentration the products consist of disordered aggregates (Sr 50%). At concentration higher than 80% no precipitate was observed. The crystal phases obtained at the different concentrations are reported in Table 10. Quite different results, not only in morphology but also in the crystal phases, were observed at 60°C .

At 60°C OCP precipitates together with DCPD only up to 5% Sr in solution. Then, only DCPD precipitation was observed. From 60% to 90% of strontium no CaP compound precipitated while at 100% Sr, SrHPO_4 was obtained.

Attention has been focused on those samples constituted only of OCP, that is on the products obtained at 70°C .

As results by the EDS analysis (Figure 41), Sr is present in the OCP powder. The results of the powder pattern fitting carried out with the Rietveld method (Figure 42), show that the cell parameters increase on passing from OCP to Sr10%-OCP to Sr15%-OCP, suggesting a partial replacement of Ca with Sr in the OCP structure (Table 11).

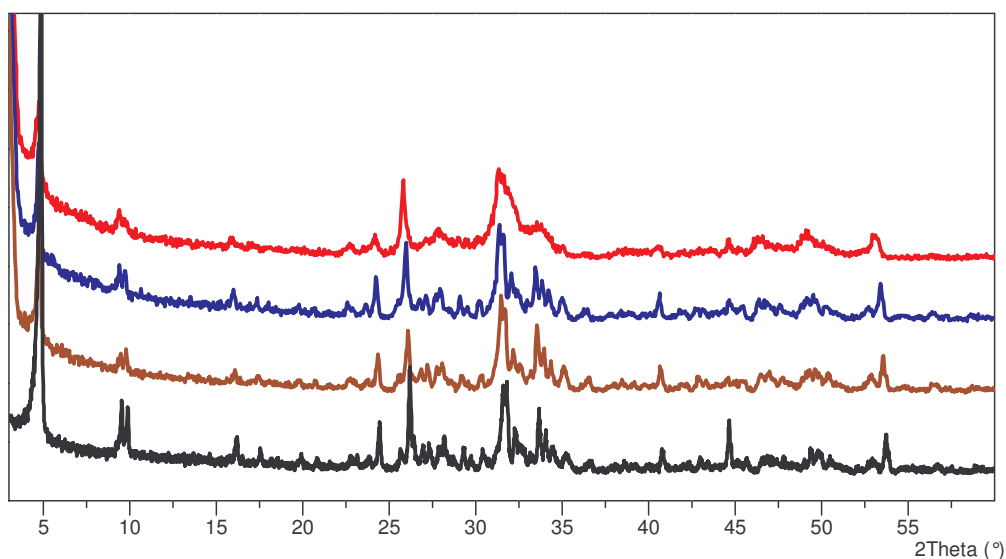
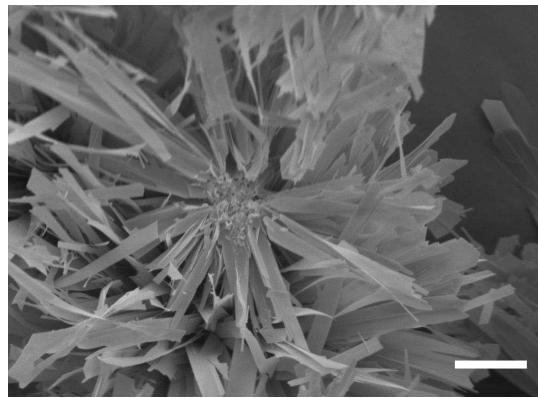


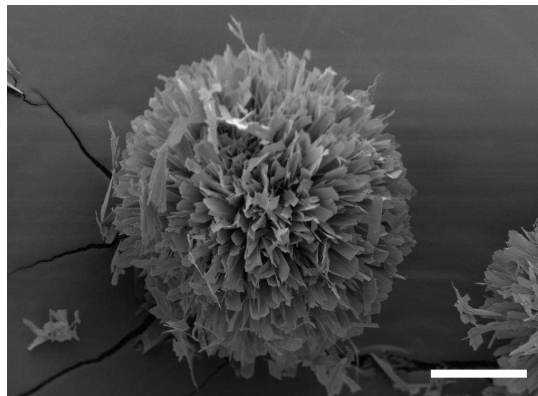
Fig. 39 - 0% (black line), 10% (brown line), 30% (blue line), 50% (red line) Sr OCP substituted XRPD patterns.

Table 10 - Crystal phases obtained by OCP synthesis in presence of Sr ions.

%Sr	T = 60°C	T = 70°C
3	OCP+DCPD	OCP
5	OCP+DCPD	OCP
10	DCPD	OCP
15	DCPD	OCP
20	DCPD	Disordered OCP
40	DCPD	Disordered OCP
50	DCPD	Disordered OCP
60	No ppt	Disordered OCP
80	No ppt	No ppt
100	SrHPO ₄	No ppt



(a)



(b)

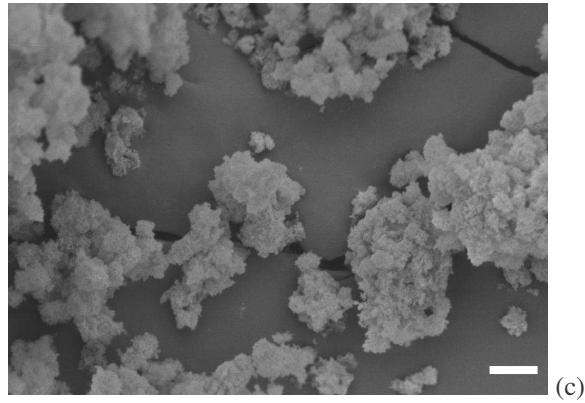


Fig. 40(a-c) - SEM images of Sr 5%, 10% [(a) and (b) respectively, scale bars 50 μ m), 50% (c, scale bar 5 μ m) OCP substituted.

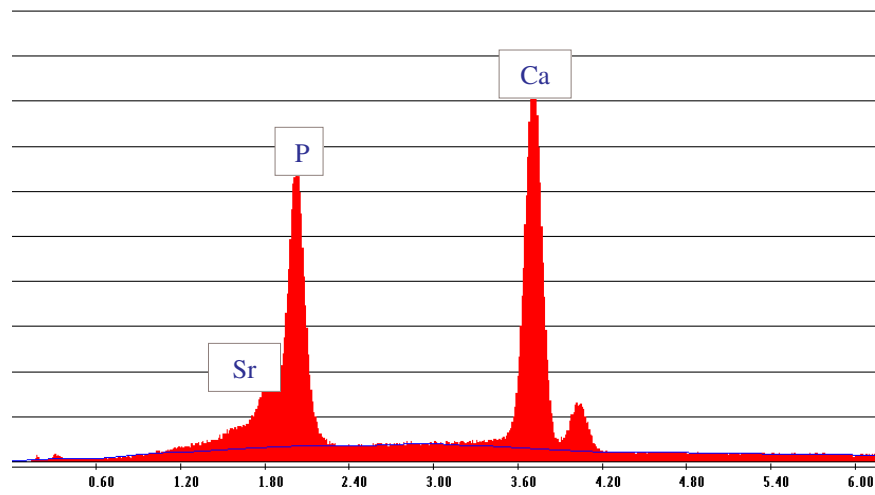


Fig. 41 - EDS analysis of OCP with a theoretical 15% Sr.

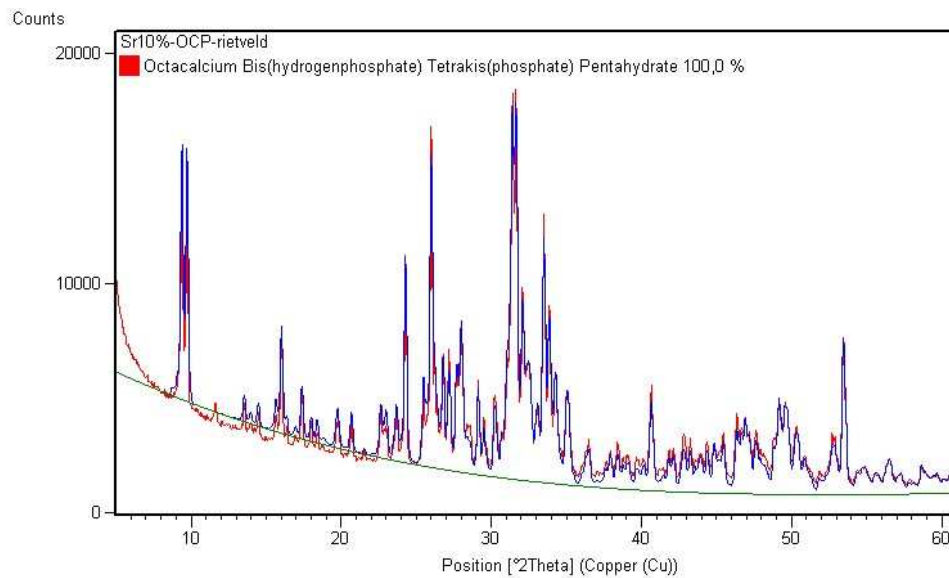


Fig. 42 - Comparison between observed and calculated Sr10% OCP diffractograms.

Table 11 - Cell parameters of OCP and Sr substituted OCP.

PARAMETER	OCP	OCP-Sr 10%	OCP-Sr 15%
<u>a</u>	19.695(5)	19.716(5)	19.75(1)
<u>b</u>	9.540(3)	9.558(4)	9.580(7)
<u>c</u>	6.834(3)	6.846(3)	6.861(4)
α	90,27(3)	90.24(3)	90.35(7)
β	92,57(3)	92.60(3)	92.59(7)
γ	108,32(3)	108,30(3)	108.27(9)
V	1218(1)	1223(1)	1231(1)

5.4.2 Magnesium Substitution

In the same way, OCP synthesis was performed in the presence of Mg. We chose to operate at 60°C or 70°C, 2 rounds per second with 1 hour dropping by adding increasing amounts of Mg. At 70°C and at a Mg content up to 15%, OCP is the only crystalline phase (*Table 12*). Then, up to 50% the crystal phase changes and DCPD forms. A further increase of Mg concentration completely inhibits precipitation. At 60°C, OCP is never observed as single phase. At low Mg concentration, the product is a mixed phase OCP/DCPD while at higher concentration only crystalline DCPD precipitates.

The XRPD patterns reported in *Figure 43*, show that OCP is obtained in the presence of little amounts of Mg ions in the reaction solution at 70°C, while at higher Mg concentration DCPD precipitates.

A morphological analysis was carried on OCP samples. At 3% of magnesium ions OCP crystals are still quite separated (*Figure 44(a)*). By increasing Mg amount (*Figure 44(b)*) the crystals tend to aggregate to form the classical OCP spherules. 15% magnesium deeply affects the morphology, so that only disordered crystal aggregates are observed (*Figure 44(c)*).

The values resulting from accurate structural refinement performed with the Rietveld method (*Figure 45*), reveals that OCP with 10% of magnesium ions exhibits reduced lattice parameters (*Table 13*) according to a smaller unit cell, suggesting a partial substitution of the smaller Mg²⁺ ion to calcium (1.00 Å calcium, 0.72 Å magnesium).

OCP obtained in the presence of Mg15% displays lattice parameters not significantly different from those of Mg10%.

Table 12 - Crystal phases obtained by OCP synthesis in presence of Mg ions.

%Mg	T = 60°C	T = 70°C
3	OCP+DCPD	OCP
5	OCP+DCPD	OCP
10	OCP+DCPD	OCP
15	DCPD	OCP
20	DCPD	OCP+DCPD
40	DCPD	DCPD
50	DCPD	DCPD
60	No ppt	No ppt
80	No ppt	No ppt
100	No ppt	No ppt

It can be hypothesized that just a limited amount of Mg can be incorporated into OCP structure, before causing a significant disorder of the structure, as indicated by the increasing broadening of the diffraction peaks observed at increasing Mg concentration (*Figure 43*).

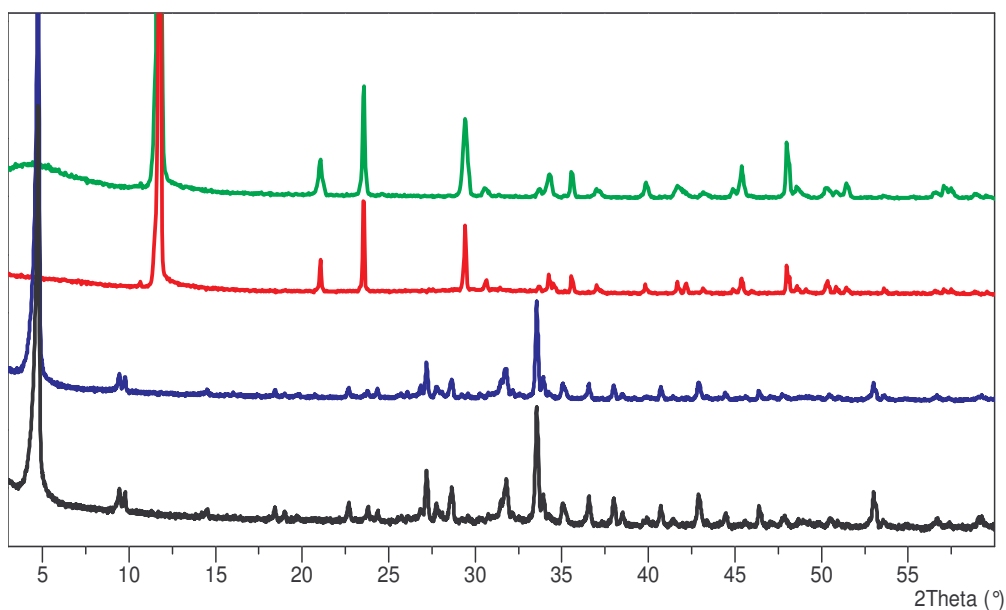


Fig. 43 - XRPD patterns of the powder obtained in presence of 3% (black line), 10% Mg ions (blue line) that correspond to OCP, 40% (red line), 50% (green line) of Mg ions that correspond to DCPD.

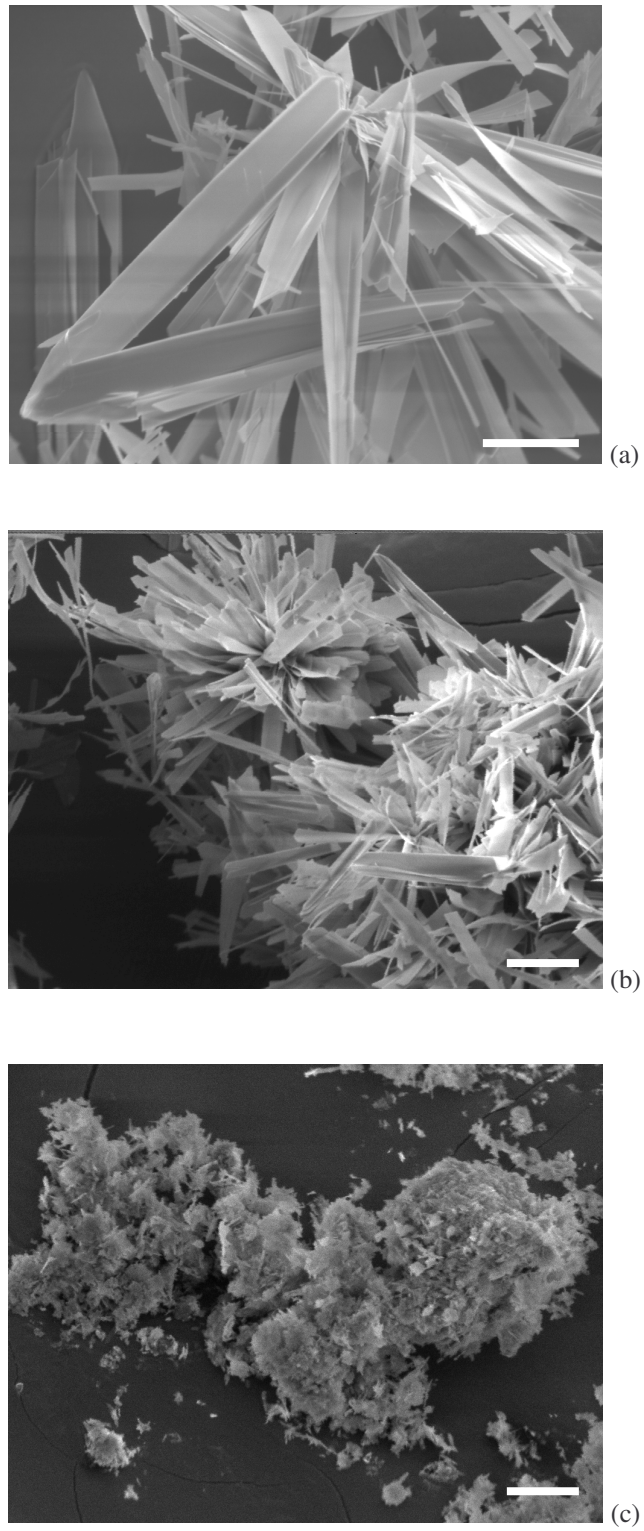


Fig. 44(a-c) - SEM images of the powder obtained in presence of 3% (a), 5% (b) and 15% (c) of magnesium ions at 70°C (scale bars = 20 μ m).

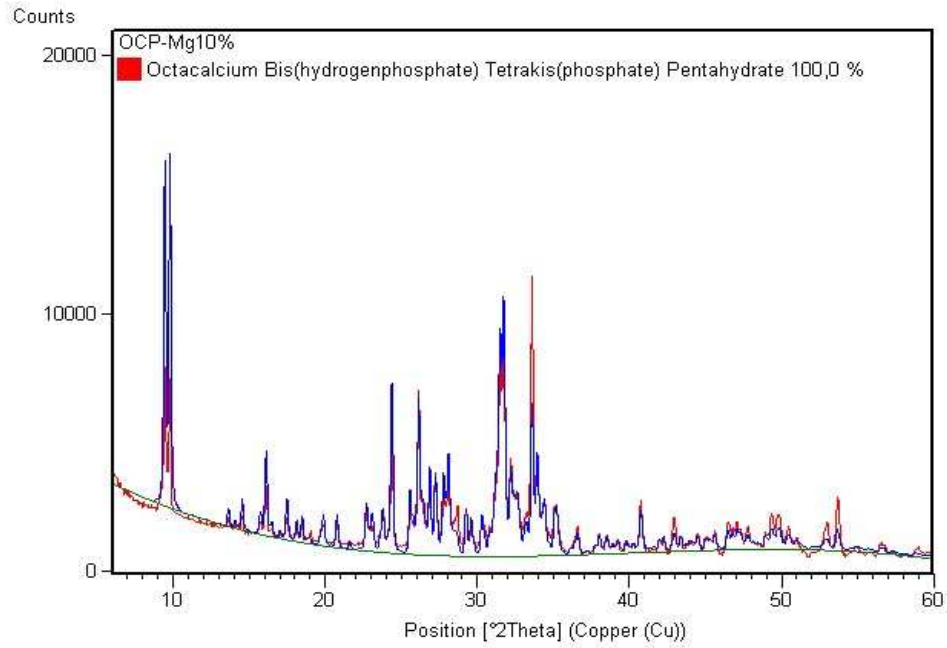


Fig. 45 - Comparison between observed and calculated Mg10% OCP diffractograms.

Table 13 - Cell parameters of OCP and Mg substituted OCP.

PARAMETER	OCP	OCP-Mg 10%	OCP-Mg 15%
a	19.695(5)	19.677(3)	19.684(7)
b	9.540(3)	9.530(3)	9.533(4)
c	6.834(3)	6.825(2)	6.829(3)
α	90,27(3)	90.22(2)	90.19(4)
β	92,57(3)	92.57(2)	92.62(4)
γ	108,32(3)	108.33(2)	108.33(4)
V	1218(1)	1213(1)	1215(1)

5.4.3 Manganese Substitution

The results of Mn ions introduction in OCP synthesis are deeply different from those observed in the case of strontium and magnesium. OCP is never obtained. Only at low percentages of Mn, a crystalline calcium phosphate phase precipitates (DCPD) both at 60 and 70°C (Figure 46).

With increasing concentrations of Mn, the precipitate is amorphous and then, up to 100%, no precipitate is obtained but at 60 °C with the 100% of Mn when $\text{Mn}_3(\text{PO}_4)_2(\text{H}_2\text{O})_7$ precipitates (*Table 14*).

Table 14 - Crystal phases obtained by OCP synthesis in presence of Mn ions.

Mn%	T = 60°C	T = 70°C
3	DCPD	DCPD
5	DCPD	DCPD
10	Amorphous phase	DCPD
15	Amorphous phase	Amorphous phase
20	Amorphous phase	Amorphous phase
40	Amorphous phase	Amorphous phase
50	No ppt	No ppt
60	No ppt	No ppt
80	No ppt	No ppt
100	$\text{Mn}_3(\text{PO}_4)_2(\text{H}_2\text{O})_7$	No ppt

From a morphological point of view DCPD crystals obtained appear deeply similar to those of pure DCPD (*Figure 47*).

The EDS analysis confirm that the products contain Mn (*Figure 48*).

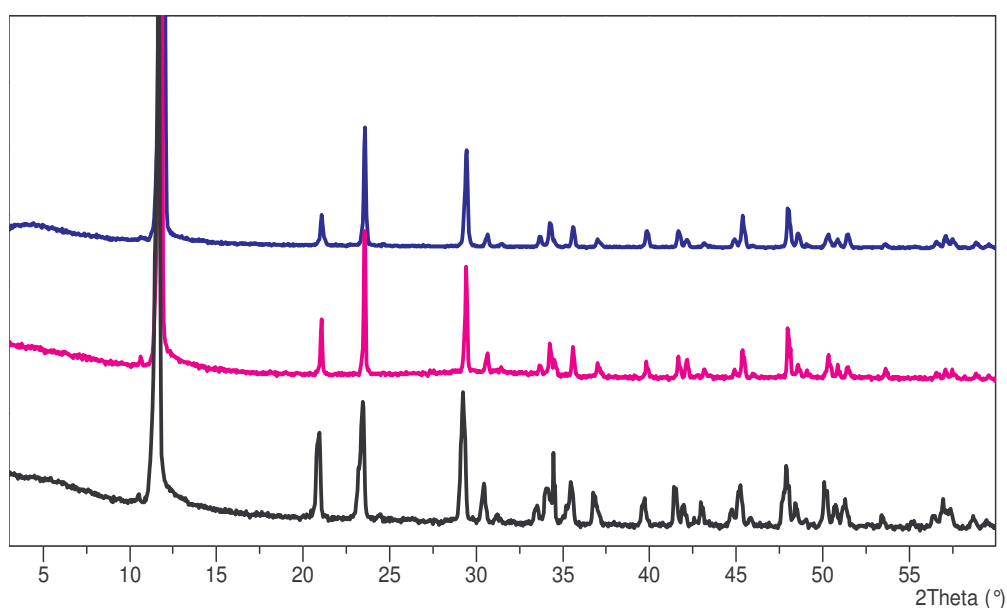


Fig. 46 - XRPD patterns of the powder obtained in presence of 3% (black line), 5% (pink line) and 10% (blue line) of Mn ions.

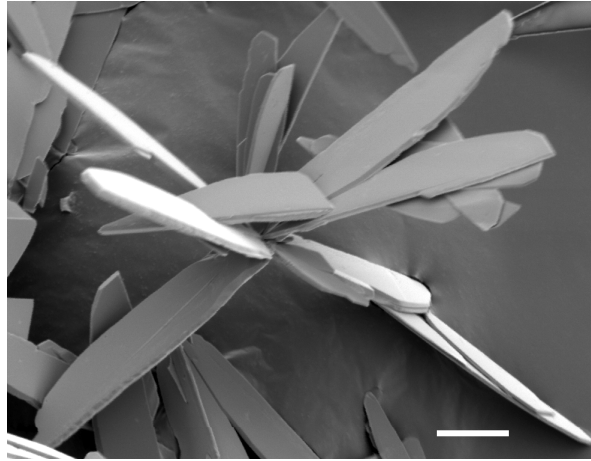


Fig. 47 - DCPD obtained by OCP synthesis produced in presence of 5% of Mn ions (scale bar = 20 μm).

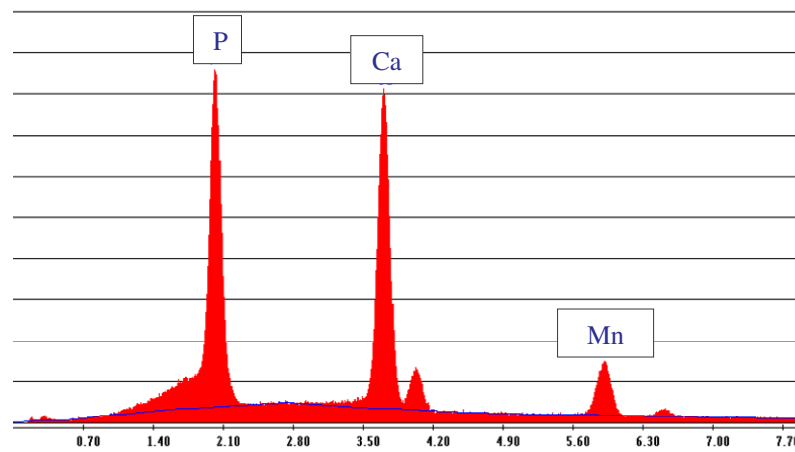


Fig. 48 - EDS image resulting by the analysis of the sample containing 15% of Mn ions.

5.5. Role of Strontium on α -TCP Hydrolysis

In view of the arising interest toward the introduction of Sr ions into the composition of calcium phosphate cements, quite often based on the hydrolysis reaction of α -TCP into HA, we examined the effect of increasing Sr concentration on α -TCP hydrolysis.

The powder X-ray diffraction patterns of the solid products obtained in the absence of Sr ions after different periods of α -TCP soaking in bidistilled water at 37°C are reported in *Figure 49*, and indicate that a mixed α -TCP/HA is present after 18 days of soaking while HA is the unique crystalline phase present after 21 days, in agreement with a complete hydrolysis of α -TCP.

When the same reaction is carried out at 60°C, 7 days are sufficient to observe the complete phase conversion into HA. The presence of strontium in solution inhibits the hydrolysis reaction: *Figure 50* reports the X-ray diffraction patterns of the products obtained after soaking at 60°C for 14 days at different concentrations, and indicates that the product obtained in the presence of 5% Sr²⁺ or more still exhibits diffraction peaks characteristic of α -TCP. The crystalline phase identified by X-ray diffraction analysis in the products of α -TCP soaking at different strontium concentrations at 37°C are reported in *Table 15*. The inhibition effect increases on increasing Sr²⁺ concentration, so that just a small amount of α -TCP appears hydrolyzed into HA after 21 days of soaking in 10% Sr²⁺ solution at 60°C.

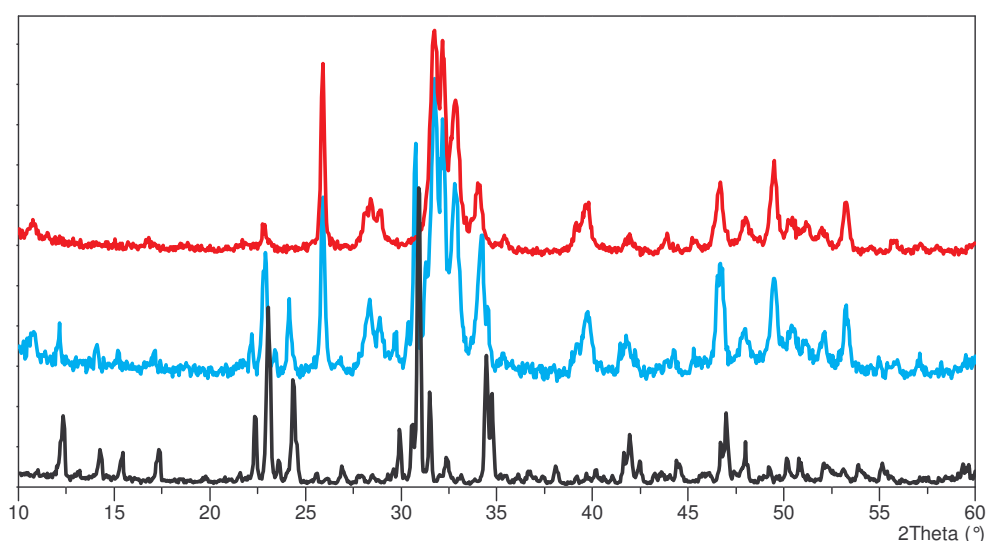


Fig. 49 - XRPD patterns of α -TCP (black line), a mixed phase α -TCP/HA obtained after 18 days of soaking (azure line) and HA (red line) obtained after 21 days of soaking.

The addition of a small amount of DCPD to the starting α -TCP powder produces an increase in the speed of phase conversion. *Table 16* reports the crystalline phases identified by X-ray diffraction analysis in the products of α -TCP soaking at different strontium concentrations at 37 or 60°C in the presence of 5% DCPD.

Table 15 – Crystalline phases present in the products of hydrolysis of α -TCP in water for different periods at 37 or 60°C.

Temperature 37°C			
% Sr ²⁺	14 days	18 days	21 days
0	α -TCP	α -TCP/HA	HA
2	α -TCP	α -TCP	α -TCP
5	α -TCP	α -TCP	α -TCP
10	α -TCP	α -TCP	α -TCP
20	α -TCP	α -TCP	α -TCP
Temperature 60°C			
% Sr ²⁺	7 days	14 days	21 days
0	HA	HA	HA
2	α -TCP	HA	HA
5	α -TCP	α -TCP/HA	HA
10	α -TCP	α -TCP	α -TCP/HA
20	α -TCP	α -TCP	α -TCP

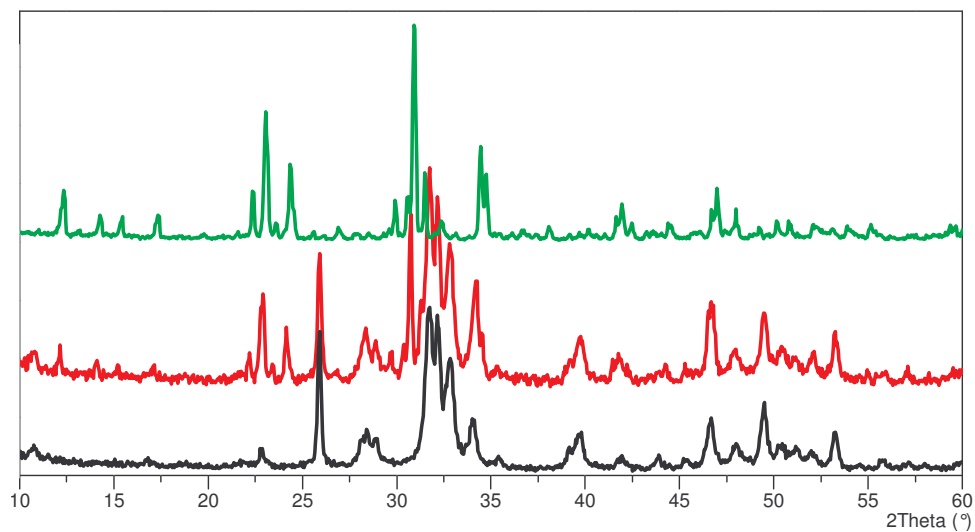


Fig. 50 - XRPD patterns of α -TCP after 14 days of soaking at 60°C in presence of 0% Sr (black line) which gives HA, 5% Sr (red line) which gives a mixed HA/ α -TCP phase and 10% of strontium ions which is still α -TCP (green line).

At 60°C, HA is the unique crystalline phase after just 24 hours when the hydrolysis is carried out in the presence of a strontium concentration up to 5%. After 12 days the hydrolysis of α -TCP is complete even in the presence of a 20% strontium concentration.

The lattice parameters of HA obtained from α -TCP hydrolysis after 12 days of soaking at 60°C are $a = 9.45(2) \text{ \AA}$, $c = 6.87(1) \text{ \AA}$, very close to those previously reported [54] and do not show any appreciable variation as a function of strontium concentration in solution (*Table 18*).

The line broadening of the 002 and 310 reflections of HA were used to evaluate the coherence lengths of the perfect crystalline domains of the crystals.

The results are reported in *Table 17* and indicate that the coherence lengths of HA crystals obtained by α -TCP hydrolysis are longer than those previously reported for synthetic HA [56]. Furthermore, the values of the coherence lengths display a decrease on increasing strontium concentration in solution.

This could be due to the presence of strontium atoms associated with the solid products of the hydrolysis reactions.

Table 16 – Products of α -TCP in water with 5% DCPD for different periods at 37 or 60°C.

37°C					
% Sr ²⁺	2 days	3 days	7 days	10 days	14 days
0	α -TCP/ HA	HA	HA	HA	HA
2	α -TCP	α -TCP	HA	HA	HA
5	α -TCP	α -TCP	α -TCP	α -TCP/ HA	α -TCP/ HA
10	α -TCP				
20	α -TCP				
60°C					
% Sr ²⁺	3 hours	6 hours	1 day	3 days	12 days
0	α -TCP/ HA	α -TCP/ HA	HA	HA	HA
2	α -TCP/ HA	α -TCP/ HA	HA	HA	HA
5	α -TCP	α -TCP/ HA	HA	HA	HA
10	α -TCP	α -TCP	α -TCP/ HA	HA	HA
20	α -TCP	α -TCP	α -TCP/ HA	α -TCP/ HA	HA

Indeed EDS analysis put into evidence the presence of strontium in the apatitic samples obtained from strontium containing solutions. *Figure 51* reports the EDS

spectra of samples obtained from solutions in the absence (*Figure 51(a)*) and in the presence of strontium (*Figure 51(b)* and *51(c)*). The amount of strontium in the samples increases with respect to calcium on increasing the strontium concentration in solution (*Figures 51(b)* and *51(c)*).

Moreover, it is possible to monitor the effect of time of strontium incorporation into CaP powder. In *Figure 52* are reported the EDS analysis of the sample containing 20% of strontium ions in the reaction solution. They show how strontium content increases from 3 (*Figure 52(a)*) days to 12 (*Figure 52(b)*) days of soaking.

Table 17 - Average dimensions of crystalline domains in (002) and (310) directions for HA samples obtained soaking α -TCP in water with 5% DCPD in 12 days at 60°C.

% Sr ²⁺	τ 002 (Å)	τ 310 (Å)
0	474 (2)	310 (1)
2	441 (5)	269 (4)
5	425 (5)	257 (5)
10	390 (4)	244 (7)
20	371 (5)	284 (6)

Table 18 – Unit cell parameters of HA obtained from α -TCP + DCPD a 60°C with different amount of strontium ions inside the solution.

% Sr ²⁺	\underline{a} parameter (Å)	\underline{c} parameter (Å)
0	9.45 (2)	6.87 (1)
2	9.42 (4)	6.87 (1)
5	9.44 (1)	6.89 (2)
10	9.48 (4)	6.90 (4)
20	9.36 (8)	6.88 (5)

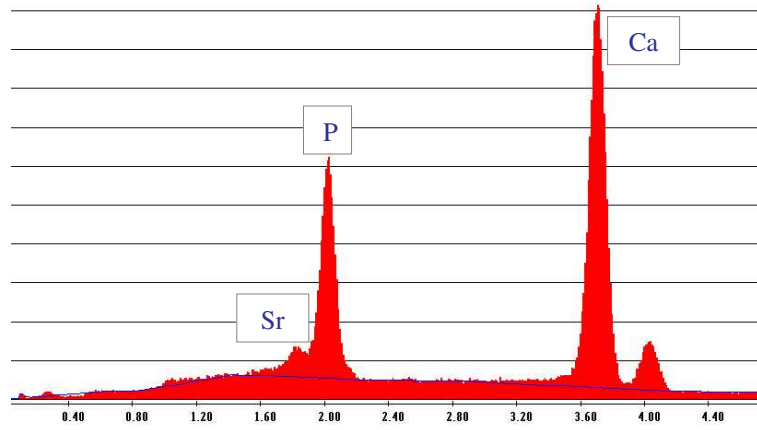


Fig. 51(a) - Sample containing 5% Sr^{2+} after 12 days of soaking in water solution.

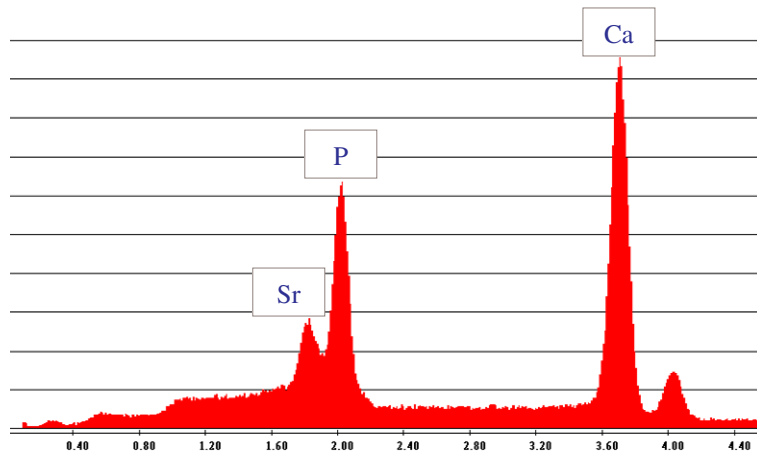


Fig. 51(b) - Sample containing 10% Sr^{2+} after 12 days of soaking in water solution.

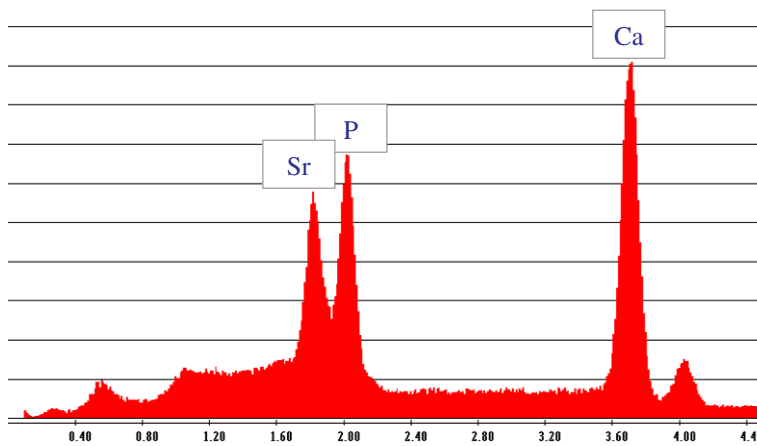


Fig. 51(c) - Sample containing 20% Sr^{2+} after 12 days of soaking in water solution.

Figure 43 reports the SEM images of the products obtained after soaking in bidistilled water at 60°C for different periods of time. α -TCP appears constituted of dense rounded blocks with the characteristic morphology of a solid-state product. The presence of added DCPD crystals, which display a plate-like morphology, is clearly appreciable in the image (*Figure 53(a)*). After a couple of hours of soaking, small HA crystals appear on the α -TCP ones (*Figure 53(b)*). After 6 hours soaking, platelet-like crystals (of HA) appear close to the α -TCP aggregates (*Figure 53(c)*). According to the results of X-ray diffraction analysis, this material contains both α TCP and HA as crystalline phases. After 12 days soaking, only platelet-like crystals of HA with dimensions of few microns are present (*Figure 53(d)*).

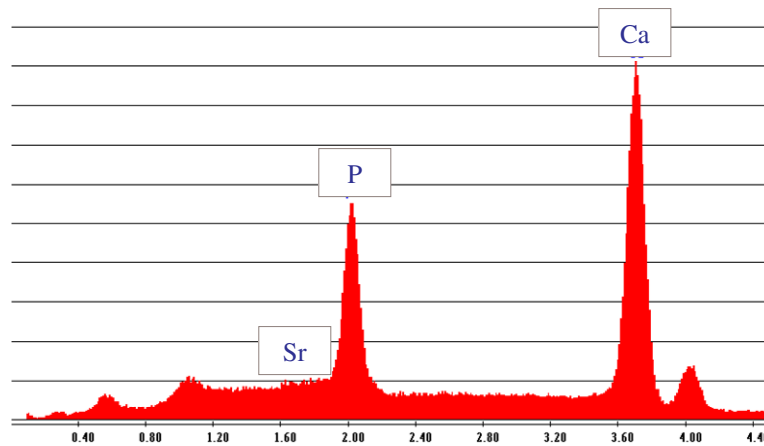


Fig. 52(a) - Sample containing 20% Sr^{2+} after 3 days of soaking in water solution: no strontium ions are present in the powder.

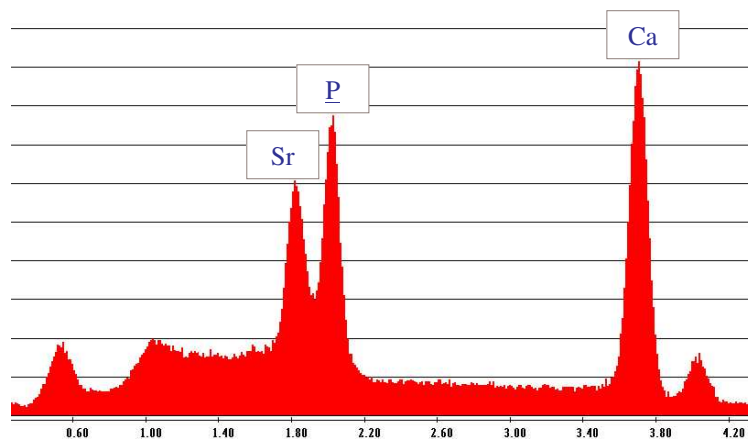


Fig. 52(b) - Sample containing 20% Sr^{2+} after 7 days of soaking in water solution.

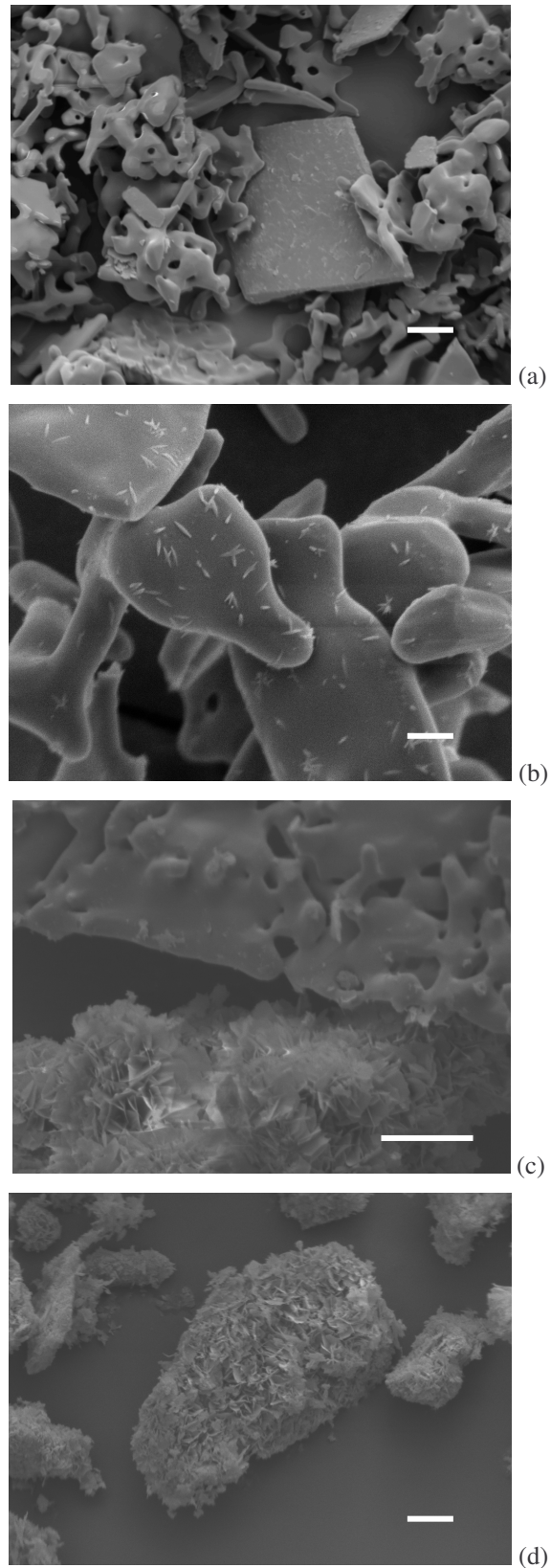


Fig. 53(a-d) - SEM images of α -TCP/DCPD powder (a) (scale bar = 10 μm), α -TCP with a few little HA crystals (b) (scale bar = 2 μm), α -TCP/HA (c) and HA(d) (scale bars = 10 μm) powder after different periods of soaking.

On the other hand, when the hydrolysis is carried out in the presence of strontium, the shape of the HA crystals obtained after 12 days appears to be different, as it can be observed in *Figure 54* that reports the SEM micrograph of HA obtained after soaking in 20% Sr^{2+} solution. Crystals are rod-like and their length is definitely shorter than 1 μm .

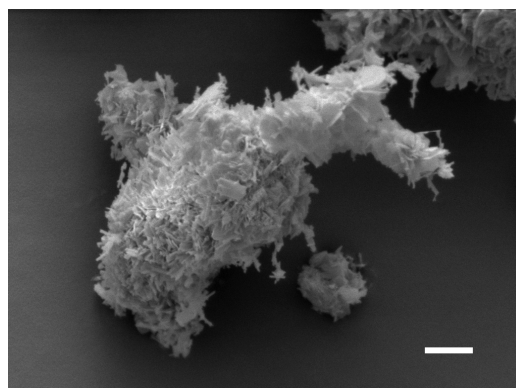


Fig. 54 - SEM image of HA obtained after soaking in 20% Sr^{2+} solution for 12 days (scale bar = 2 μm).

5.5.1 Hydrolysis in Gelatin Solutions

All samples hydrolysed in presence of gelatin were analyzed by XRPD to identify the different crystal phases (*Figure 55*). The identified crystal phases are reported on the basis of the percentage of strontium, gelatin and time of reaction (*Table 13*).

At the lower gelatin concentration (0.1%), the hydrolysis of α -TCP occurs faster than in water (*Table 14*) and the complete phase conversion into HA is observed after 14 days. On increasing gelatin concentration in solution to 0.5%, α -TCP reaction leads to the formation of an OCP/HA mixture in 3 days and HA as unique crystalline phase in 21 days; whereas at gelatin concentration of 1%, OCP may be obtained as a pure phase after just 3 days.

The presence of strontium in solution inhibits the hydrolysis reaction, so that a 2% Sr^{2+} concentration in 0.1% gelatin is sufficient to avoid any HA formation up to 35 days and the same happens for 10% and 20% Sr^{2+} concentration in 0.5% gelatin.

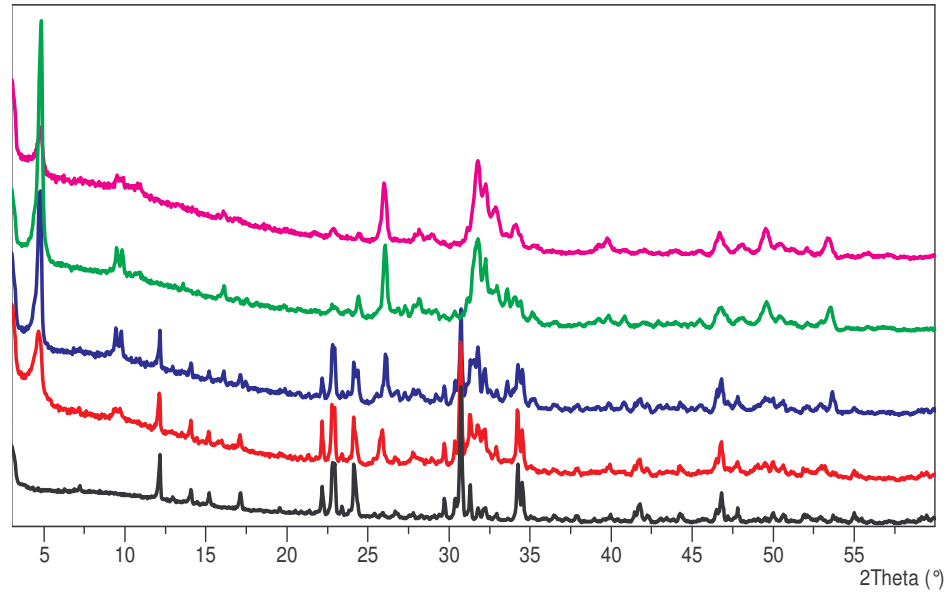


Fig. 55 - XRPD diffractograms of α -TCP soaked in gelatin solution for different time: α -TCP (black line), α -TCP/OCP (red line), OCP/ α -TCP (blue line), OCP (green line) and OCP/HA (pink line).

Table 13 - Calcium phosphate crystalline phases resulting by α -TCP soaking in 0.1, 0.5, 1% gel solution for different periods of time at 37°C.

		0.1% gel				
Sr^{2+} %		7 days	14 days	21 days	28 days	35 days
0		α -TCP	HA	HA	HA	HA
2		α -TCP	α -TCP	α -TCP	α -TCP	α -TCP
5		α -TCP	α -TCP	α -TCP	α -TCP	α -TCP
10		α -TCP	α -TCP	α -TCP	α -TCP	α -TCP
20		α -TCP	α -TCP	α -TCP	α -TCP	α -TCP
		0.5% gel				
		3 days	7 days	14 days	21 days	28 days
0		OCP/HA	OCP>HA	HA>OCP	HA	HA
2		α -TCP	OCP> α TCP	OCP>HA	OCP>HA	HA
5		α -TCP	OCP> α TCP	OCP> α -TCP	OCP> α -TCP	OCP> α -TCP
10		α -TCP	α -TCP	α -TCP	α -TCP	α -TCP
20		α -TCP	α -TCP	α -TCP	α -TCP	α -TCP
		1% gel				
Sr^{2+} %		1 days	3 days	7 days	21 days	35 days
0		α -TCP>OCP	OCP	OCP	OCP>HA	OCP>HA
2		α -TCP	α -TCP>OCP	OCP	OCP>HA	OCP>HA
5		α -TCP	α -TCP	OCP	OCP>HA	OCP>HA
10		α -TCP	α -TCP	α -TCP	α -TCP>OCP	OCP>HA
20		α -TCP	α -TCP	α -TCP	α -TCP	α -TCP>OCP

In *Figure 56* it is possible to follow the proceeding of hydrolysis reaction. SEM image shows α -TCP crystals (*a*) on which OCP crystals form (*b*). Then pure OCP crystals are visible (*c*) and after the maximum period of time considered a mixed phase OCP/HA is observed (*d*).

By means of the *QUANTO* program it was possible to quantify the percentages of the different calcium phosphate crystal phases (*Table 15*) present in the same sample. As shown in *Table 15*, this program too allow to monitor the conversion of α -TCP to hydroxyapatite which involves small portions of the sample at first, and increases with time until complete reprecipitation of the most stable calcium phosphate crystal phase.

Table 14 - Calcium phosphate crystalline phases resulting by α -TCP soaking in 0.1, 0.5, 1% gel solution for different periods of time at 37°C with 5% DCPD.

0.1% gel + 5% DCPD					
Sr ²⁺ %	1 day	7 days	14 days	21 days	35 days
0	α -TCP>>OCP	OCP>HA	HA	HA	HA
2	α -TCP	OCP>> α -TCP	HA>>OCP	HA	HA
5	α -TCP	α -TCP	HA>>OCP	Poorly cryst. HA	HA
10	α -TCP	α -TCP	α -TCP	α -TCP	α -TCP
20	α -TCP	α -TCP	α -TCP	α -TCP	α -TCP
0.5% gel + 5% DCPD					
Sr ²⁺ %	1 day	3 days	7 days	21 days	28 days
0	α -TCP>>OCP	OCP/HA	OCP>HA	HA	HA
2	α -TCP>>OCP	OCP>> α -TCP	OCP	HA>OCP	HA>OCP
5	α -TCP	OCP> α -TCP	OCP> α -TCP	HA>OCP	HA>OCP
10	α -TCP	α -TCP	α -TCP	α -TCP	OCP> HA
20	α -TCP	α -TCP	α -TCP	α -TCP	α -T CP
1% gel + 5% DCPD					
Sr ²⁺ %	1 days	5 days	7 days	21 days	35 days
0	OCP> α -TCP	OCP	OCP	OCP>HA	OCP>HA
2	α -TCP>OCP	OCP	OCP	OCP>HA	OCP>HA
5	α -TCP	OCP	OCP	OCP>HA	OCP>HA
10	α -TCP	α -TCP>OCP	OCP> α -TCP	OCP>HA	OCP>HA
20	α -TCP	α -TCP	α -TCP	α -TCP	α -TCP>>OCP

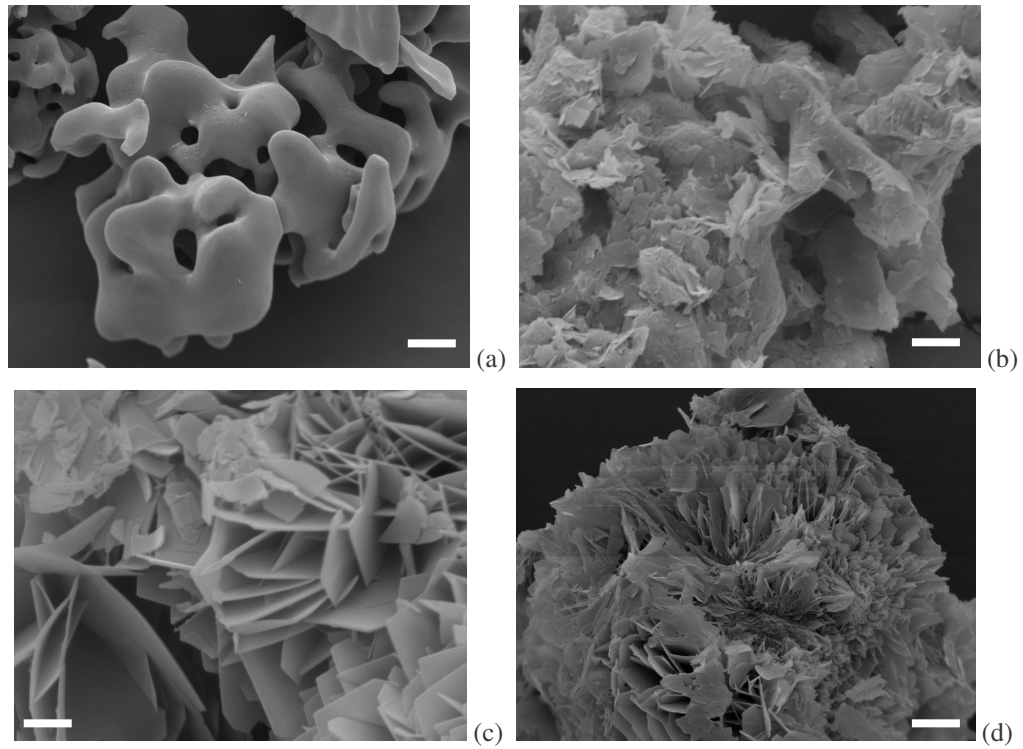


Fig. 56(a-d) - SEM images of the powder in the different steps of α -TCP hydrolysis reaction: starting material α -TCP (a) (scale bar = 5 μm), mixed phase α -TCP/OCP (b) (scale bar = 2 μm), OCP single crystalline phase (c) (scale bar = 1 μm) and mixed phase OCP/HA (d) (scale bar = 5 μm) obtained after the maximum period of soaking.

Table 15 – Percentages of the different calcium phosphates present in the products of hydrolysis.

SAMPLE	% α -TCP	% OCP	% HA
Sr0% α-TCP in H₂O			
1 day	55.8 (7)	44.2 (8)	~
21 days	~	6.5 (9)	93.9 (8)
28 days	~	19.6 (7)	80.4 (2)
35 days	~	17.5 (9)	82.5 (2)
Sr0% α-TCP + 5% DCPD in H₂O			
1 day	~	75.8 (6)	24.2 (9)
21 days	~	63.8 (8)	36.2 (7)
28 days	~	51.1 (5)	48.9 (6)
35 days	~	22.9 (9)	77.1 (3)

Sr2% α -TCP in H ₂ O			
3 days	51.1 (5)	49.9 (7)	~
21 days	~	47.8 (6)	42.2 (6)
28 days	~	52.6 (9)	47.4 (8)
35 days	~	29.4 (8)	70.6 (4)
Sr2% α -TCP + 5% DCPD in H ₂ O			
1 day	53.0 (6)	47.0 (9)	~
3 days	~	78.0 (3)	22.0 (9)
21 days	~	42.2 (9)	57.8 (9)
28 days	~	45.2 (7)	54.8 (5)
35 days	~	19.5 (8)	80.5 (3)
Sr5% α -TCP in H ₂ O			
28 days	~	47.7 (4)	52.3 (5)
35 days	~	28.6 (9)	71.4 (4)
Sr5% α -TCP + 5% DCPD in H ₂ O			
3 days	48.1 (5)	51.9 (7)	~
21 days	~	67.2 (4)	32.8 (7)
28 days	~	51.9 (4)	48.1 (5)
35 days	~	45.4 (5)	54.6 (5)
Sr10% α -TCP in H ₂ O			
35 days	~	35.7 (6)	64.3 (5)
Sr10% α -TCP + 5% DCPD in H ₂ O			
21 days	~	25.8 (7)	74.2 (5)
28 days	~	23.3 (6)	76.7 (3)
35 days	~	19.9 (5)	80.1 (3)

5.6 Microspheres

Gelatin microspheres were prepared by the so called “thermal gelation technique”: by adding a gelatin solution to stirred soy oil, a rapid cooling led to the formation of spheres.

The morphological analysis carried out on gelatin microspheres by a scanning electron microscope shows how these spheres (the cores) are smooth, spherical, with diameter dimensions of 10-20 μm (*Figure 57*).

The X-ray diffraction analysis reveals an amorphous phase (*Figure 58*).

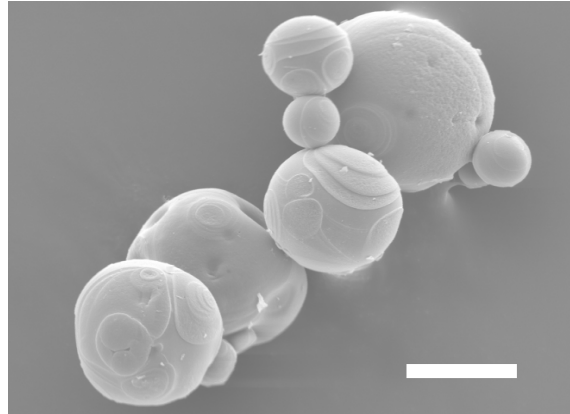


Fig. 57 - SEM image of gelatin microspheres (scale bar = 20 μm).

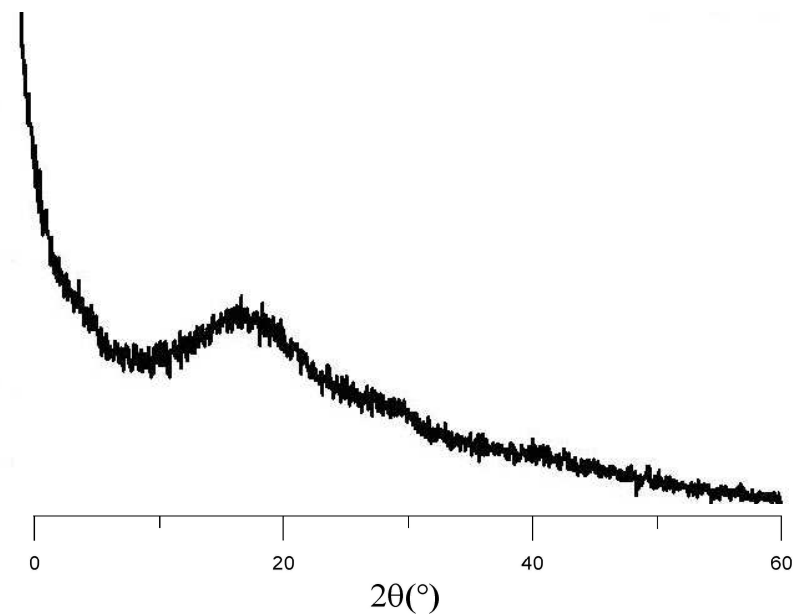


Fig. 58 - XRPD pattern of gelatin microspheres.

The second step was to coat these microspheres with a thin calcium phosphate layer. The parameters of synthesis were optimized so as to obtain homogeneous shells on microspheres' surfaces. In *Figure 59* the diffractogram displays that, even with a CaP

shell, the resulting phase is still amorphous thus precluding a deeper crystallographic analysis.

From a morphological point of view, the calcium phosphate shell appear thick and homogeneous (*Figure 60*) and no CaP precipitate independently from the gelatin microspheres.

The graph showed below (*Figure 61*) reports the percentages of gelatin released from uncoated (in blue) and coated (in red) microspheres. The values registered for coated microspheres are lower than those observed from the calculated released gelatin from uncoated microspheres. 78 hours are necessary to make 90% of gelatin released while in the same period only 60% of gelatin is released from CaP coated gelatin microspheres. This demonstrates the usefulness of CaPs coatings to modulate gelatin release.

After the optimization of gelatin microspheres synthesis, aspirin was chosen as drug model to be loaded and released from gelatin microspheres.

The XRPD pattern (*Figure 62*) of aspirin loaded gelatin microspheres is a typical amorphous diffractogram as that of unloaded gelatin microspheres was and nothing else was expected.

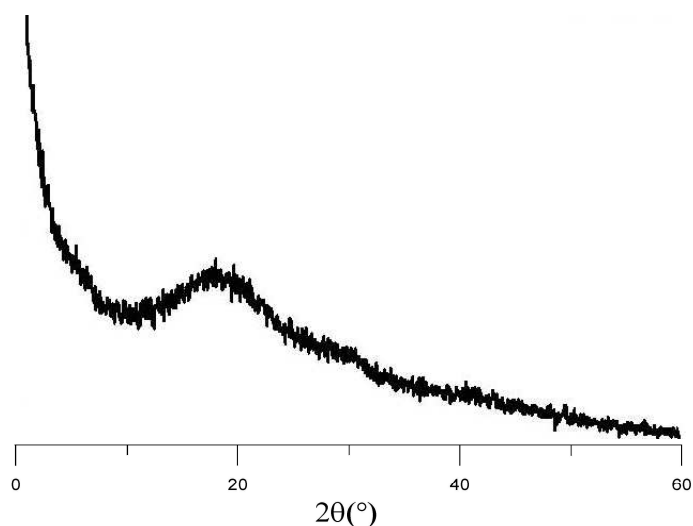


Fig. 59 - XRPD pattern of gelatin microspheres coated with a calcium phosphate shell.

From the morphological point of view, aspirin loaded gelatin microspheres appear perfectly spherical and smooth even though without regular dimensions (*Figure 63*).

After the introduction of calcium phosphate in the reaction medium, the coated microspheres were structurally analysed by XRPD. The resulting diffractogram (*Figure*

64) show an amorphous phase again, thus revealing that the calcium phosphate coating is amorphous or so thin that X-ray technique is not sufficient to determine it.

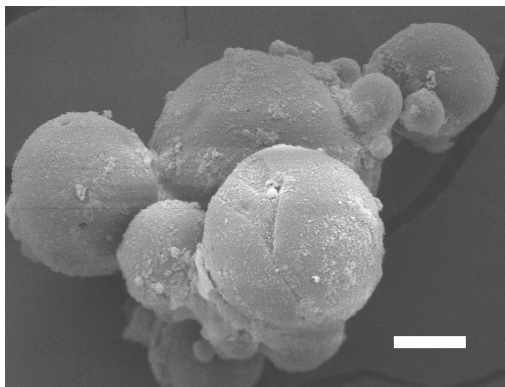


Fig. 60 - SEM image of gelatin microspheres coated with CaP (scale bar = 20 μ m).

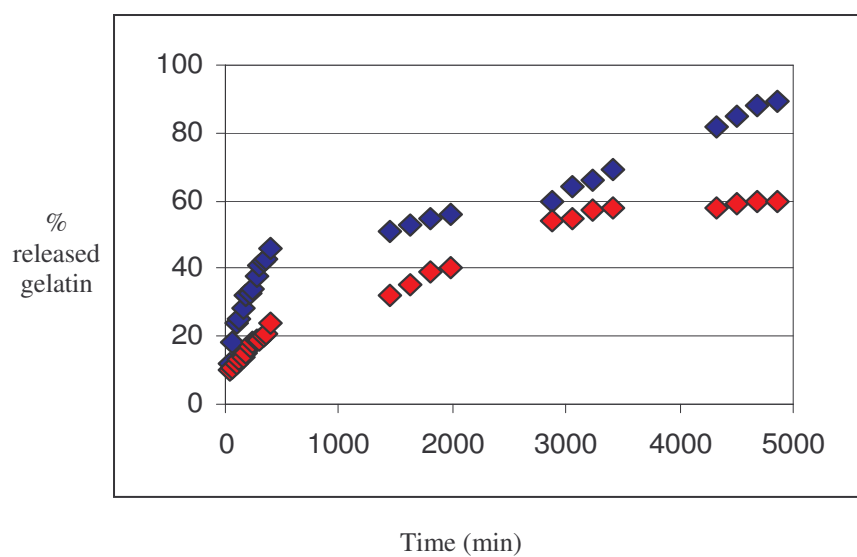


Fig. 61 - Percentage of released gelatin vs. time from uncoated (blue squares) and coated gelatin microspheres (red squares).

Aspirin loaded gelatin microspheres' coating appears not always homogeneous and even if several synthesis were performed it was not possible to reach the good homogeneousness obtained in the case of unloaded microspheres, indicating that the drug disturbs the deposition on the microspheres surface. The inorganic phase in some portions of the coating appear constituted of lamellar crystals (*Figure 65*).

The graphic below (*Figure 66*) represents the percentages of aspirin released from uncoated (green squares) and coated (pink squares) microspheres.

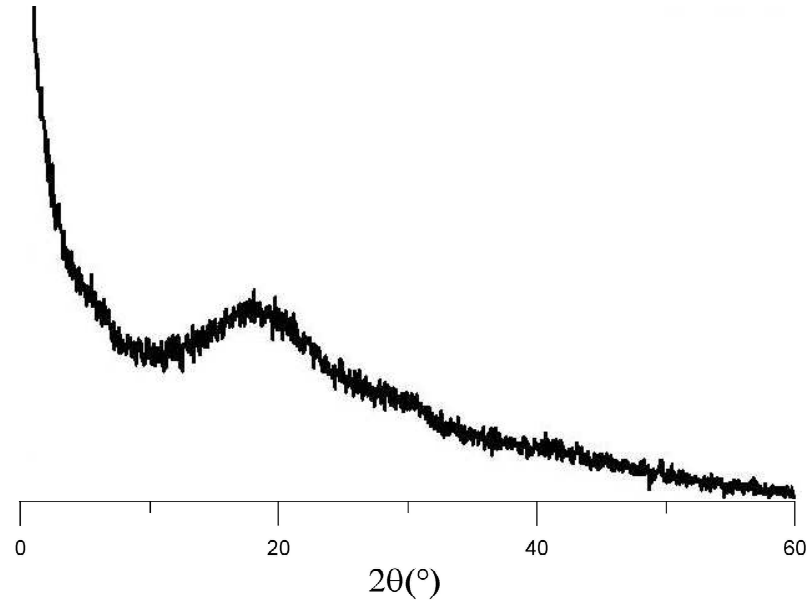


Fig. 62 - XRPD pattern of aspirin loaded gelatin microspheres.

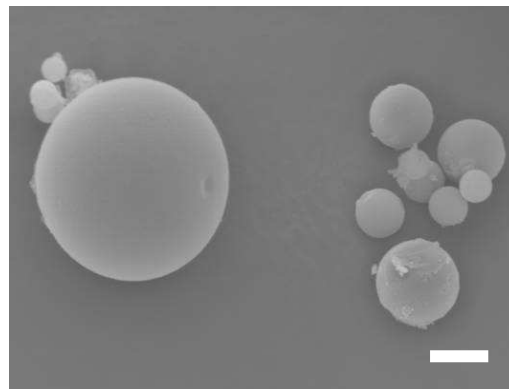


Fig. 63 - SEM images of uncoated aspirin loaded gelatin microspheres (scale bar = 5 μ m).

The kinetic of aspirin release from coated microspheres is lower than that obtained from uncoated ones only 24 hours are enough to have the 100% of aspirin released for uncoated gelatin microspheres whereas the coated gelatin microspheres release the same quantity in 48 hours.

Although aspirin is just a model, the results confirm the usefulness of CaP coating in modulating drug release.

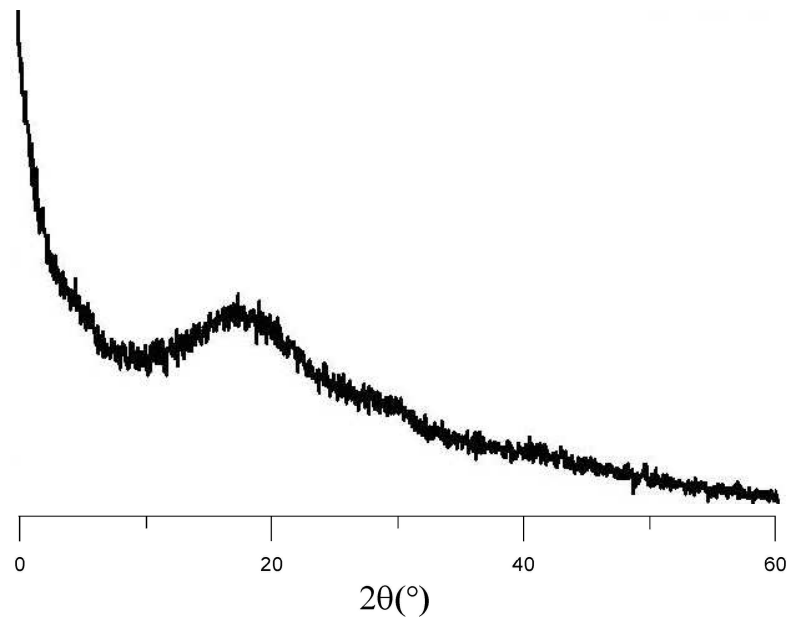


Fig. 64 - XRPD pattern of CaP coated aspirin loaded gelatin microspheres.

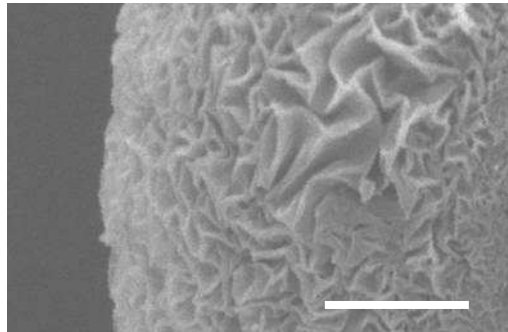


Fig. 65 - SEM images of CaP coated aspirin loaded microspheres: a particular of CaP shell (scale bar = $1\mu\text{m}$).

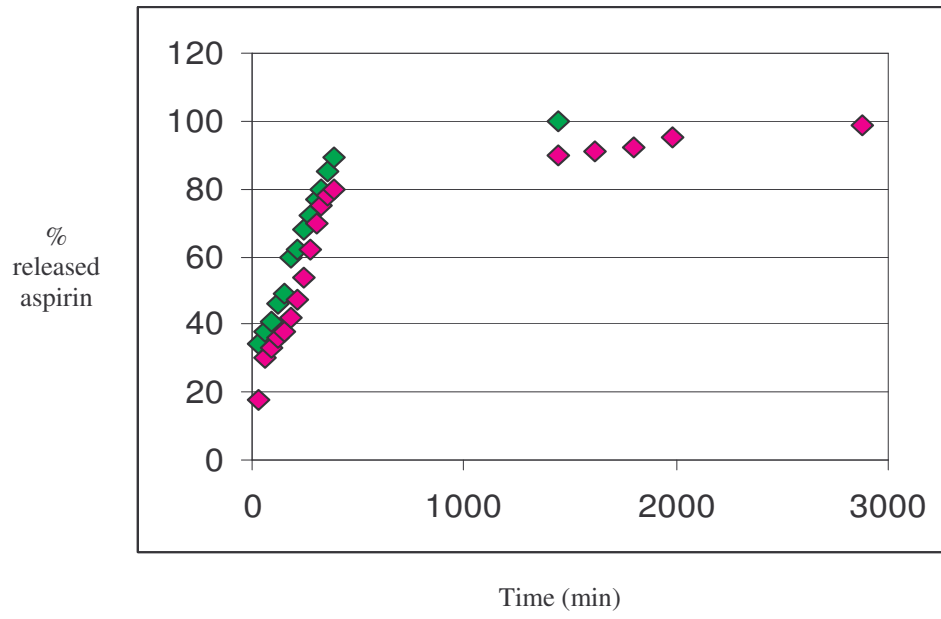


Fig. 66 - Percentage of aspirin released from uncoated (pink squares) and coated (green squares) microspheres.

6. Conclusions

The results achieved during this PhD thesis put into evidence the role of several biologically active ions and molecules on the synthesis and relative stability of a few calcium phosphates widely employed in the field of biomaterials for hard tissue repair, namely HA, OCP, α -TCP. A wide part of the investigation was addressed to study the interaction of CaPs with Sr^{2+} ion, which is known to play an active role on bone resorption and formation.

Ca–Sr–HA solid solutions have been prepared in the whole range of composition by the direct synthesis in aqueous solution with a degree of crystallinity sufficient to allow a structural analysis of the isomorphous compounds without further heat treatment. Increasing strontium substitution for calcium in the HA structure provokes a linear variation of the cell parameters and of the infrared absorption bands, in agreement with the increasing mean dimensions of the cation. At variance, the effect of strontium on crystallinity and morphology changes with composition: relatively low Sr replacement to calcium induces a decrease of the coherent length of the perfect crystalline domains and disturbs the shape of the crystals, whereas crystallinity, as well as mean dimensions of the crystals, increases at relatively high strontium contents. Similarly, although strontium distribution is not deeply different in the two cationic sites, a slight Sr enrichment of M(2) site prevails in most of the range of composition, whereas a modest preference of Sr for the smaller M(1) site can be appreciated only at a very low strontium content. This result, which is opposite to what was expected on the basis of the difference in ionic radii, is of peculiar importance for it concerns a composition in the range of strontium concentration in the bone.

The results of the *in vitro* study carried out on cultures of bone cells grown on HA nanocrystals containing up to 7% Sr indicate that this ion stimulates osteoblast activity and exerts its inhibitory effect on osteoclast proliferation even when incorporated into hydroxyapatite.

On the basis of those positive results, Pulsed Laser Deposition was successfully applied to deposit thin films of Sr substituted HA on titanium substrates. The synthesized coatings displayed a uniform Sr distribution, a granular surface and a good degree of crystallinity which slightly decreased on increasing Sr content. The results of *in vitro* tests suggested that the presence of Sr in HA thin films can enhance the positive

effect of HA coatings on osteointegration and bone regeneration, and prevent undesirable bone resorption.

At variance with the behaviour of Sr towards HA, this ion inhibits the synthesis of OCP. As a matter of fact, the presence of Sr in the synthesis reaction promotes the precipitation of DCPD, and OCP can be obtained as unique crystalline phase just when the synthesis is performed at 70°C in the presence of Sr²⁺ concentration up to 15 atom %. However, in this range of concentration, Sr enters the lattice structure of OCP, in agreement with the increase of the cell parameters observed on increasing ion concentration.

A similar behaviour was recorded for Mg²⁺ ions which provokes a reduction of the unit cell in agreement with its smaller ionic radius. The relative amount of magnesium that can substitute for calcium in OCP structure most likely is slightly less than that achievable in the case of Sr, as suggested by the minor variation of the unit cell volume.

These results are of peculiar importance since Sr-substituted OCP as well as Mg-substituted OCP, couple the osteogenetic properties of octacalcium phosphate, with the biologically relevant properties of Sr and Mg, which could be successfully exploited in the preparation of calcium phosphate based biomaterials. At variance, Mn²⁺ ion completely inhibits the synthesis of OCP, whereas it promotes the precipitation of DCPD. Further investigations could clarify if these ions are incorporated into the structure of DCPD, or simply adsorbed on crystal surface.

Sr²⁺ ion exerts an active role also in the hydrolysis of α -TCP: in the presence of increasing amounts of Sr²⁺ in solution, the speed of the conversion reaction of α -TCP into HA is highly reduced even in the presence of DCPD, which accelerates the hydrolysis reaction. However, the resulting apatitic phase contains significant amounts of Sr²⁺ suggesting that the addition of Sr²⁺ to the composition of α -TCP bone cements could be successfully exploited for its local delivery in bone defects.

The results obtained in the presence of gelatin indicate that it accelerates the hydrolysis reaction with a catalytic effect even greater than that of DCPD. Moreover, the acidic character of gelatin solution promotes the conversion of α -TCP into OCP, so that at relatively high gelatin concentration, the reaction product consists of a mixture of OCP and HA. It is conceivable to suppose that the use of gelatin in the composition of α -TCP based CPCs would not only accelerate the hardening reaction and provide a material more close to bone composition, but also lead to a fast resorption and new bone formation thanks to the presence of OCP.

The work performed during this PhD thesis allowed, furthermore, to optimize the experimental conditions to cover gelatin microspheres with an uniform layer of calcium phosphate in order to obtain useful materials for modulated drug delivery and release. The microspheres have been charged with a model drug (aspirin) to investigate the kinetics of its release from uncoated and coated microspheres. The results indicate that the presence of a calcium phosphate coating of the microspheres delays the release of aspirin thus allowing to modulate its action.

The possibility to introduce an active molecule in the implant site has been explored using MAPLE to deposit alendronate-hydroxyapatite nanocrystals at different bisphosphonate content. The mild conditions of work of this innovative technique do not affect the molecule of alendronate, which might be decomposed by the traditional PLD. As a matter of fact, MAPLE has been successfully employed to deposit thin films of HA at increasing alendronate content. The coatings exhibit a good degree of crystallinity and a positive effect on cell activity and proliferation. Osteoblast MG-63 cells cultured on the coatings displayed increased proliferation and increased values of collagen type I and osteocalcin expression on increasing alendronate content. These results indicate that it is possible to use MAPLE technique to synthesize coatings which combine the bioactivity of hydroxyapatite with the local availability of alendronate.

7. References

- [1] S. Mann, *Biomineralization. Principles and concepts in bioinorganic materials chemistry*. Oxford University Press (2001), Oxford.
- [2] A.W. Xu, Y. Ma, H. Coelfen *Biomimetic mineralization*. *J. Mater. Chem.* **17** (2007), 415–449.
- [3] G.A. Ozin, *Morphogenesis of biomineral and morphosynthesis of biomimetic forms*. *Accounts of Chemical Research* **30** (1997), 17-27.
- [4] D.M. Walsh, D.M. Hartley, Y. Kosumoto, Y. Fezoui, M.M. Condrón, A. Lomakin, G.B. Benedek, D.J. Selkoe, D.B. Teplow, *Amyloid β -protein fibrillogenesis: structure and biological activity of protofibrillar intermediates*. *J. Biol. Chem.* **274** (1999), 25945-25952.
- [5] S. Mann, *The chemistry of form*. *Angew. Chem. Int. Ed.* **39** (2000), 3392-3406.
- [6] Z. Li, S. Yang, H. Lin, J. Huang, P.A. Watkins, A.B. Mofer, C. DeSimone, X-y. Song, A. M. Diehl, *Probiotics and antibodies to TNF inhibit inflammatory activity and improve nonalcoholic fatty liver disease*. *Hepatology* **37** (2003), 343-350.
- [7] T. Cook, F. Pichaud, R. Sonnevile, D. Papatsenko, C. Desplan, *Distinction between color photoreceptor cell fates is controlled by Prospero in Drosophila*. *Dev. Cell.* **4** (2003), 853-864.
- [8] A.E. Hall, A.B. Bleecker, *Analysis of combinatorial loss-of-function mutants in the Arabidopsis ethylene receptors reveals that the *ers1 etr1* Double mutant has severe developmental defects that are *EIN2* dependent*. *The Plant Cell* **15** (2003), 2023-2041.
- [9] A.R. Boccacini, P.A. Trusty, D.M.R. Taplin, C.B. Ponton, *Colloidal processing of a mullite matrix material suitable for infiltrating woven fire performs using electrophoretic deposition*. *Journal of the European Ceramic Society* **28** (2008), 1319-1327.

- [10] J. Huang, R. Valluzzi, E. Bini, B. Vernaglia, D.L. Kaplan, *Cloning, expression, and assembly of sericin-like protein*. *J. Biol. Chem.* **278** (2003), 46117-46123.
- [11] E.Y. Kawachi, C.A. Betran, R.R. dos Reis, O.L. Alves, *Bioceramics: tendencies and perspectives of an interdisciplinary area*. *Quim Nova* **23** (2000), 518-522.
- [12] C.C. Ribeiro, C.C. Barrias, M.A. Barbosa, *Calcium phosphate-alginate microspheres as enzyme delivery matrices*. *Biomaterials* **25** (2004), 4363-4373.
- [13] M. Bohner, *Reactivity of calcium phosphate cements*. *J. Mater. Chem.* **17** (2007), 3980-3986.
- [14] L. Yubao, Z. Xingdong, K. de Groot, *Hydrolysis and phase transition of alfa-tricalcium phosphate*. *Biomaterials* **18** (1997), 737-741.
- [15] M.R. Finisie, A. Josuè, V.T. Favere, M.C.M. Laranjeira, *Synthesis of calcium-phosphate and chitosan bioceramics for bone regeneration*. *An. Acad. Bras. Cienc.* **73** (2001), 525-532.
- [16] V.P. Orlovskii, V.S. Komlev, S.M. Barinov, *Hydroxyapatite and hydroxyapatite-based ceramics*. *Inorg. Materials* **38** (2002), 973-984.
- [17] I. O. Mazali, O. L. Alves, *Morphosynthesis: high fidelity inorganic replica of the fibrous network of loof a sponge (Luffa cylindrica)*. *An Acad Bras Cienc* **1** (2005), 77.
- [18] S. Weiner, L. Addadi, *Design strategies in mineralized biological materials*. *J. Mater. Chem.* **7** (1997), 689-702.
- [19] J.D. Currey, *Physical characteristics affecting the tensile failure properties of compact bone*. *J. Biomech.* **23** (1990), 837.
- [20] L.C. Bonar, M.D. Grynblas, J.E. Roberts, R.G. Griffin, M.J. Glimcher, in *The chemistry and biology of mineralized tissues*. Ed. W.T. Butler, EBSCO Media, Birmingham (AL) (1985), 226-233.
- [21] M.J. Glimcher, in *Disorders of bone and mineral metabolism*, Eds. F.L. Coe, M.J. Favus, Raven Press New York (1992), 265-286.

- [22] S.P. Bruder, A.I. Caplan, Y. Gotoh, L.C. Gerstenfeld, M.J. Glimcher, *Immunohistochemical localization of a 66 kD glycosylated phosphoprotein during development of the embryonic chick tibia*. *Calcif. Tissue Int.* **48** (1991), 429-437.
- [23] M.D. McKee, A. Nanci, W.J. Landis, Y. Gotoh, L.C. Gerstenfeld, M.J. Glimcher, *Developmental appearance and ultrastructural immunolocalization of a major 66kDa phosphoprotein in embryonic and postnatal chicken bone*. *Anat. Rec.* **228** (1990), 77-92.
- [24] M.J. Glimcher, in *The chemistry and biology of mineralized connective tissues*. Ed. A. Veis Elsevier, Amsterdam (1981), 618-673.
- [25] R.B. Martin, D.B. Burr, *Structure, function, and adaption of compact bone*. Raven Press (1989), New York.
- [26] W. Suchanek, M. Yoshimura, *Processing and properties of hydroxyapatite-based biomaterials for use as hard tissue replacement implants*. *J. Mater. Res.* **13** (1998), 94-117.
- [27] R. Detsch, H. Mayr, G. Ziegler, *Formation of osteoclast-like cells on HA and TCP ceramics*. *Acta Biomaterialia* **4** (2008), 139-148.
- [28] D. McConnell, *Apatite, its crystal chemistry, mineralogy, utilization and geologic and biologic occurrences*. Springer-Verlag, New York (1973).
- [29] J.O. Nriagu, P.B. Moore, *Phosphate minerals*. Springer-Verlag, Berlin (1984).
- [30] A.J.G. Notholt, I. Jarvis, *Phosphorite research and development*. Geological Soc. Special publication, n. 52 London (1990).
- [31] E.S. Thian, J. Huang, S.M. Best, Z.H. Barber, Wonfield, *Silicon-substituted hydroxyapatite: The next generation of bioactive coatings*. *Materials Science and Engineering C* **27** (2006), 251-256.
- [32] E. Pecheva, T. Petrov, C. Lungu, P. Montgomery, L. Pramatarova, *Stimulated in vitro bone-like apatite formation by a novel laser processing technique*. *Chemical Engineering Journal* **137** (2008), 144-153.

- [33] A. Rabiei, T. Blalock, B. Thomas, J. Cuomo, Y. Yang, J. Ong, *Microstructure, mechanical properties, and biological response to functionally graded HA coatings*. Material Science and Engineering C **27** (2007), 423-528.
- [34] R.Z. LeGéros, *Preparation of octacalcium phosphate (OCP): a direct fast method*. Calcif. Tissue Int. **37** (1985), 194-197.
- [35] H.E. Schroeder, *Formation and inhibition of dental calculus*, Ed. Has Huber, Berne (1969).
- [36] K.J. Muenzenberg, M. Gebhardt, *Brushite, octacalcium phosphate and carbonate containing apatite in bone*. Clin. Orthop. Rel. Res. **90** (1973), 271.
- [37] P. Bodier-Houllé, P. Steuer, J.C. Voegel, F.J.C. Cuisinier, *First experimental evidence for human dentine crystal formation involving conversion of octacalcium phosphate to hydroxyapatite*. Acta Cryst. D **54** (1998), 1377-1381.
- [38] S. Kamakura, Y. Sasano, O. Suzuki, *Synthetic octacalcium phosphate (OCP) is an effective scaffold to regenerate bone*. International Congress Series **1284** (2005), 290-295.
- [39] J.J. Berzelius, *Lehbuch der Chemie Vol. 4*. Arnoldischen Buchhandlung, Dresden (1836).
- [40] W.E. Brown, *Octacalcium phosphate and hydroxyapatite: crystal structure of octacalcium phosphate*. Nature **196** (1962), 1048.
- [41] M. Mathew, W.E. Brown, L.W. Schroeder and B. Dickens, *Crystal structure of octacalcium bis (hydrogenphosphate) tetrakis (phosphate) pentahydrate, $\text{Ca}_8(\text{HPO}_4)_2(\text{PO}_4)_4 \cdot 5\text{H}_2\text{O}$* . J. Cryst. Spectrosc. Res. **18** (1988), 235-250.
- [42] G. Troemel, *Beitraege zur Kenntnis des systems kalziumoxyd-phosphorpentoxyd*. Mitt Kaiser-Wilhelm-Inst Eisenforschg **14** Dusseldorf (1932).
- [43] M. Mathew, L.W. Schroeder, B. Dickens, W.E. Brown, *The crystal structure of $\alpha\text{-Ca}_2(\text{PO}_4)_2$* . Acta Cryst. **B33** (1977), 1325-1333.

- [44] A.L. Mackay, *A preliminary examination of the structure of α - $\text{Ca}_3(\text{PO}_4)_2$* . Acta Cryst. **6** (1953), 743-744.
- [45] G.E. Moore, Am. J. Sci. **39** (1865), 43.
- [46] K. Lonsdale, *Limited studies give some details of composition, rates of growth, distribution, and possible causes*. Science **159** (1968), 1199-1207.
- [47] J.M.P.M. Borggreven, F.C.M. Driessens and J.W.E. van Dijk, *Dissolution and precipitation reactions in human tooth enamel under weak acid conditions*. Arch. Oral Biol. **31** (1986), 139-144.
- [48] L.C. Chow, W.E. Brown, *Reaction of dicalcium phosphate dehydrate with fluoride*. J. Dent. Res. **52** (1973), 1220-1227.
- [49] C.A. Beevers, *The crystal structure of dicalcium phosphate dehydrate, $\text{CaHPO}_4 \cdot 2\text{H}_2\text{O}$* . Acta Cryst. **11** (1958), 273-277.
- [50] D.W. Jones, J.A.S. Smith, *The structure of brushite, $\text{CaHPO}_4 \cdot 2\text{H}_2\text{O}$* . J. Chem. Soc. (1962), 1414-1420.
- [51] D.H.R. Kempen, L. Lu, T.E. Hefferan, L.B. Creemers, A. Maran, K.L. Classic, W.J.A. Dhert, M.J. Yaszemski, *Retention of in vitro and in vivo BMP-2 bioactivities in sustained delivery vehicles for bone tissue engineering*. Biomaterials **29** (2008), 3245-3252.
- [52] O. Suzuki, *Interface of synthetic inorganic biomaterials and bone regeneration*. International Congress Series **1284** (2005), 274-283.
- [53] S.P. Nielsen, *The biological role of strontium*. Bone **35** (2004), 583-588.
- [54] A. Bigi, E. Boanini, C. Capuccini, M. Gazzano, *Strontium-substituted hydroxyapatite nanocrystals*. Inorganica Chimica Acta **360** (2007), 1009-1016.
- [55] W. Xue, J.L. Moore, H.L. Hosick, S. Bose, A. Bandyopadhyay, W.W. Lu, K.M.C. Cheung, K.D.K. Luk, *Osteoprecursors cell response to strontium-containing hydroxyapatite ceramics*. Journal of Biomedical Materials Research Part A **79** (2006), 804-814.

- [56] Z.Y. Li, W.M. Lam, C. Yang, B. Xu, G.X. Ni, S.A. Abbah, K.M.C. Cheung, K.D.K. Luk, W.W. Lu., *Chemical composition, crystal size and lattice structural changes after incorporation of strontium into biomimetic apatite*, *Biomaterials* **28** (2007), 1452-1460.
- [57] N. Medveczky, H. Rosemberg, *Phosphate transport in Escherichia coli*. *Biochem Biophys. Acta* **241** (1971), 494-506.
- [58] M.H. Salimi, J.C. Henghebaert, G.H. Nancollas, *The crystal growth of calcium phosphates in the presence of magnesium ions*. *Am.Chem.Soc., Langmuir* **1** (1985), 119-122.
- [59] A. Bigi, B. Bracci, F. Cuisinier, R. Elkaim, M. Fini, I. Mayer, I.N. Mihailescu, G. Socol, L. Sturba, P. Torricelli, *Human osteoblast response to pulsed laser deposited calcium phosphate coatings*. *Biomaterials* **26** (2005), 2381-2389.
- [60] A. Armulik, G. Svineng, K. Wennerberg, R. Faessler, S. Johansson, *Expression of integrin subunit $\beta 1B$ in integrin $\beta 1$ -deficient GD25 cells does not interfere with $\alpha V\beta 3$ functions*. *Exp. Cell. Res.* **254** (2000), 55-63.
- [61] H. Fleisch, *Bisphosphonates: mechanism of action*. *Endocrine Rev.* **19** (1998), 80-100.
- [62] M.J. Rogers, J.C. Frith, S.P. Luckman, F.P. Coxon, H.L. Benford, J. Monkkonen, S. Auriola, K.M. Chilton, R.G.G. Russell, *Molecular mechanism of action of bisphosphonates*. *Bone* **24** (1999), 73S-79S.
- [63] R.G.G. Russell, M.J. Rogers, *Bisphosphonates: from the laboratory to the clinic and back again*. *Bone* **25** (1999), 97-106.
- [64] S.B. Woo, J.W. Hellstein, J.R. Kalmar, *Systematic review: bisphosphonates and osteonecrosis of the jaws*. *Ann. Intern. Med.* **144** (2006), 753-761.
- [65] R. Rizzoli, N. Burllet, D. Cahall, P. D. Delmas, E. F. Eriksen, D. Felsenberg, J. Grbic, M. Jontell, M. Landesberg, A. Laslop, M. Wollenhaupt, S. Papapoulos, O. Sezer, M. Sprafka, J. Y. Reginster, *Osteonecrosis of the jaw and bisphosphonate treatment for osteoporosis*. *Bone* **42** (2008), 841-847.

- [66] S.M. Ott, *Fractures after long-term alendronate therapy*. J. Clin. Endocrinol. Metab. **86** (2001), 1835.
- [67] R.G.G. Russell, *Determinants of structure-function relationships among bisphosphonates*. Bone **40** (2007), S21-S25.
- [68] E. Boanini, M. Gazzano, K. Rubini and A. Bigi, *Composite nanocrystals provide new insight on alendronate interaction with hydroxyapatite structure*. Adv. Mater. **19** (2007), 2499-2502.
- [69] E. Boanini, P. Torricelli, M. Gazzano, R. Giardino and A. Bigi, *Alendronate-hydroxyapatite nanocomposites and their interaction with osteoclasts and osteoblast-like cells*. Biomaterials **29** (2008), 790-796.
- [70] T.J. Webster, *Nanophase ceramics: the future of orthopaedic and dental implant material*. In: Ying JY, ed. Nanostructured materials New York: Academic Press (2001), 125–166.
- [71] S.P. Simon, *Orthopaedic basic science*. American Academy of Orthopaedic Surgeons, Columbus, OH (1994).
- [72] R.Z. LeGéros. *Properties of osteoconductive biomaterials: calcium phosphates*. Clin Orthop Relat Res **395** (2002), 81–98.
- [73] L. Sun, C.C. Berndt, K.A. Gross, A. Kucuk, *Material fundamentals and clinical performance of plasma-sprayed hydroxyapatite coatings: a review*. J Biomed Mater Res: Appl Biomater **58** (2001), 570–592.
- [74] Y. Yang, K.H. Kim, J.L. Ong, *A review on calcium phosphate coatings produced using a sputtering process—an alternative to plasma spraying*. Biomaterials **26** (2005), 327–337.
- [75] N. Hijon, M.V. Cabanas, J. Pena and M. Vallet-Regi, *Dip coated silicon-substituted hydroxyapatite films*. Acta Biomater. **2** (2006), 567–574.

- [76] E.S. Thian, J. Huang, S.M. Best, Z.H. Barber and W. Bonfield, *Silicon-substituted hydroxyapatite: the next generation of bioactive coatings*. Mater. Sci. Eng. C **27** (2007), 251-256.
- [77] W. Xue, H.L. Hosick, A. Bandyopadhyay, S. Bose, C. Ding, K.D.K. Luk, K.M.C. Cheung and W.W. Lu, *Preparation and cell-materials interactions of plasma sprayed strontium-containing hydroxyapatite coating*. Surf. Coat. Technol. **201** (2007), 4685-4693.
- [78] G. Socol, P. Torricelli, B. Bracci, M. Iliescu, F. Miroiu, A. Bigi, J. Werckmann and I.N. Mihailescu, *Biocompatible nanocrystalline octacalcium phosphate thin films obtained by pulsed laser deposition*. Biomaterials **25** (2004), 2539-2545.
- [79] R. Chiesa, E. Sandrini, M. Santin, G. Rondelli and A. Cigada, *Osteointegration of titanium and its alloys by anodic spark deposition and other electrochemical techniques*. J. Appl. Biomater. Biomech. **1** (2003), 91-107.
- [80] T. Kokubo, H. Kushitani, S. Sakka, T. Kitsugi and T. Yamamuro, *Solutions able to reproduce in vivo surface-structure changes in bioactive glass-ceramic A-W³*. J. Biomed. Mater. Res. **24** (1990), 721-734.
- [81] W. Mròz, M. Jedynski, A. Prokopiuk, A. Slosarczyk, Z. Paszkiewicz, *Characterization of calcium phosphate coatings doped with Mg, deposited by pulsed laser deposition technique using ArF excimer laser*. Micron **40** (2009), 140-142.
- [82] Y. Yang, K.H. Kim, J.L. Ong, *A review on calcium phosphate coatings produced using a sputtering process—an alternative to plasma spraying*. Biomaterials **263** (2005), 27-37.
- [83] Z.S. Luo, F.Z. Cui, W.Z. Li. *Low-temperature crystallization of calcium phosphate coatings synthesized by ion-beam-assisted deposition*. J Biomed Mater Res **46** (1999), 80-86.
- [84] M. Wei, A.J. Ruys, B.K. Milthorpe, C.C. Sorrell. *Solution ripening of hydroxyapatite nanoparticles: effects on electrophoretic deposition*. J Biomed Mater Res **45** (1999), 11-19.

- [85] H. Ishizawa, M. Ogino. *Formation and characterization of anodic titanium oxide films containing Ca and P*. J Biomed Mater Res **34** (1997), 15–20.
- [86] R. Chiesa, E. Sandrini, M. Santin, G. Rondelli, A. Cigada. *Osteointegration of titanium and its alloys by anodic spark deposition and other electrochemical techniques: a review*. J Appl Biomater Biomech **1** (2003), 91–107.
- [87] A. Bigi, E. Boanini, B. Bracci, A. Facchini, S. Panzavolta, F. Segatti, L. Sturba, *Nanocrystalline hydroxyapatite coatings on titanium: a new fast biomimetic method*. Biomaterials **26** (2005), 4085-4089.
- [88] Chrisey DB, Hubler GK editors, *Pulsed laser deposition of thin films* Wiley, New York (1994).
- [89] I.N. Mihailescu, E. Gyorgy, *Pulsed laser deposition: an overview*. In: T. Asakura ed. *Trends in optics and photonics*. Springer series in optical science. Springer-Verlag **201** Berlin (1999).
- [90] D. Bauerle ed., *Laser processing and chemistry*. Springer, Berlin (1996).
- [91] V. Nelea, M. Jelinek, I.N. Mihailescu. *Biomaterials: new issues and breakthroughs for biomedical applications*. In: Eason R, editor. *Pulsed laser deposition of thin films*. John Wiley, New York (2007), 421–56.
- [92] L. Clèries, J.M. Fernández-Pradas, J.L. Morenza, *Bone growth on and resorption of calcium phosphate coatings obtained by pulsed laser deposition*. J. Biomed. Mat. Res. Part A **49** (2000), 43-52.
- [93] R. Eason Ed., *Pulsed Laser Deposition of Thin Films*. John Wiley & Sons (2007).
- [94] R.A. McGill , D.B. Chrisey, 2000. *Method of producing a film coating by matrix assisted pulsed laser deposition*. Patent 6, 025, 036.
- [95] G.B. Blanchet, C.R. Fincher, C.L. Jackson, S.I. Shah, K.H. Gardner, *Laser ablation and the production of polymer films*. Science **29**, **262** (1993), 719-721.

- [96] F. Bloisi, L. Vicari, R. Papa, V. Califao, R. Pedrazzani, E. Bontempi, L.E. Depero, *Biomaterial thin film deposition and characterization by means of MAPLE technique*. *Materials science and engineering C* **27** (2997), 1185-1190.
- [97] A. Almirall, G. Larrecq, J.A. Delgado, S. Martinez, J.A. Planell, M.P. Ginebra, *Fabrication of low temperature macroporous hydroxyapatite scaffolds by foaming and hydrolysis of an α -TCP paste*. *Biomaterials* **25** (2004), 3671–3680.
- [98] T.E. Itina, V. Zhigilei, B.J. Garrison. *Matrix-assisted pulsed laser evaporation of polymeric materials: a molecular dynamics study*. *Nucl. Instrum. Methods Phys. Res. B* **180** (2001), 238-244.
- [99] K. S. TenMuisen, P.W. Brown, *Formation of calcium-deficient hydroxyapatite from α -tricalcium phosphate*. *Biomaterials* **19** (1998), 2209-2217.
- [100] A. Piqué, R.A. McGill, D.B. Chrisey, D. Leonhardt, T.E. Mslna, B.J. Spargo, J. H. Callahan, R.W. Vachet, R.Chung, M.A.Bucaro, *Growth of organic thin films by the matrix assisted pulsed laser evaporation (MAPLE) technique*. *Thin Solid Films* **535** (1999), 336-341.
- [101] S. Panzavolta, M. Fini, A. Nicoletti, B. Bracci, K. Rubini, R. Giardino, A. Bigi, *Porous composite scaffolds based on gelatin and partially hydrolized α -tricalcium phosphate*. *Acta Biomaterialia* **5** (2009), 636-643.
- [102] Q. Xu, J. T. Czemuszka, *Controlled release of amoxicillin from hydroxyapatite-coated poly(lactic-co-glycolic acid) microspheres*. *Journal of Controlled Release* **127** (2008), 146-153.
- [103] F. Caruso, M. Spasova, A. Susa, M. Giersig, R. A. Caruso, *Polymeric cores utilized include gelatin, alginate, polystyrenesulfonate*. *Chem. Mater.* **13** (2001), 109-116.
- [104] E. van den Bosch, C. Gielens, *Gelatin degradation at elevated temperature*. *International Journal of Biological Macromolecules* **32** (2003), 129-138.
- [105] R. Cortesi, C. Nastruzzi, S.S. Davis. *Sugar cross-linked gelatin for controlled release: microspheres and disks*. *Biomaterials* **19** (1998), 1641-1649.

- [106] A. Veis, *The macromolecular chemistry of gelatine*. Academic Press, New York (1964).
- [107] A. Courts and G. Stainsby, *Recent advances in gelatine and glue research*, Pergamon Press, **100** New York (1958).
- [108] P.H. Von Hippel, K.Y. Wong, *The collagen gelatin phase transition. II shape of the melting curves and effect of chain length*. *Biochemistry* **2** (1963), 1399-1413.
- [109] H. Boedker and P.J. Doty, *J. Phys. Chem.* **58** (1954), 968.
- [110] V.L. Colvin, A.N. Goldstein and A.P. Alivisatos. *J. Am. Chem. Soc.* **114** (1992), 5521.
- [111] X.G. Peng, Y. Zhang, J. Yang, B. Zou, L. Xiao and T. Li, *J. Phys. Chem.* **96** (1992), 3170-3174.
- [112] F.C. Meldrum, N.A. Kotov, J.H. Fendler, *Preparation of particulate mono- and multilayers from surfactant-stabilized, nanosized magnetite crystallites*. *J. Phys. Chem.* **98** (1994), 4506-4510.
- [113] L.L. Hench, J.M. Polak, *Third generation biomedical materials*. *Science* **295** (2002), 1014-1017.
- [114] S.I. Stupp and G.W. Ciegler, *Organoapatites: materials for artificial bone. I. Synthesis and microstructure*. *J. Biomed. Mater. Res.* **26** (1996), 169-183.
- [115] S.V. Dorozhkin and M. Epple, *Biological and medical significance of calcium phosphates*. *Angew. Chem. Int. Ed.* **41** (2002), 3130-3146.
- [116] R.Z. LeGeros, *Properties of osteoconductive biomaterials: calcium phosphates*. *Clin. Orthop.* **395** (2002), 81-89.
- [117] R. Xin, Y. Leng and N. Wang, *In situ TEM examination of octacalcium phosphate to hydroxyapatite transformation*. *J. Cryst. Growth* **289** (2006), 339-334.

- [118] O. Suzuki, S. Kamakura, T. Katagiri, M. Nakamura, B. Zhao, Y. Honda and R. Kamijo *Bone formation enhanced by implanted octacalcium phosphate involving conversion into Ca-deficient hydroxyapatite*. *Biomaterials*, **27** (2006), 2671-2681.
- [119] E. Boanini, P. Torricelli, M. Gazzano, R. Giardino, A. Bigi, *Alendronate-hydroxyapatite nanocomposites and their interaction with osteoclasts and osteoblast-like cells*. *Biomaterials* **29** (2008), 790–796.
- [120] R.Z. LeGeros, R. Kijkovska, J.P. LeGeros, *Formation and transformation of octacalcium phosphate, OCP: a preliminary report*. *Scanning Electron Microsc.* **4** (1984), 1771-1777.
- [121] A. Bigi, E. Boanini, R. Botter, S. Panzavolta, K. Rubini, *α -tricalcium phosphate hydrolysis to octacalcium phosphate: effect of sodium polyacrylate*. *Biomaterials* **23** (2002), 1849–1854.
- [122] P. Bodier-Houllé, P. Steuer, J.C. Voegel and F.J.C. Cuisinier, *First experimental evidence for human dentine crystal formation involving conversion of octacalcium phosphate to hydroxyapatite*. *Acta Crystallogr D* **54** (1998), 1377-1381.
- [123] H.P. Klug, L.E. Alexander, *X-ray diffraction procedures for polycrystalline and amorphous materials*, Wiley–Interscience, New York (1974).
- [124] A. Immirzi, *Constrained powder-profile refinement based on generalized coordinates. Application to X-ray data of isotactic polypropylene*. *Acta Crystallogr., Sect. B* **36** (1980), 2378-2385.
- [125] S. Brueckner, *Profile analysis of X-ray diffraction data from powder polymer samples*, *Chim. Ind.* **70** (1988), 48-53.
- [126] S.V. Meille, S. Bruckner, J.B. Lando, *The structure of γ -polypivalolactone: a combined analysis of single-crystal electron diffraction data and powder X-ray diffraction profiles with the Rietveld method*. *Polymer* **30** (1989), 786-792.
- [127] H.M. Rietveld *A profile refinement method for nuclear and magnetic structures*. *J. Appl. Crystallogr.* **2** (1969), 65-71.

- [128] K. Sudarsanan, R.A. Young, *Structural crystallography and crystal chemistry*. Acta Crystallogr., Sect. B 28 (1972), 3668-2670.
- [129] G. Caglioti, A. Paoletti, F.P. Ricci, *Choice of collimator for a crystal spectrometer for neutron diffraction*. Nucl. Instrum. Methods **3** (1958), 223-228.
- [130] S. Brunauer, P.H. Emmet, E.J. Teller, *Adsorption of gases in multimolecular layers*. J. Am. Chem. Soc. **60** (1938), 309-319.
- [131] Luo ZS, Cui FZ, Li WZ. *Low-temperature crystallization of calcium phosphate coatings synthesized by ion-beam-assisted deposition*. J Biomed Mater Res **46** (1999), 80-86.
- [132] C. Capuccini, P. Torricelli, E. Boanini, M. Gazzano, R. Giardino, A. Bigi *Interaction of Sr-doped hydroxyapatite nanocrystals with osteoclast and osteoblast-like cells*. Journal of Biomedical Materials Research DOI: 10.1002/jbm.a.319751.
- [133] G.M. Blake, M.A. Zivanovic, A.J. McEwan, *Sr-89 therapy: Strontium kinetics in disseminated carcinoma of the prostate*. Eur. J. Nucl. Med. **12** (1986), 447-454.
- [134] E. Shorr, A.C. Carter, *The usefulness of strontium as an adjuvant to calcium in the remineralization of the skeleton in man*. Bull. Hosp. Joint. Dis. Orthop. Inst. **13** (1952), 59-66.
- [135] E. Canalis, M. Hott, P. Deloffre, Y. Tsouderos, P.J. Marie, *The divalent strontium salt S12911 enhances bone cell replication and bone formation in vitro*. Bone **18** (1996), 517.
- [136] M.D. Grynpas, E. Hamilton, R. Cheung, Y. Tsouderos, P. Deloffre, M. Hott, P.J. Marie, *Strontium increases vertebral bone volume in rats at a low dose that does not induce detectable mineralization defect*. Bone **18** (1996), 253-259.
- [137] P.J. Marie, P. Ammann, G. Boivin, *Mechanisms of action and therapeutic potential of strontium in bone*. C. Rey, Calcif. Tissue Int. **69** (2001), 121-129.

- [138] S.G. Dahl, P. Allain, P.J. Marie, Y. Mauras, G. Boivin, P. Ammann, Y. Tsouderos, P.D. Delmas, C. Christiansen, *Incorporation and distribution of strontium in bone*. *Bone* **28** (2001), 446-453.
- [139] A. Bigi, F. Marchetti, A. Ripamonti, N. Roveri, E. Foresti, *Magnesium and strontium interaction with carbonate-containing hydroxyapatite in aqueous medium*. *J. Inorg. Biochem.* **15** (1981), 317-327.
- [140] B.O. Fowler, Infrared studies of apatites. I. *Vibrational assignments for calcium, strontium, and barium hydroxyapatites utilizing isotopic substitution*. *Inorg. Chem.* **13** (1974), 194-207.
- [141] T. Kikuchi, Y. Sugiura, H. Tanaka, *Two types of molybdenum sites in Mo enzymes, characterized by the new indicator of ESR parameters*. *Inorganica Chimica Acta* **66** (1982), L5-L8.
- [142] J.C. Elliott, *Structure and chemistry of the apatites and other calcium orthophosphates*. Elsevier Sci, The Netherlands (1994).